



City Research Online

City, University of London Institutional Repository

Citation: Eckhardt, H.S (2009). Gas analysis in the deep ultraviolet wavelength region using fibre-optics and spectrophotometric detection. (Unpublished Doctoral thesis, City, University of London)

This is the accepted version of the paper.

This version of the publication may differ from the final published version.

Permanent repository link: <https://openaccess.city.ac.uk/id/eprint/19753/>

Link to published version:

Copyright: City Research Online aims to make research outputs of City, University of London available to a wider audience. Copyright and Moral Rights remain with the author(s) and/or copyright holders. URLs from City Research Online may be freely distributed and linked to.

Reuse: Copies of full items can be used for personal research or study, educational, or not-for-profit purposes without prior permission or charge. Provided that the authors, title and full bibliographic details are credited, a hyperlink and/or URL is given for the original metadata page and the content is not changed in any way.

City Research Online:

<http://openaccess.city.ac.uk/>

publications@city.ac.uk

**Gas analysis in the deep ultraviolet
wavelength region using fibre-optics
and spectrophotometric detection**

by

Hanns Simon Eckhardt

**A thesis submitted to City University for the Degree of
Doctor of Philosophy (PhD)**

**CITY University London
School of Engineering and Mathematical Sciences
Northampton Square, London EC1V 0HB**

April 16, 2009

Contents

1	Introduction and background	1
1.1	Aims and objectives of the work	4
1.2	Review of analysis equipment for matter in the gas phase	5
1.2.1	Electrical sensors	5
1.2.2	Gas Chromatography (GC) [Gottwald, 1995]	6
1.2.3	Infrared spectroscopy	10
1.2.4	Mass spectroscopy (MS)[Hogan, 1996]	14
1.2.5	UV detection systems	15
1.3	Light power flow in a fibre-optic-based sensor system	16
1.4	The Bouguer-Lambert-Beer Law	19
1.5	Analysis of limitations in a spectroscopic measurement	20
1.5.1	Deviations from Bouguer-Lambert-Beer Law	21
1.5.2	Errors in an intensity measurement	21
1.5.3	Errors within an absorbance measurement	22
1.6	Physical principles of absorption spectroscopy[Atkins, 1996; Ban- well and McCash, 1994; Jaffé and Orchin, 1962]	25
1.6.1	Rotational transitions	25
1.6.2	Vibrational transitions	27
1.6.3	Electronic states and electronic transitions	29
1.7	Structure of the thesis	34
 2	 Fibre Optics	 42
2.1	Introduction	42
2.2	Fibre types available for UV-applications	43
2.3	AS-UV-fibres	44
2.3.1	Basic and UV-Induced attenuation	44
2.3.2	Studies on basic attenuation and UV induced defects	46

2.3.3	Influence of UV induced loss on fibre optic measurements [Belz et al., 2008]	52
2.4	UV-HCW	55
2.4.1	Optical properties of hollow core waveguides	57
2.5	Summary and discussion	60
3	Lamp System	67
3.1	Abstract	67
3.2	Introduction	67
3.3	Influence of coupling optics	69
3.4	Nitrogen purge for lamp housing	71
3.5	Experimental determination of lamp stability	71
3.6	Experimental results	73
3.7	Summary	75
4	Development and characterization of fibre-optic spectrometer	78
4.1	Abstract	78
4.2	Different techniques for wavelength separation [Hardwick, 1998; Loewen, 2005; Margaritondo and Staehli, 1994]	78
4.3	Influence of entrance slit & Cross section converter	84
4.4	Important parameters for spectrophotometers	85
4.5	Measurements on different spectrometers for gas analysis	89
4.6	Characterization of HRUV prototypes	91
4.7	Measurement results	94
4.8	Summary and Discussion	97
5	Development of an intrinsic absorption cell for gas analysis	102
5.1	Abstract	102
5.2	Existing concepts	102
5.3	Concepts for new applications	103

5.3.1	Measurement of trace gases	103
5.3.2	Measurement of GC effluent	103
5.4	Realization of hollow core waveguide sensor cell for the detection of gas chromatographic effluent	104
5.4.1	Coupling efficiency	105
5.4.2	Dimensions of absorption cell	108
5.4.3	Construction and Heating of the measurement cell	112
5.5	Summary	114
6	Measurements with GC-UV Detection systems	117
6.1	Introduction	117
6.2	Measurements with existing GC-UV detector	117
6.3	Characterization of fibre-optic UV detection system for gas chro- matography	123
6.3.1	Fibre-optic UV detector	123
6.3.2	Measurement of systems short-term noise and drift be- haviour	123
6.4	Measurements with fibre-optic UV detection system for gas chro- matography	126
6.4.1	Measurement of UV Test sample	126
6.4.2	Linearity and minimum detection limits	127
6.5	Coupling of fibre-optic GC-UV system with a mass spectrometer (GC-UV-MS)	130
6.6	Comparative measurements with modified sample	131
6.7	Measurement on polycyclic aromatic hydrocarbons	135
6.8	Summary	138
7	UV Absorption measurements for Trace Gas Analysis	144
7.1	Introduction	144

Contents

7.2	Comparison of extinction coefficients in the UV and MIR wavelength region	145
7.3	Measurement technique / Linearity	148
7.4	Possible Applications	149
7.4.1	Medical / health care applications	149
7.4.2	Monitoring of exhaust gas compounds	150
7.5	Summary	152
8	Conclusions & Future Work	154
8.1	Summary of work carried out	154
8.2	Future Work	157
9	List of Publications	159
9.1	Publications related to fibre-optic gas analysis	159
9.2	Publications related to fibre-optic characterization and applications	160
A	Appendix	162
A.1	Short-term Stability measurements of fibre optic UV detection system	162
A.2	Engineering drawings of measurement system	165

List of Tables

2-1	Spectral attenuation, measured with UVM fibres	47
3-1	D2-Lamp 30W, supplier A	77
3-2	D2-Lamp 30W, supplier B	77
3-3	Fiberlight Lamp, Heraeus	77
4-1	Maximum Signal to noise values for different digital resolutions, considering only noise due to AD conversion	89
4-2	Overview on compared spectrometers	90
4-3	Overview on HRUV prototype spectrometers	94
4-4	Measurement of photometric accuracy, HRUV1 spectrophotome- ter	98
4-5	Measurement of photometric accuracy, HRUV2 spectrophotome- ter	98
5-1	Absorption peak length for 2 ml/min flow and 1 s peak duration	112
6-1	Composition of UV test sample	120
6-2	GC method and data acquisition parameters	120
6-3	Noise and drift behaviour of fibre-optic measurement system under operation conditions	125
6-4	Measurement of linearity, absorption peak area based on chro- matogram, absolute percentual deviation in brackets	129
6-5	Measurement of linearity, absorption peak area based on corre- lation method, absolute percentual deviation in brackets	129
6-6	Composition of UV/MS test sample	132
6-7	Calculated peak areas of the UV and MS detector, values with an asterisk have not been used	133
6-8	Correlation coefficients (R) and standard deviations (SD) of lin- ear fit	134
6-9	Overview on detected PAHs	139

List of Figures

7-1	Extinction coefficients of sulfur dioxide	147
7-2	Gradient, correlation coefficient R and standard deviation SD of linear fits	149
7-3	Exhaled trace gases indicating illnesses [Diskin et al., 2003; Fet- zer et al., 2003; A. T. Society, 1999]	150
7-4	Typical exhaust gases from automobiles	151

List of Figures

1.1	Schematic drawing of optical system	17
1.2	Relative error of an absorbance measurement, for Reference val- ues of 500, 1000, 10000, and 60000 counts	24
1.3	A Diatomic molecule treated as two masses, joined by a rigid bar.	26
1.4	A diatomic atom as a harmonic oscillator	27
1.5	Energy levels in a vibrating diatomic atom	29
1.6	Overview on energy levels present in molecules	31
1.7	Overlap of wavefunctions of the ground state and the excited state	32
2.1	Variation in basic attenuation of an all-silica fibre	45
2.2	System for solarization measurements	47
2.3	Measurement of induced attenuation in all-silica fibres, initial spectrum (black) and after UV-irradiation (red)	48
2.4	Variation of induced attenuation in all-silica fibres, standard type (black and green) and improved material (red)	49
2.5	Measurement procedure for UV fibres, for determination of tran- sient defects	51
2.6	Time dependent of UV-damage and annealing at 215 nm, UV irradiation from 0 to 4 hours (first run) and from 24 to 26 hours (second run), no UV irradiation from 4 to 24 hours	52

List of Figures

2.7	Spectral UV-damage and annealing of fibre with 2 m length. 4 hour damage during first run (upper curve), 2 h damage during second run (middle curve) and 20 hour annealing (lower curve)	53
2.8	Fibre-optic based measurement system	54
2.9	Structure of a hollow core waveguide	56
2.10	Reflection on a wall of aluminium	57
2.11	Spectral attenuation of a hollow core waveguide	58
2.12	Measurement of the numerical aperture by the inverse farfield method	59
2.13	Numerical Aperture of a hollow core waveguide [Kötschau, 2002]	59
2.14	Length dependence of numerical aperture [Kötschau, 2002] . . .	60
3.1	Setup of standard deuterium lamps	68
3.2	Fiberlight setup without fibre coupler	68
3.3	The optical projection	69
3.4	Illustration of the Chromatic abberation	70
3.5	Lamphousing and attached imaging optics, illustrated gas flow (red) and light path (blue)	72
3.6	Experimental characterization of noise and drift	73
3.7	Comparison of spectral intensity with spectrometer: supplier A (red), supplier B (black), Fiberlight multiplied by a factor of 100 (blue)	74
4.1	Diffraction of incident light on a grating [Loewen, 2005]	81
4.2	Czerney Turner Setup	83
4.3	Rowland circle setup	84
4.4	Schematic drawing of a cross section converter produced of 19 optical fibres, side of fibre-optic connector (left), side of entrance slit (right)	85

List of Figures

4.5	Single wavelength illuminating a detector chip. The wavelength accuracy, spectral resolution, pixel resolution and temperature drift can be deduced	87
4.6	Influence of spectral width	91
4.7	Measurement setup for characterization of spectrometer, according to ASTM procedures	93
4.8	Determination of spectral slit width with the ratio of minimum and maximum absorption of toluene in hexane, HRUV1 (black), HRUV2 (red)	95
4.9	Determination of spectral slit width with the absorption of benzene vapour, HRUV1 (black), HRUV2 with an offset of 0.4 AU (red), spectral slit width of approx. 1.6 nm, with an offset of 0.7AU (green)	96
4.10	Determination of stray radiant power ratio: HRUV1 (black), HRUV2 (red)	97
4.11	Measurement on photometric accuracy: from bottom to top: 20, 40, 60, 80, 100 mg/ml	98
5.1	Schematic of measurement cell	105
5.2	Measurement setup for determination of coupling efficiency . . .	106
5.3	Measurement of coupling efficiency with displacement along the x-Axis, Distances fibre endface - HCW1000: 1 mm (black), 3 mm (red), 5 mm (green)	107
5.4	Measurement of coupling efficiency with displacement along the x-Axis, Distances fibre endface - HCW500: 1 mm (black), 5 mm (red)	108
5.5	Measurement of coupling efficiency with displacement along the z-Axis, HCW1000 (black), HCW500 (red)	109
5.6	Schematic drawing of a "gas plugs" within the separation column	109
5.7	Schematic drawing of a chromatogram	110

List of Figures

5.8	Simulated influence of time-equivalent volume on chromatographic resolution: 0.2 s (black), 1 s (red), 2 s (green), 4 s (blue)	111
5.9	Simulated UV-signal (top) and differentiated UV-signal (bottom) for time-equivalent volume of 2 s (black) and 4 s (red) . . .	112
5.10	Cell setup	113
6.1	Schematic setup	118
6.2	Chromatogram for wavelength 185 to 300 nm	119
6.3	Chromatogram of UV test sample, calculated from 185 to 300 nm	121
6.4	Schematic measurement setup of fibre-optic UV detection system	122
6.5	Measurement setup for the characterization of the UV detection system, illustrating the path of GC effluent within the system . .	124
6.6	Intensity signal of the measurement system, flushed with nitrogen at a temperature of 180 °C	125
6.7	Determination of short time stability, at a wavelength of 186 nm, under Measurement conditions	126
6.8	Chromatogram of the UV test sample, detected with the UV detector	127
6.9	Absorption spectra of the compounds within the UV test sample, Carbon disulfide (A), Ethylbenzene (B), Bromobenzene (C), trans-decahydronaphtalene (D), cis-decahydronaphtalene (E) and Butyrophenone (F)	128
6.10	Chromatogram of the UV test sample, detected with the UV detector (top) and the mass spectrometer (bottom)	131
6.11	Absorbance spectra of bromobenzene for a sample containing 1000 (black), 100 (red) and 10 ng (green)	132
6.12	Linearity of Ethylbenzene (green), Bromobenzene (red) and Butyrophenone (black), measured with UV detector	134
6.13	Linearity of Ethylbenzene (green), Bromobenzene (red) and Butyrophenone (black), measured with the MS detector	135

List of Figures

6.14	Mass spectra of phenantrene (top) and anthracene (bottom) . . .	136
6.15	UV absorption spectra of phenantrene (top) and anthracene (bottom)	137
6.16	Chromatogram of the PAH sample, UV detector (top), MS de- tector (bottom)	138
7.1	Measurement System for trace gas analysis	146
7.2	Absorption spectrum of 8.4 ppm sulfur dioxide in the infrared wavelength region, measured with a pathlength of 1 m	146
7.3	Absorption spectrum of 1.1 ppm sulfur dioxide in the ultraviolet wavelength region, measured with a pathlength of 1 m	147
7.4	Linear regression of concentration over absorptions of Nitrogen dioxide at 220.9 (black), 227 (red), 242.3 (green) and 326.6 nm (blue)	148
7.5	Absorption spectra of oxygen (black) and 828ppm of nitrogen dioxide in oxygen (red), with an offset of 0.5 AU	152
A.1	Determination of short time stability under Measurement con- ditions at 180 nm	162
A.2	Determination of short time stability under Measurement con- ditions at 186 nm	163
A.3	Determination of short time stability under Measurement con- ditions at 200 nm	163
A.4	Determination of short time stability under Measurement con- ditions at 217 nm	164
A.5	Overview on measurement system	165
A.6	Drawing of base plate of measurement setup	166
A.7	Overview on lamp setup	167
A.8	Drawing of lamp housing	168
A.9	Drawing of imaging optics	169
A.10	Drawing of lens holder	170

List of Figures

A.11 Drawing of lens ring	170
A.12 Overview on measurement cell	171
A.13 Explosion drawing of measurement cell	172
A.14 Drawing of measurement cell - base plate for gas cell	173
A.15 Drawing of measurement cell - side parts	174
A.16 Drawing of measurement cell - front and rear part	175
A.17 Drawing of measurement cell - base plate	176
A.18 Drawing of measurement cell - top cover	177
A.19 Drawing of measurement cell - punched plate insulation, bottom	178
A.20 Drawing of measurement cell - punched plate insulation, top . .	179
A.21 Drawing of measurement cell - insulation, top and bottom . . .	180

”It was recognized very early in the development of spectroscopy that the study of molecular spectra is one of the most important tools for the determination of molecular structures.”

Gerhard Herzberg, Nobel Prize Lecture, 1971

Acknowledgements

I wish to express my thanks to Prof. K.-F. Klein for his advice and guidance throughout this work. In addition I would like to acknowledge his patience in reviewing this manuscript.

I am deeply indebted to Prof. K.T.V. Grattan and Prof. T. Sun for their supervision of this work and also for providing their valuable time to discuss problems of all sorts.

I wish to acknowledge the support and hospitality of Prof. B. Spangenberg and R. Brämer of HS Offenburg during very exciting measurement campaigns.

I am grateful to H. Befort-Riedl, H. Dominick, J. Mannhardt, J. Gerstel, G. Kuka, G. Nelson and U. Schröder also representing their associated colleagues and companies for their co-operation and fruitful discussions.

I am most grateful to the present and past personnel at the laboratory of optical communications and waveguides for their understanding, loyalty and fruitful discussions during my time in the laboratory.

I take my head off to the machine shop of Fachhochschule Giessen-Friedberg who manufactured a variety of different parts on short notice with highest precision, thank you Klaus, Gerd and Jürgen.

Finally I would like to pay a special tribute to Christian, Cornell, Hellge, Jalal, Michael, Walter, Valentin, Mareike & Ulrich, Ulrike & Heinz, Karin & Heinz and especially my family, Annette and Hannah, who have supported me in many ways throughout the course of my studies and to whom this thesis is dedicated.

I grant powers of discretion to the University Librarian to allow this thesis to be copied in whole or in part without further reference to me. This permission covers only single copies made for study purposes, subject to normal conditions of acknowledgement.

Abstract

This thesis reports on the development of deep ultraviolet fibre-optic sensor systems for gas analysis. Several parameters affecting the stability and sensitivity of such sensor systems are studied and discussed. These fibre-optic systems might be used for the analysis of gas chromatographic effluent or alternatively for on-line and real time analysis of gases. These systems are suitable for measurement tasks within the environmental, health care, high technology, chemical engineering or food safety field.

Basic design aspects and components of an analytic system based on absorption measurement are described. In this context, the transmission properties of all-silica optical fibres in the UV-region, including their solarization behaviour, have been taken in consideration. A central point was the development of a spectrophotometer, with suitable wavelength range and spectral resolution for the absorption measurements in the vapour phase. In addition, the development of a fibre-optic absorption cell was carried out. The influence of the absorption length and the associated cell volume was studied in detail.

A variety of samples, previously separated by an upstream gas chromatograph has been measured with the described measurement system. The interconnection of the presented detection system with an additional downstream mass spectrometric detector was studied as an interesting alternative for better analyses. Coupling of both detection systems proved to give complementary information on the reference sample. The linearity of the measurement system has been demonstrated, too. Due to the small volume, a minimal detectable absolute mass in the nanogram range has been determined.

List of Symbols

a	area of fibre end face
N_2O	nitrous oxide
NO	nitric oxide
NO_2	nitrogen dioxide
NH_3	ammonia
$B_{Power}(\lambda)$	wavelength-dependent power budget [dB]
$P_D(\lambda)$	power reaching the detector [W]
$P_S(\lambda)$	power emitted from a light source [W]
G_i	geometric extend of component i
S_i	area of component i [mm^2]
NA_i	numerical aperture of component i
λ	wavelength [nm]
L_i	power loss within component i
$I(\lambda)$	light intensity measured with a spectrometer (uncalibrated A/D output of spectrometer) [$counts$]
$I_{sam}(\lambda)$	sample intensity measured with a spectrometer [$counts$]
$I_{ref}(\lambda)$	reference intensity measured with a spectrometer [$counts$]
$I_{dark}(\lambda)$	dark intensity measured with a spectrometer [$counts$]
$I_{corr}(\lambda)$	dark-signal corrected intensity measured with a spectrometer [$counts$]
c	molar concentration [$mol \cdot l^{-1}$]
l	optical path length [cm]
$\varepsilon(\lambda)$	molar absorption coefficient [$l \cdot mol^{-1} \cdot cm^{-1}$]
$A(\lambda)$	Absorbance [AU]
$T(\lambda)$	Transmission [%]
$a.u.$	arbitrary units
AU	absorbance units

List of Symbols

SNR	Signal to noise ratio [dB]
σ_I	standard deviation of spectroscopic intensity measurement
ΔI	(estimated) error of spectroscopic intensity measurement
E' -Centre	Defect in fused silica due to solarization, absorption maximum at 215 nm
$NBOH$	Non-bridging oxygen hole, defect in fused silica due to solarization, absorption maximum at 265 nm
$\alpha(\lambda)$	attenuation [$dB \cdot m^{-1}$]
$L_{UV}(\lambda)$	UV-induced loss [dB]
Θ	angle of acceptance
m	order or diffraction
d	grating constant
θ	blaze angle
R	resolving Power of a grating
$\Delta\lambda$	spectral resolution (optical)
ADC	Analogue digital converter
$SRPR$	Stray radiant power ratio
$FWHM$	full width half maximum
$HRUV$	high resolution UV spectrophotometer
R	grade of separation (in gas chromatography) [s]
$t_{dr,i}$	retention time of compound i [s]
w_i	peak duration of compound i [s]
$S_{GC}(t)$	signal of a GC detector [$a.u.$]
$S_{UV}(t)$	signal of a UV-detector [$a.u.$]
w_{cell}	time-equivalent volume of absorption cell [s]
L_p	length of gaschromatographic peak in absorption cell [cm]
A_{Cell}	cross-sectional area of measurement cell [$10^{-3} \cdot mm^2$]
F	flow rate [$ml \cdot s^{-1}$]
$\bar{A}(t)$	chromatogram calculated as a mean value [AU]

List of Symbols

$C(t)$	chromatogram calculated by auto correlation
$GC-UV$	Combination of gas chromatography with a spectrophotometric UV detector
$GC-UV-MS$	Combination of gas chromatography with a spectrophotometric UV and a mass spectrometric detector
MS	Mass spectrometer
MSD	Mass spectrometric detector
PAH	Polycyclic aromatic hydrocarbons
SO_2	sulfur dioxide
ppm	parts per milion

1 Introduction and background

The determination of the composition of matter in all states of aggregation has always been a major concern for the scientific and industrial world. Therefore, new techniques of many kinds have been developed in the field of analytic chemistry, which are capable to do qualitative and quantitative analyses of mixtures. In addition to the accuracy of the measurement, the measurement time plays a major role in process analytics and process control.

Separation techniques, such as gas chromatography (GC), high precision liquid chromatography (HPLC) and thin layer chromatography (TLC) are applied in laboratories throughout the world. In 1957, M.J.E. Golay introduced the capillary column, which influenced the applicability and further improved the selectivity of gas chromatography. In contrast to the packed (rigid) columns, the capillary columns with long length and high separation power could be installed easily by coiling the capillary. In addition, a variety of detection systems allow both the registration and analysis of complex samples, as well as the sensitive detection of traces in different matrices.

Spectroscopic and spectrophotometric techniques allow the analysis of samples, depending on its interaction with light. The study of the electronic, vibrational and rotational transitions permit the exploration of molecular structures. These techniques have been established for the analysis of solids, liquids and gases with different sensor cell setups and wavelength ranges [Banwell and McCash, 1994; Jaffé and Orchin, 1962; Svanberg, 2001]. Mainly in the mid infrared (MIR) range of the spectrum optical methods are established for the use in chemical laboratories. In addition, the analysis of solids and liquids are carried out in the ultraviolet and visible (UV/VIS) wavelength range.

Evolving computational power allowed the automation of measurement setups. In addition, data acquisition, storage and computer-based interpretation of large amounts of spectral data enabled efficient analyses, leading to comput-

erized analytical systems for laboratory and process environments. On the instrumental side, the implementation of two techniques allow a very efficient data acquisition; within the Fourier transform IR (FTIR) spectrometer an interferogram from an interferometer can be transferred into a spectrum by Fast Fourier transformation within fractions of a second. On the other hand the development of linear sensor arrays, mainly for the ultraviolet and visible wavelength region, allow the fast acquisition of spectra in polychromator setups. The interconnection of different analytic techniques can be reasonable, if the sample is very complex and the information for characterizing the sample is not sufficient. Most common combination is the gas chromatographic separation and mass selective detection system (MSD), which allows an identification of the compounds eluting from the GC column. The high sensitivity of the MSD allows very low detection limits. However, the detection principle relies on the fragmentation of the molecules, which accounts for difficulties when isomers need to be analyzed.

The combination of GC and infrared detection (IRD) which has been introduced firstly in 1967 [Low and Freeman, 1967], provides structural information of the molecules which caused a development of a commercially available detection system. In the ultraviolet wavelength range, the interfacing was proposed in 1962 [Kaye, 1962]. Subsequently, two different approaches for efficiently detecting eluent have been described. The construction of a light pipe setup within a laboratory spectrophotometer [Lagesson, 1992] and the combination of fibre-optic components with an absorption cell [Müller, 1992].

While the mismatch of the absorption cell or "light pipes" volume and the eluent of the separation column was reducing the efficiency of the measurement system in both spectral ranges, high absorptions resulting in low detection limits for the ultraviolet detector have been reported.

In the ultraviolet wavelength range, below 250 nm, degradation and solarization effects of components like lenses, windows and mainly optical fibres,

caused by the higher energies of ultraviolet light, hindered the further development of measurement systems. In this wavelength range the attenuation properties of fibres were studied, and solarization effects, which could influence the measurement, were minimized [Fabian et al., 1991; Khalilov et al., 2004, 2006; Klein et al., 1997, 2001].

In addition, the development of a hollow core waveguide, originally designed for the transportation of ultraviolet high power laser light [Matsuura and Miyagi, 1999; Matsuura et al., 2000; Miyagi et al., 1987], made available an efficient optical waveguide. Furthermore, the low volume within this waveguide, which is based on internally coated capillaries made it an excellent candidate for an intrinsic sensor.

In addition, the analysis of trace gases with high precision in a short measurement time and the quick determination of constituents in low concentration are necessary in the context of environmental regulations, health care or quality control: The determination of the toxic and hazardous minor components of automobile or combustion exhaust gain importance in the environmental context. The non-invasive detection of trace gases in exhaled breath can be used for the early indication of diseases. Finally, monitoring the purity of gases for applications in the high technology and food industry both allow maintaining a high production and minimizing risk for the customer.

1.1 Aims and objectives of the work

The research described in this work discusses the development of a fibre-optic-based polychromatic chemical sensor system for gas analysis in the ultraviolet range of the light spectrum at wavelengths below 300 nm. Investigations are carried out in respect to a range of design aspects of a sensor system which ultimately may have laboratory and field use.

The principle aims and objectives of the thesis are as follows:

- The development of a fibre-optic based polychromatic chemical sensor system.
- The investigation of the underpinning physics of the sensor systems considered.
- The development, setup and characterization of a novel UV polychromator setup; including the comparison of techniques for determining essential parameters of spectrophotometers.
- The development and characterization of a series of absorption cells in terms of their performance at varying temperatures representing the extremes in field application.
- A range of measurements with the sensor systems on a number of chemicals to determine their applicability.
- A comparative measurement on different light sources and detector systems to determine the limits of the system proposed in terms of sensitivity, thermal stability and accuracy.
- Conclusions of the research and suggestions for future work.

1.2 Review of analysis equipment for matter in the gas phase

After the discovery of nitrogen by Daniel Rutherford in the 1770s, and his following studies on its properties the era of gas analysis began.

The first quantitative analysis of gases was published by Robert Bunsen in 1857. His "Gasometrische Methoden" describes a volumetric method, where a volume of gas is analyzed in a closed system [Bunsen, 1857]. In several steps the gas is interacting with different absorbing materials, either solids or liquids, and the change of volume after every step indicates the quantity of gas adsorbed by the specific absorbent.

Beside the chemical analysis carried out in laboratories like colorimetric, titrimetric and gravimetric methods, sensing schemes for the use in automated instruments have been developed over the years. In addition, methods have been developed which utilize existing gas analysis equipment with matter that is in the vapour phase only at elevated temperatures. The following section discusses gas and vapour analysis, which is performed by automated instruments. Only sensing schemes offering the opportunity to distinguish between different components in a mixture, qualitative analysis, and furthermore quantifying the components will be discussed.

1.2.1 Electrical sensors

The first instrumental method for gas analysis was developed in the 1880s, where the quantity of a component was measured. The concept was based on the specific thermal conductivity of a component, and its ability to cool an electrically heated wire, by passing it. The amount of a gas component within a mixture is proportional to the current, necessary to maintain a constant temperature. In 1913 the first apparatus was patented by the "Siemens and

Halske Co.” as a viable tool for quantifying gas components in binary or quasi binary mixtures. A binary mixture is a mixture of two gases with different thermal behaviour.

In 1999 an improved method of this technique was patented [Grunewald, 1999], where the sensor is given not a constant but a sinusoidal wave around a constant value over time as set point for the temperature. As the thermal conductivity of the gases changes with temperature, the current necessary to reach the setpoint is modulated and generates additional frequencies that can be separated by the use of a fast Fourier transformation (FFT). With a calibration of the behaviour of thermal conductivity of gases the system can quantify the composition of a mixture of up to five gases. The detection limit of this technique is in the lower percentage range with a measurement time of approx. 1s for 90 percent accuracy.

1.2.2 Gas Chromatography (GC) [Gottwald, 1995]

The concept of separating molecules and compounds by using a mobile and a stationary phase was applied in paper chromatography very early. Mikhail Tswett described the process detailed for the separation and following analysis of plant pigments in botanical studies and coined the name ”chromatography” in 1906 [Tswett, 1906a,b].

The basic principle is, that a mobile phase (petrol ether / ethanol mixture) and a sample (plant extract) was put onto a stationary phase (calcium carbonate) which acted as an adsorbent. The mobile phase carries molecules of the sample, and arrange them according to the adsorption series in the direction of the mobile stream.

In addition to this type of chromatography on plates, the development of liquid column chromatography, which is nowadays known as high-performance liquid chromatography (HPLC) or liquid chromatography (LC), was firstly predicted

in 1941 by Martin and Synge [Martin and Synge, 1941a]. In addition, in a following publication they suggested applying this technique for the separation of vapours [Martin and Synge, 1941b]. In 1952, Martin and Synge succeeded in building the first gas-liquid partition chromatography instrument and received the Nobel Prize in chemistry for the development of partition chromatography. In gas chromatography, a typically liquid sample is injected and evaporated in a heated injector. A carrier gas stream of inert gas, like nitrogen, hydrogen, helium or CO₂ carries the vapour into the separation column.

This separation column can be set up by various different designs: A packed column, a rod from stainless steel, glass or silica, with a diameter between 1 to 4 mm and filled (or packed) with particles, which have been coated with liquid stationary phase for the separation, alternatively solid stationary phases can be used. In addition, a small inner diameter (typically between 0.25 and 0.53 mm) stainless steel or fused silica capillary with an internal coating of liquid stationary phase on the inner surface can be used for separation. The length of both columns and the liquid phase used vary, depending on the mixture and the required separation for each sample. In general, packed columns are used if higher amounts of samples are injected. Furthermore, they can be tailored for applications, by putting particles with different coatings into them. This is a very effective method for reducing the measurement time in a well known sample, where the quantification of the compounds is of interest. In most cases, the capillary column is chosen for standard laboratory equipment. Within the capillary a variety of stationary phases can be deposited as thin films, with typical thicknesses between 0.1 and up to 7 μm . The thickness of the film has an influence on the amount of sample that can be adsorbed and separated efficiently.

Stationary phases are commercially available by a various companies producing capillary columns and coated particles for packing columns. Mainly, the stationary phases are divided into polar and nonpolar phases, stating their

capability to separate polar and nonpolar constituents. The available columns range from fully polar to fully nonpolar, with percentual mixtures available in between. In addition to laboratory based applications gas chromatography moved towards an instrument for industrial and automated applications. Therefore, the suppliers for capillary columns offer different columns for a variety of applications with described parameters for the analysis in particular applications.

While the mobile phase is moving through the column without interfering with the stationary phase, the analytes are diffusing into the stationary phase and released some time thereafter. The analytes delay in moving through the column is called retention.

Depending on the column chosen the gaseous component of the sample are separated depending on their polarity, size and boiling point. By changing the temperature of the column or more practically the temperature of the GC-Instruments oven, the speed of the components in the capillary is influenced, and subsequently the grade of separation which is reached at the end of the capillary. However, keeping the temperature low would result in a very time-consuming measurement and therefore the selection of initial and end temperature and the steepness of temperature ramps in between has to be balanced between time for analysis and grade of separation. Within a GC measurement the information on the analyte is given by the retention time. The retention time is the time needed for an analyte to travel through the column. If a quantitative detector is used, the identification of analytes can be achieved by comparing the retention times, only within a known mixture. However, the retention time might change in the established gas chromatographic method, due to changes in the temperature program, column length, carrier gas flow and film thickness. Consequently, deviations might occur.

A wide variety of sensors are in use allowing the detection of gas chromatographic effluent at the end of a separation column. Most of them are only

quantitative, but non selective to the compounds. These detectors include flame ionisation (FID) and photo ionization detectors (PID). Both detectors are based on the principle that the ionisation of the molecules lead to an electrical signal at the collector. However, the ionization is realized with different techniques: The FID uses a hydrogen and synthetic air flame, while the PID uses a high energetic ultraviolet light source. Other quantitative detectors like the electron capture detector (ECD) and the thermal conductivity detector (TCD) can be used as well. In the case of the ECD a constant source of beta particle radiation (electrons) is realized with a Nickel-63 foil. When operated in a nitrogen atmosphere, the carrier gas its self does not absorb any electrons from this beta source. If a sample passes through the detector the molecules capture electrons and a change in the current can be measured. The TCD can distinguish between compounds having higher or lower thermal conductivities compared to the carrier gas and therefore giving positive and negative peaks for samples travelling through it.

From above detectors most can be used for analysis, however their selectivity and sensitivity has to be taken into account. The FID can only detect molecules including carbon, while the PID only can detect molecules that can be ionized by UV irradiation. TCD and ECD can virtually detect all molecules, as long as they do not have the same properties as the carrier gas used. In terms of the sensitivity the ECD can detect lowest concentrations with an excellent dynamic range. It is 10 to 1000 times more sensitive than the FID and up to a million times more sensitive than the TCD. However, also the reliability of the detectors have to be taken into account and therefore the most commonly used detector is the FID.

In the case of more complex samples or if the full analysis of an unknown sample is necessary, a more sophisticated detector is required. Most of these detectors are used and capable for analysis in the laboratory. However, the hyphenation of these techniques gives additional information which eventually simplifies

the analysis of complex samples. These detectors include mass spectroscopy, optical spectroscopy and atomic emission detectors (AED). Mainly mass spectroscopy (MS) is used as a standardized technique in laboratories nowadays. Optical spectroscopy detectors like Fourier transform infrared (IR) detectors and ultraviolet detectors give information on the structure of molecules. The operation principle of the IR is more detailed described in section 1.2.3. In case of the UV detector for gas chromatography (GC-UV or GC/UV) the first measurements have been reported in 1962 and 1964 [Kaye, 1962; Kaye and Waska, 1964]. In addition measurements have been carried out with a redesigned system starting in the 1990s [Lagesson, 1992]. In chapter 1.2.5 the development of this detection principle will be discussed. The MS is described in more detail in section 1.2.4.

Recent developments in gas chromatography have been realized with the coupling of two different columns, where the first column "injects" a sample in the second column that does a fast separation. The separated compounds have very small differences in the retention time, and therefore a fast detector like a time of flight mass spectroscopy detector is necessary. This technique is called GC times GC-MS (GCxGC MS). An annual held symposium provides an excellent overview on recent development in capillary GC and GCxGC [Sandra, 2006].

1.2.3 Infrared spectroscopy

In the infrared wavelength region the energy provided by irradiation is absorbed by vibrational and rotational transitions within the molecules. These absorptions cause characteristic spectra in the wavelength region and provide excellent information on the structure of molecules: The transitions are represented in the wavelengths of the absorption peaks, which are characteristic for the bonds within the molecules, while the quantity of the gas species can be determined with the strength of the absorption. However, there are different

techniques and methods applied to use this basic material property for analysis. In addition the strength of the absorption bands varies, depending on the gas and the selected wavelength region. For the detection of gases the mid Infrared (MIR: $\lambda \geq 2.5 \mu m$) is used mainly for the measurement of gases in medium and low concentrations, while the near infrared (NIR: $800 nm \leq \lambda \leq 2.5 \mu m$) is mainly used for the analysis of liquids. However, traces of gases with absorption bands in this wavelength region can be detected in the percent range.

In general, the absorption bands are measured with dispersive techniques, which give information over a wide wavelength range, with a good resolution allowing to distinguish between different absorption bands. Using broadband infrared light sources, the wavelength information is gathered by different techniques: The classical monochromator setup for the MIR is based on the diffraction of light at an optical grating. The spectrum is recorded by turning the grating in order to select the wavelength which is registered by a detector. Depending on the line distance on the grating and the focal length of the optical setup, the spectral resolution over a spectral range can be selected. The dimension of the slit influences the spectral resolution of the system. As the broadband light sources available for this wavelength range provide little spectral intensity, the measurement times are rather long and sometimes Lock-In amplifiers are required to obtain a good signal to noise ratio (SNR). The development of indium gallium arsenide arrays allowed a different setup for NIR spectrometers: In principal the light can be diffracted by a Czerny-Turner setup. However, transmission gratings with lenses for focusing or flat-field setups can be used as an alternative. All of them provide the spectral information imaged onto a linear InGaAs sensor, where the light can be measured on a number of pixels in a very short time, as no mechanical changes of the setup are necessary anymore. Due to the fast data acquisition the detection systems are excellent candidates for the use in process analysis applications. Finally, another technique for efficient spectral measurements in the MIR and

NIR wavelength range came up in the instrumental analytic with increasing computational power: The incident light is passing through an interferometer, where it is split up by a beam splitter and travels different path lengths, depending on the variation of the mirror position. After the combination of the light from the two different paths an interference-pattern occurs, depending on the mirror position. The signal resulting from the interference is recorded by a detector as a function of the mirror position, containing masked wavelength information. By fast Fourier transformation (FFT) an intensity spectrum over wavelength is obtained.

In order to efficiently use the described measurement schemes, an excellent SNR is essential. However the low spectral intensity of the light sources and the mostly demanded cooling of the detectors required to achieve the systems performance can be considered as a drawback of this measurement technique. In addition, the time for acquiring a single spectrum can take up to 60 seconds or longer. The time is influenced by different reasons: Within a monochromator setup, the time needed to perform the rotation of the grating and gathering data points. In the FTIR measurement, single spectra are accumulated in order to improve the SNR behaviour.

In the past, numerous researchers have been reporting the development and applications of a GC detector based on the FTIR technique. The development of the instrument, the optimization of the measurement setup, the gas handling and optimized triggering were studied and reported in different publications [Griffiths, 1977; Low and Freeman, 1967; Yang et al., 1984; Yang and Griffiths, 1984]. Additional publications provide information on Light pipe dimensions and volumes, and discuss the Signal to noise ratio and other instrumental aspects. Furthermore, a variety of different applications have been reported [Brown and Lennon, 1991; Brown et al., 1985; Giss and Wilkins, 1984; Griffiths and Wilkins, 1988; Haaland et al., 1993; Hasenoehrl et al., 1992; Mark and Griffiths, 2002; Smith et al., 1983; Wang and Edwards, 2006].

For the analysis of gases, which have not been separated, additional techniques for analysis have been developed, based on the research with highly selective techniques described above: The so-called non dispersive infrared detector (NDIR) uses a broadband light source, where the desired wavelength range for the absorption measurement of one gas component is selected with a filter. This technique offer the opportunity to do relatively fast measurements, but the wavelength region of the filter has to be chosen carefully. In addition a cross sensitivity to other gases with an absorption in the same wavelength region is possible. The use of a filter wheel offers the opportunity to detect more than one gas component in this setup and can minimize the measurement error resulting from overlapping absorption bands.

The development of tuneable diode lasers (TDL), both for the NIR and MIR wavelength regions allowed the scan of absorption bands in a limited wavelength region [Fetzer et al., 2002, 2003; Stewart et al., 1997]. This technique can be used for the selective measurement of single gases, scanning over one absorption band, with a wide variety of different gas cell setups (e.g. White-cells, cavities, evanescent field sensors)[Kleine et al., 2000; White, 1942; Willer et al., 2004] . Due to the higher power of the light source shorter measurement times are possible. In contrast to the NDIR method this Tuneable Diode Laser Absorption Spectroscopy (TDLAS) technique is more selective, due to the scanning of a small wavelength range the absorption of gases to be measured and a neighbouring absorption can be distinguished. With further development of laser sources attractive sensing techniques can be realized; e.g. quantum cascade lasers (QCL) working at room temperature and at new wavelengths in the MIR and additional wavelengths of laser sources in the NIR.

1.2.4 Mass spectroscopy (MS)[Hogan, 1996]

Based on the work of J.J. Thomson in the late 1890s with electrons and cathode rays, and Wien's work on the deflection of positive rays in electric and magnetic fields a technique was developed, where ionized components of gases can be sorted and detected by their mass/charge ratio. Within the first mass spectrometers the process was carried out under atmospheric pressure. By minimizing the pressure in a vacuum chamber the influences of ambient air decreases, with increasing accuracy of the measurement. In addition, different techniques to measure the mass charge ratio were developed, beginning with a semicircular magnetic field, where the selection is done by the strength of the magnetic field, chosen to get an ion of a certain mass/charge ratio to the detector, continuing with a time of flight separation. In most instruments, so-called quadrupoles are used, which are mass filters controlled by radiofrequency and constant voltages applied on two pairs of parallel rods. The resulting electromagnetic field between them allows only ions with a selected mass/charge ratio a stable trajectory through the mass filter and onto the detector. By alternating the electrical field of the mass filter a scan over different mass/charge ratios can be done. In addition to gas analysis the MS Systems can also be used for the characterization of numerous solids, vaporized by plasmas or by incident laser power.

In case of the hyphenation to a gas chromatograph there are two options, depending on the time necessary for the measurements; when using the more economically prized quadrupole setup, the detection of single or a series of chosen mass/charge ratios with a very short measuring time during a GC run, or alternatively using the full scan mode of the MS, where all detectable mass/charge ratios are measured. However, for short retention times the sampling time needs sufficiently short to provide a good time resolution of chromatographic peaks. Applications like the GCxGC technique require a comparatively high

price Time of Flight MS (TOF-MS). This detector allows the detection of a wide mass/charge ratio range in a short time, as the molecules are accelerated at the same time and detected by their time needed to reach the detector after crossing a so-called flight tube with a defined length.

1.2.5 UV detection systems

Ultraviolet spectrophotometers have a long tradition in analytical chemistry [Gauglitz, 1983; Perkampus, 1992a, 1995; Sommer, 1989], mainly for the analysis of liquid and solid samples. For the liquid in solid phase absorption spectra are available [Perkampus, 1992b]. While these systems are considered limited in the capability to produce valuable information concerning the composition, structure and conformation, the advantage of UV systems can be seen in their ability to quantify accurately in the trace contamination level [Talmi, 1982]. The classical setup for measuring the absorption of the sample is the monochromator setup with a double beam passing through a reference and a sample cell. The ratio between sample and reference cell is measured by an amplifier circuit and recorded by an analogue digital converter (ADC) or an x-y-plotter. A measurement with this technique is rather time consuming, as the wavelength separation is done by a mechanical rotation of the grating in the monochromator. Typically a measurement time of one second per nanometer needs to be considered. In the late 70s, a new setup, capable of faster data acquisition was developed. Based on optoelectronic imaging devices, the so-called photodiode array (PDA) was developed and tested for the use in spectrophotometric applications. These detectors allow to measure up to 2048 points (pixel) in the wavelength axis with variable integration time. After the first tests in existing monochromator systems, suitable polychromator setups with a flat spectral image were developed [Zeiss, 1982]. The application of the new polychromator systems allowed optimization of the whole systems performance resulting

in comparatively short sampling time for a spectrum, depending on the light intensity, good Signal to Noise ratio (SNR) and good stray light behaviour, which is comparable to most laboratory systems. In addition, the higher data acquisition rates allows the monitoring of dynamic processes, where in the past several samples have been taken for a later analysis. Some applications for real-time measurements are published for dissolution testing of drugs or water monitoring [Belz, 1998; Schatz, 2001]. For specialized applications, where only a number of known compounds need to be quantified, non-dispersive systems can be realized for measurements in the UV. For the improvement of the system, a gas discharge lamp, filled with nitrogen monoxide [Leippe et al., 2004; Wiegleb, 2004] was used, to enhance the sensitivity of the measurement system. The light passes a beam splitter, and is divided into two beams. The first one hits a detector for referencing the power. The second passes through a gas absorption cell before the detection. In front of the light source and in front of the detector used for the measurements a filter wheel can be used to select wavelength regions belonging to different gases. With this measurement setups a measurement of up to 4 components (N_2O , NO , NO_2 , NH_3) is possible. The duration of a measurement is depending on the time needed for the filter wheel to turn to the next filter.

1.3 Light power flow in a fibre-optic-based sensor system

In fibre-optic sensor schemes based on multimode fibres, the measurement of intensity changes due to absorption is most convenient. The approach of this section is to establish some performance criteria and formalize a general system description of a fibre-optic sensor scheme. The optical elements of a fibre-optic-based sensor system are shown in Fig. 1.1, comprising a light source, a fibre coupler, input and output fibres, a sensor cell and a detector. The performance of such a measurement arrangement is dependent on a

number of factors, such as sensitivity, noise, signal-to-noise ratio, resolution, range, accuracy, temperature, stability, range and response time [Belz, 1998]. In addition, transient responses caused by the measurand or the sensor system might occur and should be considered.

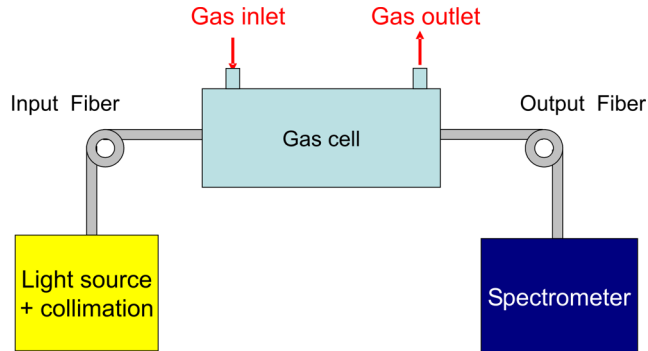


Figure 1.1: Schematic drawing of optical system

The key factor in designing a polychromatic sensor system, as envisaged in this work, is the wavelength-dependent power budget, which may be defined as $B_{Power}(\lambda)$:

$$B_{Power}(\lambda) = 10 \cdot \log \left(\frac{P_S(\lambda)}{P_D(\lambda)} \right) \quad (1-1)$$

where $P_S(\lambda)$ is the light power emitted from the source and $P_D(\lambda)$ the light power detected at a particular wavelength, λ . Thus, the goal in designing a polychromatic sensor system is to match the spectral dependence or sensitivity of the individual optical components, to obtain an acceptable signal-to-noise ratio over the desired wavelength range. However, the transfer and conservation of light power depends on a number of factors, including the efficiency of light coupling from one optical component to the next. This most important factor, the coupling of light between the optical components, is characterized by what is termed the geometric extent G_i , which describes the ability of each

optical component to accept light [Geckeler, 1990]. This is defined by

$$G_i = \pi S_i (NA_i)^2 \quad (1-2)$$

where S_i is the area of the emitting source and NA_i is a generalized value of the numerical aperture of the optical components. A difference in the geometric extend G_i leads to additional coupling losses. The other aspects of the loss function depend on a range of intrinsic aspects of the optical components. These can be described by the equation given below for the resultant intensity at the polychromatic detector as a function of wavelength, λ , source size, S , numerical aperture, NA , ambient temperature of the sensor system, T , and time, t , taking the lifetime of the light source and the degradation of the optical components by the UV radiation present, into account.

The light power collected by the polychromatic detector, $P_{D,dB}(\lambda)$, is given by a function comprising several factors and their dependencies can be seen in the following equation [Belz, 1998]:

$$\begin{aligned} P_D(\lambda, S_D, NA_{Det}, t, T) &= P_S(\lambda, S_S, NA_S, t, T) \\ &\quad - L_C(\lambda, S_C, NA_C) \\ &\quad - L_{IF}(\lambda, S_{IF}, NA_{IF}, t, T) \\ &\quad - L_{Sensor}(\lambda, S_{Sensor}, NA_{Sensor}, t, T) \\ &\quad - L_{OF}(\lambda, S_{OF}, NA_{OF}, t, T) \end{aligned} \quad (1-3)$$

where P_S is the spectral power of the light source, L_C is the coupling loss from the light source to the fibre input, L_{IF} and L_{OF} are the losses inside the input and output fibres respectively and L_{Sensor} is the optical loss inside the sensor cell, caused by sample modulation and guiding losses. With knowledge of the above, the power budget, can be optimized in the choice of the components used. The optical configuration mainly used and investigated in this work comprises a deuterium lamp as a light source, a lens or UV achromate used to couple light into the input fibre, solarization resistant input and output

fibres, for improved flexibility of the system, a spectrophotometer and a sensor cell. The performance of each part and the system will be discussed in the subsequent chapters.

1.4 The Bouguer-Lambert-Beer Law

A mathematical-physical basis of light-absorption measurements to determine the molar concentration of certain substances in gases and liquids is defined by the Bouguer-Lambert-Beer (BLB) law in the ultraviolet, visible and infrared part of the light spectrum. The reduction of intensity, $dI(\lambda)$, at a wavelength λ , that occurs when light of a monochromatic incident intensity $I(\lambda)$, passes through a sample of thickness dz along the z -axis, containing an absorbing species with a molar concentration c , can be expressed by:

$$-dI(\lambda) = I(\lambda) \cdot c \cdot k(\lambda) \cdot dz \quad (1-4)$$

by integration over the pathlength l :

$$\int_{I_{ref}(\lambda)}^{I_{sam}(\lambda)} \frac{1}{I(\lambda)} \cdot dz = k(\lambda) \cdot \int_0^l c \cdot dz \quad (1-5)$$

where $I_{ref}(\lambda)$ is the initial, or so-called reference intensity, $I_{sam}(\lambda)$ is the intensity transmitted through the sample, the so-called sample intensity, and $k(\lambda)$ as a proportionality factor. Assuming that the concentration, c , is uniform and independent of z , this will result in:

$$\ln \frac{I_{ref}(\lambda)}{I_{sam}(\lambda)} = k(\lambda) \cdot c \cdot l \quad (1-6)$$

and

$$I_{sam}(\lambda) = I_{ref}(\lambda) \cdot e^{-k(\lambda) \cdot c \cdot l} \quad (1-7)$$

Equation 1-7 indicates that the intensity decreases exponentially with the sample thickness and concentration. However, the BLB law is often expressed as:

$$I_{sam}(\lambda) = I_{ref}(\lambda) \cdot 10^{-\varepsilon(\lambda) \cdot c \cdot l} \quad (1-8)$$

with $\varepsilon(\lambda)$ as the molecular absorption coefficient of the absorbing species observed. Then the absorbance, $A_{sam}(\lambda)$, and the Transmission, $T_{sam}(\lambda)$, can be defined as:

$$A_{sam}(\lambda) = \log_{10} \left(\frac{I_{ref}(\lambda)}{I_{sam}(\lambda)} \right) = \varepsilon \cdot c \cdot l \text{ [AU]} \quad (1-9)$$

and

$$T_{sam}(\lambda) = 100 \cdot \frac{I_{sam}(\lambda)}{I_{ref}(\lambda)} \text{ [%]} \quad (1-10)$$

respectively, with the dimensions for $A_{sam}(\lambda)$ in absorbance units, AU, for T_{sam} in %, for $\varepsilon(\lambda)$ in $l \cdot mol^{-1} \cdot cm^{-1}$, for c in $mol \cdot l^{-1}$ and for length l in cm . The concentration c can be calculated by

$$c = \frac{A(\lambda)}{\varepsilon(\lambda) \cdot l} \quad (1-11)$$

The BLB law is usually valid for dilute analyte solutions, for strongly monochromatic, parallel and coherent radiation and in optically homogeneous (isotropic) media. There should be no luminescence or scattering in the solution observed and the optical path length should be strictly defined. Its validity is demonstrated by strictly linear plots of $A(\lambda)$ versus cell path length, l , or concentration, c , of the absorbing analyte in solution. The sensitivity of the measurement can be elevated by increasing the path length in case of species with low molar absorption coefficients. In addition an improvement of the systems SNR would result in an extended dynamic range and in reduced uncertainties of the measurement. A more detailed description may be found in several texts, [Atkins, 1996; Banwell and McCash, 1994; Jaffé and Orchin, 1962; Perkampus, 1992a].

1.5 Analysis of limitations in a spectroscopic measurement

In order to estimate the reliability and repeatability of measurements done with a spectrophotometric system, the possible errors have to be analysed. Within error analysis the possible errors are divided into two groups. The first

group are the systematic errors, which should be avoided during the design and the construction phase of the system. Secondly, random errors can occur during the measurement and their influence on the measurement has to be analyzed in detail.

1.5.1 Deviations from Bouguer-Lambert-Beer Law

During the measurement of a sample, the applicability of the BLB law is paramount for a successful measurement. The main effects that interfere are stray light, lack of monochromasy, radiation scattering, fluorescence, changes in the refractive index, change in the chemical equilibrium and instrumental deviations. The effects are discussed in more detail in [Belz, 1998; Gauglitz, 1983; Sommer, 1989].

1.5.2 Errors in an intensity measurement

During the process of acquiring spectral data with a detection system based on a photodiode array the accuracy of the measurement is influenced by the following parameters: The residual output of the unilluminated detector, known as dark signal and the deviation of the acquired signal, which can be considered as Gaussian noise, mainly. Both effects have an influence on the applicability of the Boguer-Lambert-Beers law during a spectroscopic measurement.

The real sample intensity can be determined only by two measurements. The first measurement is the measurement of the residual output, referenced as the dark signal $I_{dark}(\lambda)$, with no light within the system and the actual sample measurement $I_{sam}(\lambda)$. The real intensity measured can be determined with the following formula:

$$I_{corr}(\lambda) = I_{sam}(\lambda) - I_{dark}(\lambda) \quad (1-12)$$

Under the presence of noise, which can be considered as a random error with a Gaussian density function, the intensity's mean value can be determined as:

$$\bar{I}(\lambda) = \frac{1}{N} \sum_{i=1}^N I_i(\lambda) \quad (1-13)$$

The mean value $\bar{I}(\lambda)$ is close to the real intensity value (the center of the density function), if a sufficient number of measurements N have been done. Furthermore, the deviation of the single measurements from the mean value has to be taken into account. This deviation in the measurement can be described as standard deviation σ_I . The standard deviation can be determined as:

$$\sigma_I = \sqrt{\frac{1}{N-1} \sum_{i=1}^N I_i(\lambda) - \bar{I}(\lambda)} \quad (1-14)$$

In general, the standard deviation σ_I describes an interval around the mean value which comprises approx. 68% of all measurement points; if a Gaussian density function is considered. Both values provide information about a measurement series, such as precision and repeatability. The measurement result is usually described as:

$$I = \bar{I}_\lambda \pm \sigma_I \quad (1-15)$$

In the case of a single measurement it is not possible to determine mean value and standard deviation. However, an error ΔI can be estimated for a single measurement $I(\lambda)$:

$$I(\lambda) = I(\lambda) \pm \Delta I \quad (1-16)$$

1.5.3 Errors within an absorbance measurement

During an absorbance measurement three intensity measurements have to be performed. Each of these measurements is influenced by noise. Therefore the uncertainty of the single intensity measurement and the absorbance measurement have to be evaluated [Belz, 1998; Mark and Griffiths, 2002]. In other references, the dark signal and the reference signal are considered a noise free

value, and their influence on the error within an absorbance measurement is neglected. Calculating the absorbance according to formula 1-9, considering the subtraction of dark signal in formula 1-12, the absorbance can be described as:

$$A(\lambda) = \log_{10} \left(\frac{I_{corr,ref}(\lambda)}{I_{corr,sam}(\lambda)} \right) = \log_{10} \left(\frac{I_{ref}(\lambda) - I_{dark}(\lambda)}{I_{sam}(\lambda) - I_{dark}(\lambda)} \right) = \log_{10} \left(\frac{R - D}{S - D} \right) \quad (1-17)$$

taking into account the presence of a dark signal $D = I_{dark}(\lambda)$, while $S = I_{sam}(\lambda)$ is the sample intensity and $R = I_{ref}(\lambda)$ is the reference intensity. The error on the absorbance can be determined according to the partial differentiation regarding to the dark, signal and reference intensities, as described within the error propagation:

$$\Delta A = \sqrt{\left(\frac{\delta A}{\delta R} \cdot \Delta R \right)^2 + \left(\frac{\delta A}{\delta S} \cdot \Delta S \right)^2 + \left(\frac{\delta A}{\delta D} \cdot \Delta D \right)^2} \quad (1-18)$$

resulting in:

$$\Delta A = \frac{1}{\ln(10)} \sqrt{\left(\frac{1}{(R - D)} \cdot \Delta R \right)^2 + \left(\frac{-1}{(S - D)} \cdot \Delta S \right)^2 + \left(\frac{R - S}{(R - D)(S - D)} \cdot \Delta D \right)^2} \quad (1-19)$$

Taking into account the illumination independent behaviour of a photodiode array, a constant error for the dark, reference and sample intensity can be estimated. Therefore, the error from the intensity measurement ΔI can be taken out of the square root.

$$\Delta A = \frac{1}{\ln(10)} \cdot \Delta I \sqrt{\left(\frac{1}{(R - D)} \right)^2 + \left(\frac{-1}{(S - D)} \right)^2 + \left(\frac{R - S}{(R - D)(S - D)} \right)^2} \quad (1-20)$$

Analyzing each term under the square root, the second term is strongly influenced by the sample intensity. For high absorbance values, the sample intensity becomes small and the relative error increases.

According to formular 1-20, the relative error was calculated and displayed in

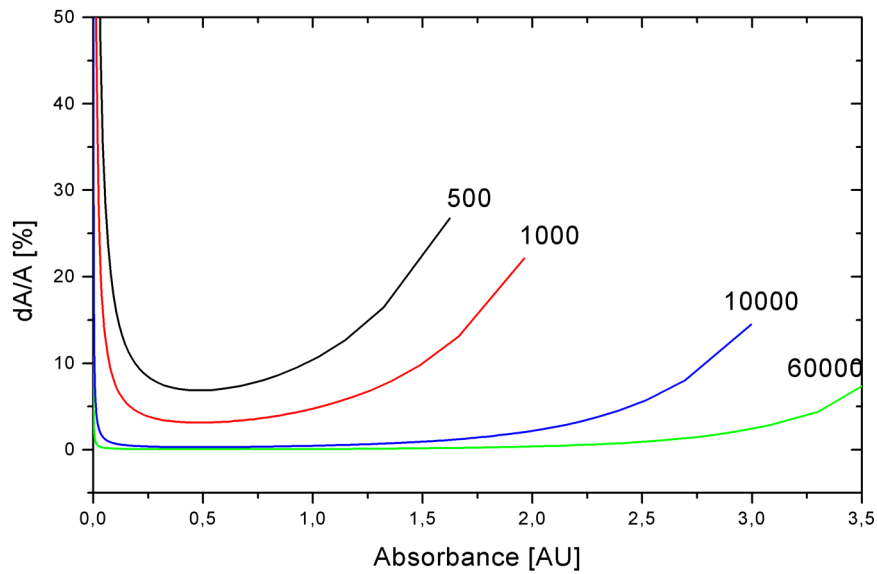


Figure 1.2: Relative error of an absorbance measurement, for Reference values of 500, 1000, 10000, and 60000 counts

figure 1.2. A dark signal with a mean intensity of 80 counts and a peak to peak noise representing an estimated ΔI of 10 counts was used. Reference intensities between 500 and 60000 counts were chosen. The relative error decreases significantly with a high reference intensity. Consequently, absorbances with rather low reference intensities comprise large relative errors. This effect has to be taken into account during an analytic measurement. The influence of the decreasing sample intensity is also visible, as the relative error is increasing strongly for higher absorbance values.

1.6 Physical principles of absorption spectroscopy[Atkins, 1996; Banwell and McCash, 1994; Jaffé and Orchin, 1962]

When continuous radiation passes through a transparent material, a portion of this radiation may be absorbed. This absorption is caused by transitions between different energy levels. The difference ΔE is necessary for a transition between the ground E_g and the excited E_e state. The energy needed for this transition can be described by the frequency of the absorption ν and the Planck's constant h :

$$\Delta E = E_e - E_g = h\nu \text{ with } h = 6.626 * 10^{-34} \text{ Js} \quad (1-21)$$

This frequency can be expressed as wavelength λ ,

$$\lambda = \frac{c}{\nu} \text{ [m]} \quad (1-22)$$

or as wave number:

$$\tilde{\nu} = \frac{\nu}{c} \text{ [m}^{-1}\text{]} \quad (1-23)$$

Absorption at optical wavelengths is due to rotational, rotational-vibrational and electronic transitions. Electronic transitions usually include rotational and vibrational interaction.

1.6.1 Rotational transitions

On a rigid diatomic molecule the rotational changes can be discussed: A linear molecule, as shown in Figure 1.3, consists of two single atoms with the masses m_1 and m_2 and a rigid bond of the length r_0 . The molecule rotates around the axis ω , which is intersecting point C, the center of gravity, which is defined by the moment:

$$m_1 \cdot r_1 = m_2 \cdot r_2 \text{ with } r_0 = r_1 + r_2 \quad (1-24)$$

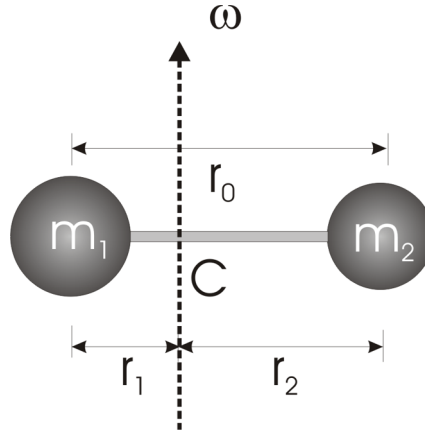


Figure 1.3: A Diatomic molecule treated as two masses, joined by a rigid bar.

The inertia of the system, I, can be described as:

$$I = \frac{m_1 \cdot m_2}{m_1 + m_2} \cdot r_0^2 = \mu \cdot r_0^2 \quad (1-25)$$

with μ describing the reduced mass of the system. By the use of the Schrödinger equation it might be shown that the rotational energy levels allowed to the rigid atomic molecule are given by the expression:

$$E_J = \frac{h^2}{8 \cdot \pi^2 \cdot I} \cdot J(J + 1) [J] \text{ with } J = 0, 1, 2, \dots \quad (1-26)$$

In this expression h is the Planck's constant, and I is the inertia of the system. The quantity J is the rotational quantum number: As this value is not arbitrary, only certain discrete rotational energy levels are allowed in the molecule. Formula 1-26 represents the energy levels in Joules. However, for spectroscopy the wavenumbers or wavelengths of the energies are of interest. The following formula gives the energies in wavenumbers with the unit $[cm^{-1}]$:

$$\varepsilon_J = \frac{E_J}{h \cdot c} = \frac{h}{8 \cdot \pi^2 \cdot I \cdot c} \cdot J(J + 1) [cm^{-1}] \text{ with } J = 0, 1, 2, \dots \quad (1-27)$$

c represents the speed of light. Above equation can be simplified with the rotational constant B:

$$\varepsilon_J = B \cdot J(J + 1) \text{ with } B = \frac{h}{8 \cdot \pi^2 \cdot I \cdot c} [cm^{-1}] \text{ and } J = 0, 1, 2, \dots \quad (1-28)$$

1.6.2 Vibrational transitions

For the description of molecular stretching vibrations, the diatomic molecule can be converted into a harmonic oscillator, as shown in figure 1.4. The atoms are considered to be masses and the bonding force is considered as a spring. Furthermore one of the atoms is fixed and the displacement x , out of the equilibrium position r_{eq} of the second causes a force F on the mass:

$$F = -k \cdot x \quad (1-29)$$

The constant k represents the force constant of the system. The force is correlated with the potential energy of the molecule by $F = -dV/dx$. Due to this relationship the potential energy can be described as:

$$V = \frac{1}{2}kx^2 \quad (1-30)$$

For above formula, the energy curve equals a parabola.

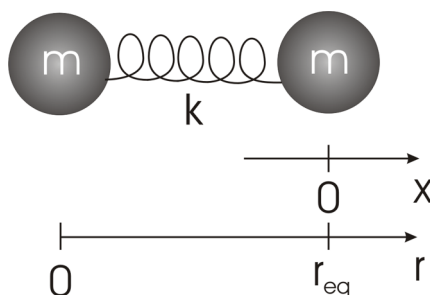


Figure 1.4: A diatomic atom as a harmonic oscillator

In this case, the angular oscillation frequency of the system can be calculated with:

$$\omega_{osc} = \frac{1}{2 \cdot \pi} \sqrt{\frac{k}{\mu}} \quad [Hz] \quad (1-31)$$

where μ is the reduced mass of the system. The oscillation frequency can also be represented in wavenumbers:

$$\tilde{\omega}_{osc} = \frac{1}{2 \cdot \pi \cdot c} \sqrt{\frac{k}{\mu}} \quad [cm^{-1}] \quad (1-32)$$

The vibrational energies of the system can be calculated from the Schrödinger equation:

$$E_v = \left(v + \frac{1}{2}\right) h \cdot \omega_{osc} [J] \text{ with } v = 0, 1, 2, \dots \quad (1-33)$$

where v is representing the vibrational quantum number. Converting this equation into spectroscopic units, we have:

$$\varepsilon_v = \frac{E_v}{h \cdot c} = \left(v + \frac{1}{2}\right) \tilde{\omega}_{osc} [cm^{-1}] \quad (1-34)$$

as the only energies allowed for this simple harmonic vibrator. The potential energy curve of the molecules is not homogenous as shown above with Hooke's law: If the bond between the atoms is stretched, there will be a point when breakage will occur. In cases of compressions there is a minimal radius to be obeyed between the atoms. The Morse function V_{Morse} describes a good approximation of this behaviour:

$$V_{Morse} = D_e [1 - \exp\{a(r_{eq.} - r)\}]^2 \quad (1-35)$$

The displacement x from the Hooke's law equation is exchanged by the difference of the molecules distance in equilibrium $r_{eq.}$ and the actual position r . Furthermore a dissociation energy D_e is given for the energy needed to separate the bond, when the internuclear distance increases. a is a constant for a particular molecule. For the calculation of the vibrational energy level the pattern of the allowed energy levels is found to be:

$$\varepsilon_v = \left(v + \frac{1}{2}\right) \bar{\omega} - \left(v + \frac{1}{2}\right)^2 \bar{\omega} \cdot x_e \text{ for } v = 0, 1, 2, \dots \quad (1-36)$$

where $\bar{\omega}$ is the oscillating frequency in wavenumbers, and x_e is the corresponding anharmonicity constant, which for bond stretching vibrations, is always small and positive, so that the vibrational levels crowd more together with increasing v . For the values of $0 \leq v \leq 6$ the Morse function has a good overlap to the energy functions in molecules. As equation 1-35 is an approximation,

the energy levels for higher ν require cubic and quadratic terms in $(\nu + \frac{1}{2})$ with additional anharmonicity constants:

$$\varepsilon_\nu = \left(\nu + \frac{1}{2}\right) \bar{\omega} - \left(\nu + \frac{1}{2}\right)^2 \bar{\omega} \cdot x_e + \left(\nu + \frac{1}{2}\right)^3 \bar{\omega} \cdot y_e + \dots \quad (1-37)$$

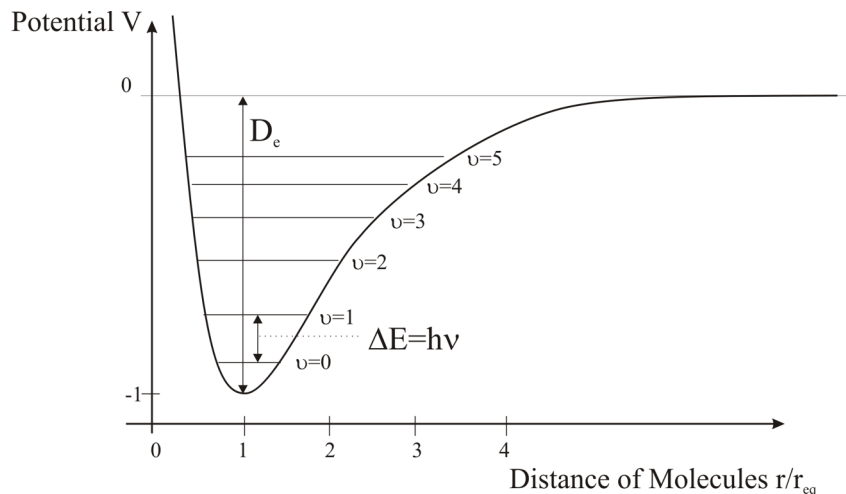


Figure 1.5: Energy levels in a vibrating diatomic atom

For comparison of the harmonic oscillator with the anharmonic oscillator equation 1-36 can be rewritten as:

$$\varepsilon_\nu = \bar{\omega}_e \cdot \left\{ 1 - x_e \left(\nu + \frac{1}{2} \right) \right\} \left(\nu + \frac{1}{2} \right) \quad (1-38)$$

Compared with equation 1-33 the oscillating frequency of the anharmonic oscillator, $\bar{\omega}_e$ can be written as:

$$\bar{\omega}_{osc.} = \bar{\omega}_e \left\{ 1 - x_e \left(\nu + \frac{1}{2} \right) \right\} \quad (1-39)$$

It is obvious, that the anharmonic oscillator behaves like the harmonic oscillator, but with an oscillating frequency which decreases steadily with increasing ν . For the ground state ($\nu = 0$) the both oscillation energies are the same.

1.6.3 Electronic states and electronic transitions

The structure of atoms is well known: A positively charged nucleus, contributing nearly all mass of the system, is surrounded by a number of negatively

charged electrons in sufficient number to balance the nuclear charge. In contrast to laws of classical mechanics the behaviour of electrons can be described by quantum theory, which was recognized by Bohr, firstly. He described the propagation of electrons on circular trajectories, representing certain quantized energies, around the nucleus. The energy difference between two orbits is dependent on the atom. While using classical mechanics on this model the electrons would have to irradiate light. Therefore, a modification was done: The electron is not considered to move in a trajectory, but in waves, described by wave functions, ψ . This function behaves like a mathematical function and contains the information necessary to describe positions of electrons around the nucleus (or nuclei in molecules). A propagation of one electron is possible without emitting energy, when a standing wave is formed, where the amplitude squared of the wave function $|\psi^2|$ is the probability density of the electrons position. Due to the bonding of different atoms into molecules an overlay of orbitals occurs and new orbitals are formed. In contrast to vibrational and rotational changes, the energies of electronic transitions can not be described in a simple analytical form. Therefore a more qualitative explanation of the effects will be given.

When an electronic transition takes place an electron changes the orbital from the ground into the excited state. After the transition, due to the changed force-field, the molecule might start to vibrate. The vibrational structure can be resolved in gaseous samples. In liquid and solid samples the lines merge together and result in a broad band. Superimposed on the vibrational transitions, which accompany the electronic transition of a molecule, is an additional branch structure that arises from rotational transitions. A principal overview on the energy levels present in a molecule is given in figure 1.6.

In addition, selection rules govern which transitions between allowed states of a molecule will be observed in its electronic spectrum. The interaction of electronic and vibrational transitions is described by the Franck-Condon-

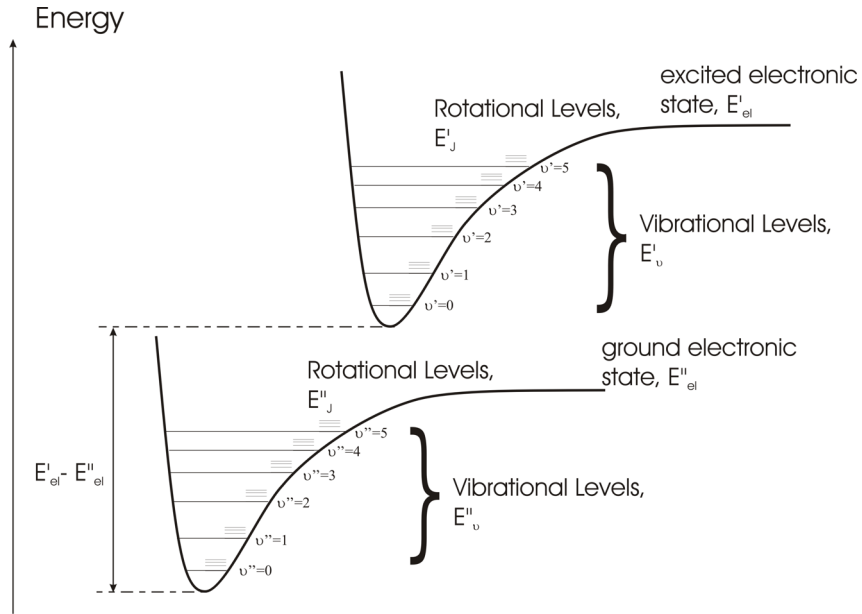


Figure 1.6: Overview on energy levels present in molecules

principle: Due to the higher mass of the nuclei compared to the electrons, the electronic transition takes place much faster, than the nuclei can respond. Due to the transition a different force field is influencing the nuclei. After the transition has taken place a changed force field within the molecule initiates and affects the vibrations of the molecule. For the selection of transition a transient dipole moment can be calculated:

$$\mu_{2,1} = -e \int \psi_2^* \cdot r \cdot \psi_1 d\tau \quad (1-40)$$

Where ψ_2 and ψ_1 are the combined electronic and vibrational wavefunctions of the system before and after the transition and r the distance of the electrons. The intensity of the transition is proportional to the squared transient dipole moment, $|\mu_{2,1}^2|$. Looking only at the vibrational wave functions, the overlapping integral can be calculated as:

$$S_{v'',v'} = \int \psi_{v''}^*(r) \cdot \psi_{v'}(r) d\tau \quad (1-41)$$

It is the overlapping integral of the vibrational wavefunctions of the system

before and after the transition. In this formula $\psi_{v''}$ describes the ground state and $\psi_{v'}$ the excited state. The squared overlapping integral $S_{v'',v'}$ is known as the Frank-Condon-Factor. It describes the relative excitation of the vibrational transition: With increasing overlap of the vibrational wavefunctions in the upper electronic state with the vibrational wavefunction in the lower electronic state, vibration is excited stronger. Figure 1.7 illustrates the overlap of the wavefunction $v = 0$ in the ground state and $v = 10$ in the excited state [Atkins, 1996].

To combine the different transitions, a formalism that is known as the Born-

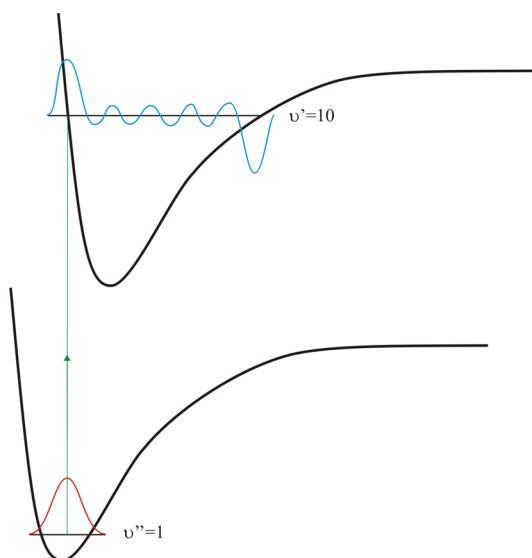


Figure 1.7: Overlap of wavefunctions of the ground state and the excited state

Oppenheimer approximation is used to describe the effects within molecules. Different effects causing absorptions are considered to be independent of each other. In this approximation the electronic transitions are independent of stretching and bending vibrations while the energies of the moving electrons are calculated.

$$E_{total} = E_{electronic} + E_{vibration} + E_{rotation} \quad (1-42)$$

Formula 1-42 shows the different energies present in molecules: Electronic,

vibrational and rotational energies. The change of the total energy, interesting for absorbant or emittant effects can be described as:

$$\Delta E_{total} = \Delta E_{electronic} + \Delta E_{vibration} + \Delta E_{rotation} [J] \quad (1-43)$$

or as wavenumbers:

$$\Delta \varepsilon_{total} = \Delta \varepsilon_{electronic} + \Delta \varepsilon_{vibration} + \Delta \varepsilon_{rotation} [cm^{-1}] \quad (1-44)$$

The orders of magnitude in these changes are, for diatomic molecules:

$$\Delta \varepsilon_{electronic} \approx \Delta \varepsilon_{vibration} \cdot 10^3 \approx \Delta \varepsilon_{rotation} \cdot 10^6 \quad (1-45)$$

Within this equation information on the structure of the absorption spectra is given: The rotational changes produce a "fine structure" and the vibrational changes a "coarse structure" on the spectra of electronic transition.

1.7 Structure of the thesis

A brief review on gas analysis is given in Chapter 1, mainly citing corresponding literature offering a review of the relevant aspects. Following that, a simple model, describing the light power flow within a fibre-optic sensor system is presented. Then, the measurement principle of the Bouguer-Lambert-Beer Law is described, discussing the range of absorbance measurements and possible deviations. The physical background and the basic aspects of absorption, caused by electronic, vibrational and rotational transitions are summarized, subsequently.

In Chapter 2, an overview on specialty fibres available for the transmission of light in the ultraviolet wavelength region is given. The optical characteristics of these fibre types are condensed. Furthermore, the transmission properties of all-silica fibres, including basic and UV-induced attenuation, have been analyzed in respect to their influence on absorption measurements.

Possible light sources for the use in the ultraviolet wavelength region are outlined in Chapter 3. This is followed by the discussion of the design criteria and the construction and development of a lamp system, consisting of a 30 W deuterium bulb and imaging optics, for the application in the deep ultraviolet wavelength range.

The physical background of wavelength separation is described in Chapter 4. Several available detection systems have been tested for the absorption measurements of gases, emphasizing the need for an extended wavelength range and adequate acceptance aperture for fibre-optic applications. A newly developed spectrophotometer has been characterized.

A variety of fibre-optic absorption cells are introduced in Chapter 5 and their applicability are discussed. For volume critical applications the volume is crucial points for successfully setting up a fibre-optic measurement cell. While the successful analysis of trace gases does not necessarily rely on the volume

of the absorption cell, this parameter strongly influences the sensitivity and time resolution of gas chromatographic detection system. In consideration of gas chromatic peak parameters, a model for identifying the optimum volume of the measurement cell is introduced.

Consequently, Chapter 6 reports on measurements with different detectors for GC effluent, using an existing measurement setup as a reference. The newly developed system has been characterized in terms of stability and linearity. Especially, the influence of the absorption cells volume and the performance of the system compared with a mass spectroscopy detector are descibed.

The potential for the applicability of a measurement system for trace gas analysis is discussed in Chapter 7. Applications within the environmental field and the health care sector are presented as case studies.

Conclusions and suggestions for further work are included, as are detailed reference lists following every chapter.

References

- P. Atkins. *Physical Chemistry (in German)*. VCH, Weinheim, 1996.
- C. N. Banwell and E. M. McCash. *Fundamentals of molecular spectroscopy*. McGraw-Hill Book Company, London, 1994.
- M. Belz. *Pollutant monitoring with fiber optic in the deep ultra violet*. PhD thesis, City University London, UK, 1998.
- R. Brown and J. Lennon. Factors affecting sensitivity in lightpipe gas chromatography fourier transform infrared interfaces. *Journal of Applied Spectroscopy*, 45, Number 4:667–672, 1991.
- R. S. Brown, J. R. Cooper, and C. L. Wilkins. Lightpipe temperature and other factors affecting signal in gas chromatography/fourier transform infrared spectrometry. *Anal. Chem.*, 57:2275–2279, 1985.
- R. Bunsen. *Gasometrische Methoden*. Vieweg, Braunschweig, 1857.
- H. Fabian, G. U., K.-H. Woerner, and K.-F. Klein. Optical fibre for UV-applications. In *Proc. SPIE 1513*, 168, 1991.
- G. Fetzer, A. Pittner, W. Ryder, and B. D.A. Tunable diode laser absorption spectroscopy in hollow core waveguides. *Appl. Opt.*, 41:3613–3621, 2002.
- G. Fetzer, A. Pittner, and P. Silkoff. Mid-infrared laser absorption spectroscopy in coiled hollow core waveguides. In *Proc. SPIE Int. Soc. 4957*, 124, 2003.
- G. Gauglitz. *Applied Spectroscopy (in german: Praktische Spektroskopie)*. Attempo Verlag, Tübingen, 1983.
- S. Geckeler. *Optical fibre transmission systems, in german*. Springer-Verlag, 1990.

- G. N. Giss and C. L. Wilkins. Effects of lightpipe dimensions on gas chromatography/ fourier transform infrared sensitivity. *Journal of Applied Spectroscopy*, 38, Number 1:17–20, 1984.
- W. Gottwald. *GC für Anwender*. VCH, Weinheim, 1995.
- P. R. Griffiths. Optimized sampling in the gas chromatography-infrared spectroscopy interface. *Journal of Applied Spectroscopy*, 31, Number 4:284–288, 1977.
- P. R. Griffiths and C. L. Wilkins. Quality criteria for digital infrared reference spectra. *Journal of Applied Spectroscopy*, 42, Number 4:538–545, 1988.
- A. Grunewald. Method and device for determining gas concentration in a gas mixture. Technical report, European Patent EP000001222454A1, German Patent DE000019949327A1, 1999.
- D. M. Haaland, E. V. Thomas, and D. S. Blair. Improvements in methods for spectral combination of gas chromatography/fourier transform infrared spectroscopic data. *Journal of Applied Spectroscopy*, 47, Number 10:1612–1619, 1993.
- E. J. Hasenoehrl, J. H. Perkins, and P. R. Griffiths. Rapid functional group characterization of gas chromatography/fourier transform infrared spectra by a principal components analysis based expert system. *Anal. Chem.*, 64: 705–710, 1992.
- J. Hogan. *Specialty Gas Analysis*. Wiley-VCH, New York, 1996.
- H. Jaffé and M. Orchin. *Theory and Applications of ultraviolet spectroscopy*. Wiley, New York, 1962.
- W. Kaye. Far-ultraviolet spectroscopic detection of gas chromatograph effluent. *Anal. Chem.*, 34:287–293, 1962.

- W. Kaye and F. Waska. A rapid-scan far ultraviolet spectrophotometer for monitoring gas chromatograph effluent. *Anal. Chem.*, 36:2380–2381, 1964.
- V. Khalilov, K.-F. Klein, and N. G. Low-OH all-silica fiber with broadband transparency and radiation resistance in the UV-region. In *Proc. SPIE 5317-09*, 2004.
- V. K. Khalilov, K.-F. Klein, J. Belmahdi, R. Timmerman, and G. Nelson. High-OH fibers with higher stability in the UV-region. In *Proc. SPIE 6083-08*, 2006.
- K.-F. Klein, P. Schliessmann, E. Smolka, G. Hillrichs, M. Belz, W. Boyle, and K. Grattan. UV-stabilized silica based fiber for applications around 200 nm wavelength. *Sensors and Actuators B*, 39:305–309, 1997.
- K.-F. Klein, R. Arndt, G. Hillrichs, M. Ruetting, M. Veidemanis, R. Dreiskemper, J. Clarkin, and G. Nelson. UV-fibers for applications below 200 nm. In *Proc. SPIE 4258-08*, 2001.
- D. Kleine, H. Dahnke, J. Lauterbach, P. Stry, P. Weber, M. Mürtz, W. Urban, P. Kleinermanns, and P. Hering. Trace gas analysis in the atmosphere with cavity ring-down spectroscopy. In *Proceedings of Workshop "Chemical Behavior of Aromatic Hydrocarbons in the Troposphere", 27.2. - 29.2.2000 in Valencia / Spain*, 2000.
- V. Lagesson. *Micro gas chromatographic separation combined with UV- and IR-spectrophotometric detection/identification with applications within the occupational hygiene field using diffusive and active sampling followed by a direct thermal desorption technique*. PhD thesis, University of Göteborg & University of Linköping, Sweden, 1992.
- G. Leippe, B. Lenzen, P. Spurk, W. Fabinski, M. Moede, H. Pongratz,

- W. Schindler, and W. Schiefer. Neues system zur Messung von Stickstoffkomponenten im Einsatz an SCR-Katalysatoren. *MTZ*, 65:392–399, 2004.
- M. J. D. Low and S. K. Freeman. Measurement of infrared spectra of gas-liquid chromatography fractions using multiple-scan interference spectrometry. *Anal. Chem.*, 39, No. 2:194–198, 1967.
- H. L. Mark and P. R. Griffiths. Analysis of noise in fourier transform infrared spectra. *Journal of Applied Spectroscopy*, 56, Number 2:633–639, 2002.
- A. Martin and R. Synge. A new form of chromatogram employing two liquid phases. *Biochemical Journal*, 35:1358–1368, 1941a.
- A. Martin and R. Synge. Separation of the higher monoamino-acids by counter-current liquid-liquid extraction: the amino-acid composition of wool. *Biochemical Journal*, 35:91–121, 1941b.
- Y. Matsuura and M. Miyagi. Aluminum-coated hollow glass fibers for ArF-excimer laser light fabricated by metallorganic chemical-vapor deposition. *Applied Optics*, 38:2458–2462, 1999.
- Y. Matsuura, T. Yamamoto, and M. Miyagi. Delivery of F2-excimer laser light by aluminum hollow fibers. *Optics Express*, 6:257, 2000.
- M. Miyagi, Y. Hiratani, T. Taniguchi, and N. s. Aluminum anodizing technique for fabricating optical thinfilm waveguides. *Applied Optics*, 26:970–971, 1987.
- P. Müller. *Development of an UV spectrometric detectors for gas chromatographic applications, in German: "Entwicklung eines UV-spektrometrischen Detektors für die Gaschromatographie"*. PhD thesis, University Würzburg, 1992.
- H. Perkampus. *UV-VIS Spectroscopy and its applications*. Springer, 1992a.

- H. Perkampus. *UV-VIS Atlas of organic compounds*. VCH, Weinheim, 1992b.
- H. Perkampus. *Ecyclopedia of spectroscopy*. VCH, Weinheim, 1995.
- P. Sandra. (chairman) 29th international symposium on capillary chromatography and 3rd GCxGC symposium. In *Conference, Riva del Garda, Italy*, 2006.
- C. Schatz. *Spectroscopic techniques and fiber optics in dissolution testing: increasing efficiency in pharmaceutical quality control*. PhD thesis, ETH Zurich, Switzerland, 2001.
- S. L. Smith, S. E. Garlock, and G. E. Adams. Industrial applications of a capillary gas chromatography/fourier transform infrared system. *Journal of Applied Spectroscopy*, 37, Number 2:192–196, 1983.
- L. Sommer. *Analytical Absorption Spectrophotometry in the Visible and Ultraviolet, the principles*. Elsevier, 1989.
- G. Stewart, W. Jin, and B. Culshaw. Prospects of fibre-optic evanescent field gas sensors using absorption in the near infrared. *Sensors and Actuators B*, 28-29:42–47, 1997.
- S. Svanberg. *Atomic and molecular spectroscopy*. Springer, Berlin, 3rd edition, 2001.
- Y. Talmi. Spectrophotometry and spectrofluorometry with the self-scanned photodiode array. *Applied Spectroscopy*, 36:1–18, 1982.
- M. S. Tswett. Physical chemistry studies on chlorophyll, the adsorptions (in german: Physikalische-chemische Studien über das Chlorophyll. Die Adsorptionen.). *Berichte der Deutschen Botanischen Gesellschaft*, 24:316–323, 1906a.

- M. S. Tswett. Adsorption analysis and chromatographic methods, application on the chemistry of chlorophyll, (in german: Adsorption Analyse und chromatographische Methode, Anwendung auf die Chemie des Chlorophylls). *Berichte der Deutschen Botanischen Gesellschaft*, 24:384–393, 1906b.
- F. Wang and K. Edwards. The separation of C2-naphthalenes by gas chromatography x fourier transform infrared spectroscopy (GCxFTIR): A two-dimensional separation approach. In *29th International Symposium on Capillary Chromatography, Riva del Garda, Italy, 2006*.
- J. White. Long optical paths of large aperture. *J. Opt. Soc. Am.*, 32:285, 1942.
- G. Wiegleb. UV-gassensor zum Nachweis von Stickoxiden. In *Forschungsforum Trafo, Düsseldorf, Germany, 2004*.
- U. Willer, C. Bohling, P. Geiser, and W. Schade. Infrared evanescent-field fiber sensor for in situ mapping of volcano gases. In *Second European Workshop on Optical Fibre Sensors, 2004*.
- P. Yang, E. Ethridge, J. Lane, and P. Griffiths. Optimization of GC/FTIR measurements I: Construction of light pipes. *Journal of Applied Spectroscopy*, 38, Number 6:813–816, 1984.
- P. W. J. Yang and P. Griffiths. Optimization of GC/FT-IR measurements II: Optical design. *Journal of Applied Spectroscopy*, 38, Number 6:816–821, 1984.
- Zeiss *Parallelspectrometer in german: "Simultanspektrometer" Productinformation of C. Zeiss, Oberkochen, Mai 1982*.

2 Fibre Optics

2.1 Introduction

The invention of the optical fibre by Kao in 1966 [Kao and Hockham, 1966] has initiated an improvement and development of a wide variety of fibres for different applications. Based on the principle of total internal reflection, light is confined inside the high refractive index core of the fibre, surrounded by a lower refractive index cladding. The difference in the refractive index can be produced by doping either the core or the cladding, when the fibre is produced from a single basis material. Commonly used base materials for ultraviolet, visible and near infrared wavelengths are fused silica, glass and polymers. Typical combinations for fused silica are an undoped core, and a fluorine doped cladding or an undoped cladding surrounding an germanium doped core. Depending on the application the number of modes carried within the fibre is of interest. For telecom applications a very low dispersion of the signal is desired to transport large bit rates. This can be achieved with the so-called single mode fibre, where the core diameter is smaller than $10\ \mu\text{m}$, allowing only one mode to be transported. Larger core diameters allow a high number of modes travelling through the fibre. Typically, the core diameter of multimodal fibres is between 50 and $200\ \mu\text{m}$, but can be bigger for special applications (e.g. spectroscopy for analytical applications). Fused silica based fibres usually provide a good light transportation with a very low attenuation over a wide spectral range, typically from $200\ \text{nm}$ to $2.4\ \mu\text{m}$ [Klein et al., 1998]. Alternatively, the combination of fused silica as a core material with a polymer cladding can be used, too. In addition to the lower price per meter, the main advantage of this design is the wider range of refractive indices provided in polymers, which allows a wide variety of numerical apertures. The Polymer cladded silica fibre (PCS), also named as hard clad silica fibre (HCS), is a good compromise for short haul data communications, for example in automobile technology

[Clarkin et al., 2005]. However, the wavelength range is limited from 350 to 900 nm, with typically higher attenuation compared to all-silica fibres. Furthermore, all-polymer fibres can be used as an alternative to HCS fibres in this wavelength range. They provide similar transmission properties, superior flexibility and can be very low cost. However, they have a lower temperature range of operation.

The refractive index change can alternatively be produced by producing air holes in a specific base material, surrounding the core to lower the refractive index seen by the light in the cladding region. So-called photonic crystal fibres (PCF), holey or micro structured fibres have been studied in detail within the scientific community and a wide area of applications have been described [Barton et al., 2004; Bjarklev et al., 2004; Issa, 2004; Klein et al., 2005; van Eijkelenborg et al., 2004; Wadsworth et al., 2004]. As the optical properties of the fibres are influenced mainly by the geometry and size of the holes, virtually every fibre type can be realized.

2.2 Fibre types available for UV-applications

Due to the variety of fibre types, a selection of the fibres depending on the application is required. Usually the applicability of some fibres are limited by their transmission or numerical aperture properties. For more detailed studies within this work two different types of fibres are available for applications in the ultraviolet wavelength region, below 300 nm: all-silica fibres for the transportation of ultraviolet light, which have been studied in detail to improve both their basic attenuation in the ultraviolet wavelength region, as well as their solarization behaviour since the 1990s. In addition, hollow core waveguides, originally designed for the transportation of high power ultraviolet laser light down to 157 nm, can be utilized in this wavelength range.

2.3 AS-UV-fibres

It was recognized early, that fused silica is the material of choice for the fibre based transportation of light in a wide wavelength range and especially in the ultraviolet wavelength region below 300 nm [Klein and Mühlich, 1988]. The transmission properties are defined by the basic attenuation of the fibre, that is mainly influenced by the purity of the material. Furthermore induced damages generated either by the transported UV-light below 250 nm, or by gamma irradiation influence the transmission behaviour. The reduction of the basic UV attenuation in optical fibres is paramount, when they are to be used in deep UV gas analysis applications. Ideally wavelength ranges as low as 175 to 180 nm should be transmitted in order to measure absorption of gases [Lagesson-Andrasko and Lagesson, 2005]. In addition, the characterization and selection of fibres in terms of their time-dependent behaviour ensure a stable measurement system for long term measurements.

2.3.1 Basic and UV-Induced attenuation

The total transmission in all-silica fibres below 300 nm is influenced by Fresnel losses $L_{fresnel}$, the transmission of the fibre core T_{fibre} , including Rayleigh-scattering proportional to λ^{-4} and UV induced losses $L_{defects}$ [Bates, 1976; Klein and Mühlich, 1988; Klein et al., 1997]:

$$T_{total} = (1 - L_{fresnel})^2 T_{fibre} \cdot (1 - L_{defects}) \quad (2-1)$$

The intensity change (dI) within a defect free fibre without UV-induced losses, can be described along its length (z direction) as follows:

$$-\frac{dI}{dz} = \alpha \cdot I + \beta \cdot I^2 \quad (2-2)$$

It is influenced by a linear attenuation coefficient $\alpha(\lambda)$ and a non-linear attenuation coefficient $\beta(\lambda)$. By integration, the internal transmission of the fibre

can be determined:

$$\frac{1}{T} = \frac{I_0}{I(l)} = \left(1 + I_0 \frac{\beta}{\alpha}\right) \exp(\alpha \cdot l) - \frac{I_0 \cdot \beta}{\alpha} \quad (2-3)$$

Where I_0 represents the input intensity and $I(l)$ the output intensity at the fibre length l . In the UV-wavelength region below 300 nm, the basic attenuation $\alpha(\lambda)$ is dependent on Rayleigh scattering and the tail of the intrinsic UV absorption band. In addition, the losses due to two photon absorption, described by the non-linear coefficient $\beta(\lambda)$ are intensity dependent. With increasing fibre length, decreasing wavelength and high light intensities (e.g. lasers), these effects dominate the transmission [Dressel et al., 1990; Taylor et al., 1988]. However, for applications with deuterium lamps such non-linear effects can be neglected.

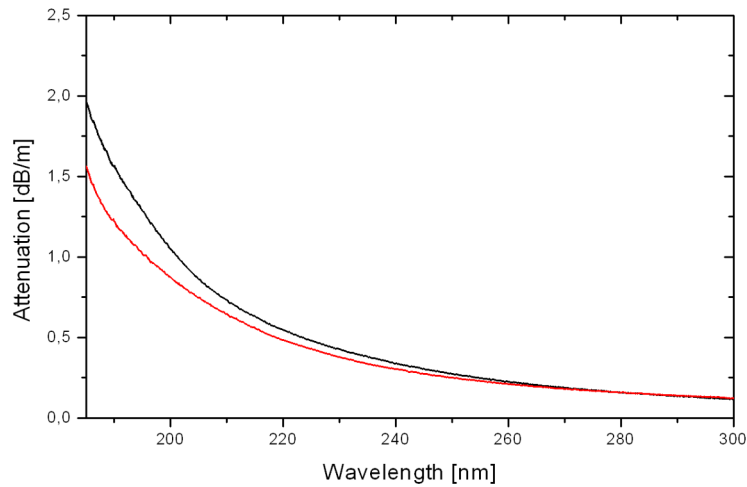


Figure 2.1: Variation in basic attenuation of an all-silica fibre

The second mechanism influencing the attenuation are the generation of defects by irradiating UV light or gamma rays, as described in [Friebele and Griscom, 1979; Griscom, 1984, 1985; Weeks, 1994; Weeks et al., 1992]. These defects influence the transmission properties at different wavelengths. A good overview

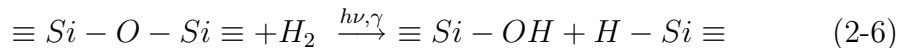
on defect centres in silica fibres can be found in literature [Hübner et al., 2000; Khalilov et al., 2004]. The dominant mechanism for the generation of defects in the fibre material is described below, dependent on gamma radiation γ , or UV irradiation $h\nu$:



In addition small chlorine content in the fibre leads to an additional defect:



In both cases E'-centres are generated, causing an additional or induced loss with a maximum at a wavelength of 215 nm. A smaller effect can be observed by the non-bridging oxygen hole-centres (NBOHC) ${}^\circ O - Si \equiv$ at 265 nm. The passivation of these main defects can be reached by hydrogen loading of the fibre, shown for 215 nm defects [Klein et al., 1998]:



The E'-center is passivated and the absorbing UV-defect is no longer present. In 2004 and 2006 [Khalilov et al., 2004, 2006] significant improvements on reducing fibre damage by UV-light have been reported for both, material with high-OH and low-OH content. The minimum basic spectral attenuation has been determined down to 180 nm with a corresponding value of 2.65 dB/m for standard fibres. Furthermore, the time depending dynamics of transient effects in the standard fibre material and R&D samples, which are available as a commercial product since two years, have been studied in detail.

2.3.2 Studies on basic attenuation and UV induced defects

The analysis of basic attenuation can be carried out analogue to the cut-back method, which is a standard method for the determination of attenuation in fibres [Marcuse, 1981]. Within this measurement, an intensity spectrum of the

long fibre is measured. Then the fibre is cut to a shorter length and a second spectrum is measured. The basic attenuation is determined according to the following equation:

$$\alpha(\lambda) = \frac{10}{\Delta l} \cdot \log_{10} \left(\frac{I_{short}(\lambda)}{I_{long}(\lambda)} \right) \text{ with } \Delta l = l_{long} - l_{short} \quad (2-7)$$

In contrast to other wavelength ranges, the measurement needs to be carried out in a nitrogen atmosphere to prevent measurement errors in the wavelength region below 198 nm, due to the absorption of ambient air and ozone generation [Kötschau et al., 2003], an absorption spectrum of oxygen is shown in figure 7.5. In addition, the time necessary for the measurement is critical, as solarization effects have to be taken into account.

Depending on the purity of the fibre preform and the fibre drawing parameter,

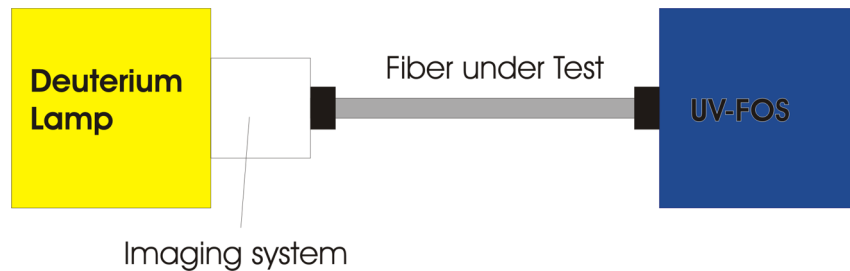


Figure 2.2: System for solarization measurements

variations in the basic attenuation can be observed, as exemplified in figure 2.1 for two different batches. Basic attenuations from 0.8 to 5 dB/m at 200 nm can be measured in different batches [Klein et al., 2001]. A typical measurement result of the spectral attenuation is shown in table 2-1.

Table 2-1: Spectral attenuation, measured with UVM fibres

Wavelength [nm]	180	185	190	195	200	210	220	230
Min. spectral attenuation [dB/m]	2.65	1.56	1.25	1.01	0.87	0.63	0.5	0.4

For the analysis of UV-induced effects in optical fibres a measurement system has been developed, as shown in figure 2.2. Within this system the light of a Deuterium lamp is coupled into a fibre under test with an imaging system, optimized for UV wavelengths below 250 nm [Klein et al., 1998]. The transmitted light is detected with a fibre optic spectrometer. For solarization measurements, the power distribution over wavelength range is critical in order to achieve repeatable measurements. To keep the measurements comparable, the input power at 214 nm is checked regularly with a bandpass filter and a photodiode. This wavelength is closest to maximum of the E'-centres at 215 nm. For these measurements a fibre length of 2 m has been selected as a standard length and the fibres are typically measured over a time frame of 4 hours.

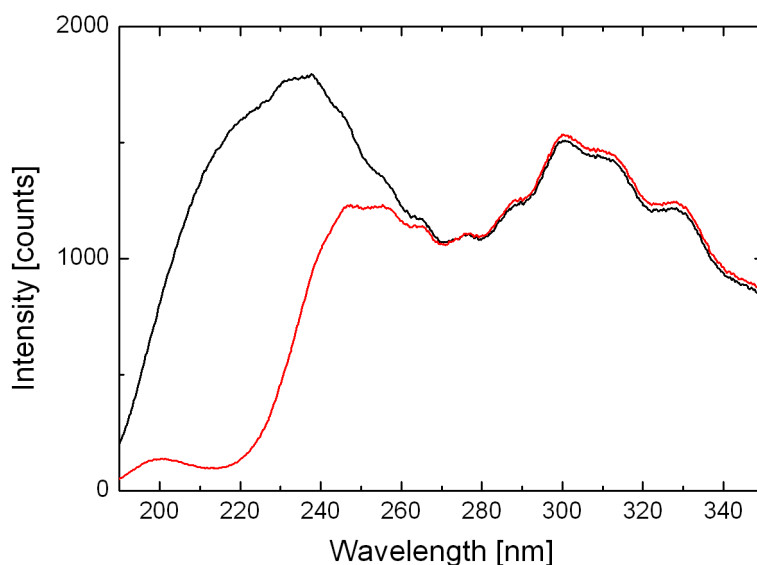


Figure 2.3: Measurement of induced attenuation in all-silica fibres, initial spectrum (black) and after UV-irradiation (red)

In figure 2.3, typical intensity spectra received from the measurements are shown. The initial spectrum shows the lamp spectrum transported through

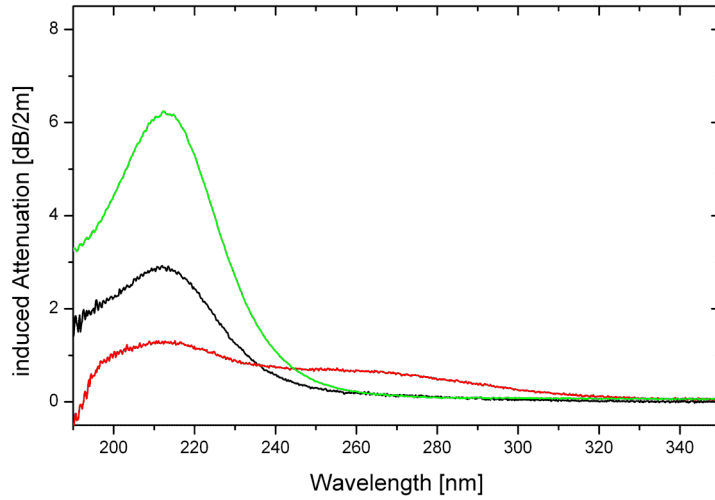


Figure 2.4: Variation of induced attenuation in all-silica fibres, standard type (black and green) and improved material (red)

the fibre, in the second spectrum UV damages cause a reduced signal in the wavelength region below 260 nm, after UV-irradiation. The resulting additional attenuation $\alpha_{UV}(\lambda)$ is usually calculated from the two spectra according to the following formula:

$$\alpha_{UV}(\lambda, t) = 10 \cdot \log_{10} \left(\frac{I_{initial}(\lambda)}{I_{damaged}(\lambda, t)} \right) \quad (2-8)$$

Where $I_{initial}(\lambda)$ represents the first spectrum measured at the beginning of the measurements $t = 0$ and $I_{damaged}(\lambda, t)$ represents the spectrum after the measurement time t . As the testing is carried out with fixed fibre lengths of typically 2 m, the UV-induced attenuation $\alpha_{UV}(\lambda)$ [dB/2m] will be used synonymous with the UV-induced loss $L_{UV}(\lambda)$ [dB]. For standard UV-fibres E⁺-centre concentrations are so strong that UV-induced loss is higher than 15 dB, measured with the standard fibre length of 2m. With improved preform material [Vydra and Schötz, 1999], fibres show a significantly reduced loss of approx. 5 dB/m. Using standard drawing conditions, the tolerances of

UV induced losses are shown in figure 2.4 (black and green curve). In addition a new type of improved material has been measured [Khalilov et al., 2006].

As an additional parameter, the time behaviour of the solarization can be analyzed. In the past transient defects have been studied only within hydrogen loaded fibres [Belz, 1998; Hübner et al., 2000], where the hydrogen caused the annealing of the induced defects, when the fibre was not illuminated. The time frames of recovery have been in the two hours range. However, this measurements showed, that the level of UV-damaging reaches a saturation level, if a sufficient long time is given. For more detailed measurements on the transient effects in unloaded fibres, a measurement program has been developed, which allowed to measure the dark annealing of the fibre. The test procedure is shown in figure 2.5. Defects are generated within the fibre over a time frame of approx. 4 hours of UV irradiation, where they reach a saturation level. After this fixed time, the shutter of the light source is closed mechanically and the fibre starts to recover. During the recovery, the shutter is periodically opened for a short time in order to gather information on the annealing of the defects. Typical recover times were between 16 and 24 hours in the tests carried out, but could be adjusted to the fibre type. After that, a second continuous UV irradiation follows over a period between 15 minutes and 2 hours. During the measurements, the dark signal of the detector was monitored as well.

Figure 2.6 shows the temporal behaviour of the transient defects in a $600\ \mu\text{m}$ fibre with a length of 2 m; a defect free fibre is inserted into the measurement setup and the first solarization process is observed between point 1 and 2, showing the generation of E'-centres at 215 nm wavelength. Then, the light is shuttered mechanically and the transient defects in the fibre recover between point 2 and 3 over 20 hours. The second degradation measurement starts at point 3, where the fibre is illuminated continuously again to monitor the degradation process.

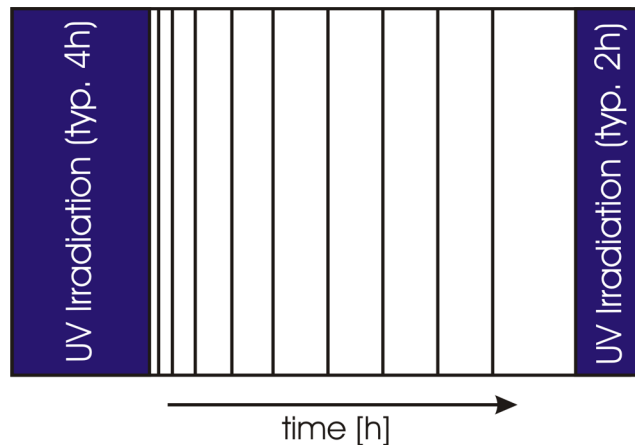


Figure 2.5: Measurement procedure for UV fibres, for determination of transient defects

After 4 hours, the additional loss was approx. 1.1 dB. During the annealing phase, a recovery of 0.1 dB could be determined. The additional loss, which starts at 14 hours can be attributed to the system drift. The drift was confirmed during the second run, when an increased loss of 0.25 dB was measured for the fibre.

The corresponding spectral gain and loss of these measurements are shown in figure 2.7. During the first 4 hours of irradiation, the generation of defects causes an additional loss within the fibre, which can be seen in the upper curve. Without UV-irradiation, the transient defects in the fibre recover, represented in a spectral "gain", when comparing the intensity spectra after the 4h UV damaging and the recovery (lower curve). After the recovery the UV-damage was repeated and the spectral loss due to the UV-damaging is shown in the middle curve. These UV-induced transient losses are slightly higher due to the system drift, which can be observed in figure 2.6.

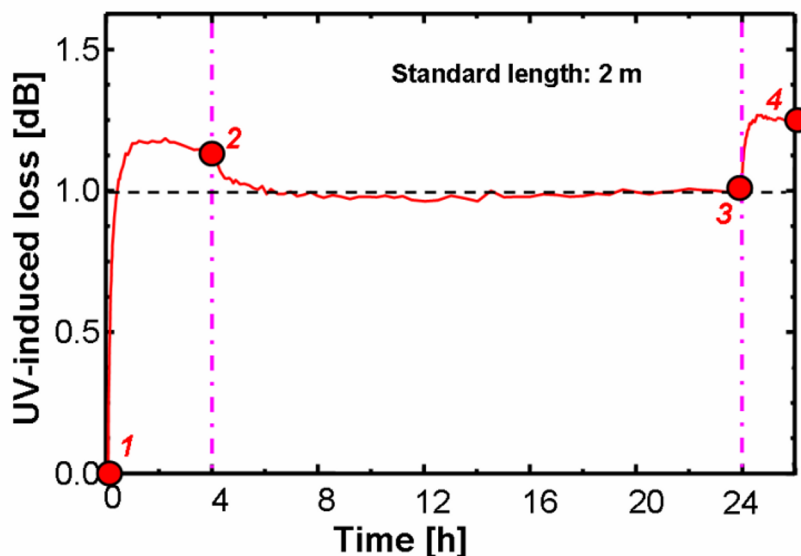


Figure 2.6: Time dependent of UV-damage and annealing at 215 nm, UV irradiation from 0 to 4 hours (first run) and from 24 to 26 hours (second run), no UV irradiation from 4 to 24 hours

2.3.3 Influence of UV induced loss on fibre optic measurements [Belz et al., 2008]

The application of fibres and their UV-induced damages influence strongly the measurement systems performance. It is clear, that the transient defects behaviour will be different to the time behaviour as shown in figure 2.6, as the lamp systems in analytical instruments are designed to give a well balanced spectrum of UV-light in order to successfully carry out the desired measurements. Due to this reason, the time for reaching a saturation level will be longer. According to the measurements shown above, the fibres additional loss, due to UV-damages, is a combination of permanent and transient defects:

$$L_{UV}(\lambda) = L_{UV,p}(\lambda, t, P_{in\,fibre}, l) + L_{UV,t}(\lambda, t, P_{in\,fibre}, l) \quad (2-9)$$

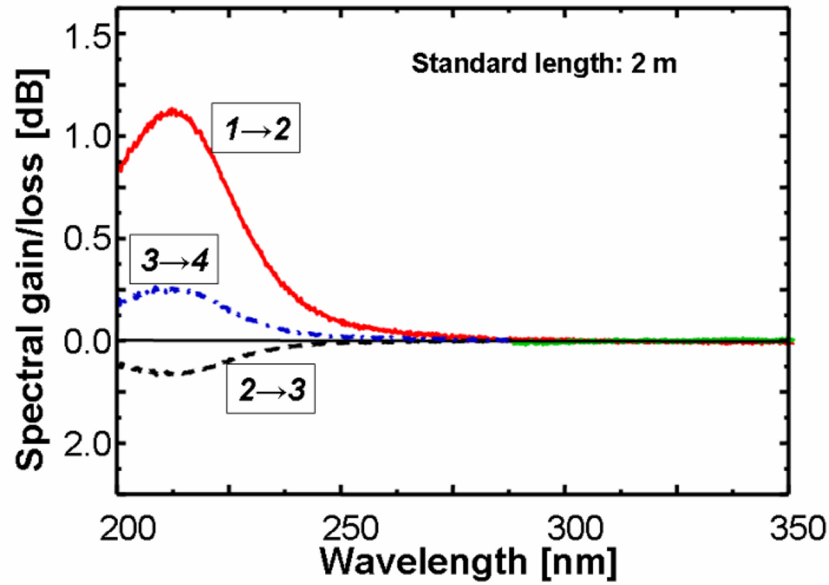


Figure 2.7: Spectral UV-damage and annealing of fibre with 2 m length. 4 hour damage during first run (upper curve), 2 h damage during second run (middle curve) and 20 hour annealing (lower curve)

These depend on the exposure time t , the wavelength λ , the input power $P_{in\,fibre}$ coupled into the fibre and the fibre length l . In addition, there is a position dependency of the UV-induced attenuation, taking the light power $P(Z)$ at a certain position Z into account.

According to formula 1-9, describing the absorbance value and 2-8, which is used for the calculation of the UV-induced loss, the UV-induced loss and the spectral absorbance can be linked:

$$L_{UV}(\lambda) [dB] = 10 A_i(\lambda) [AU] \quad (2-10)$$

Next a fibre optic detection system, consisting of a fibre-optic light source, a measurement cell and a spectrometer, as shown in figure 2.8 is evaluated. In this system, light is coupled into and out of the measurement cell via two

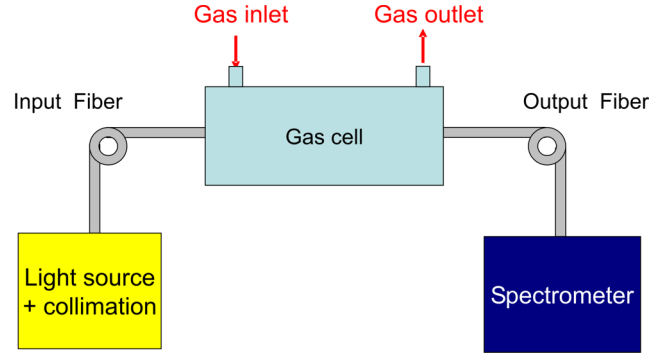


Figure 2.8: Fibre-optic based measurement system

optical fibres. Taking into account that drift of the light source and detector is negligible, the measured absorbance $A_{system}(\lambda)$ is dependent on the sample absorbance and the absorbance produced by the input and output fibre:

$$A_{system}(\lambda) = \frac{1}{10}L_{UV,IF}(\lambda, t, P_{in,IF}, L_{IF}) + A_{Sam}(\lambda) + \frac{1}{10}L_{UV,OF}(\lambda, t, P_{in,OF}, L_{OF}) \quad (2-11)$$

where L_{UV-IF} and L_{UV-OF} represent the total UV-induced loss of the input fibre and output fibre respectively, and $A_{Sample}(\lambda)$ is the sample absorbance. The variation in the absorbance $A_{system}(\lambda)$ of the system due to transient defects in the fibres may disturb the measurement signal. Therefore, the time difference, Δt , between measuring the reference and sample measurement will lead to the following formula for its variation during operation:

$$\Delta A_{system}(\lambda) = \frac{1}{10}A_{UV,IF}(\lambda, \Delta t, P_{in,IF}, L_{IF}) + \frac{1}{10}A_{UV,OF}(\lambda, \Delta t, P_{in,OF}, L_{OF}) \quad (2-12)$$

If the time difference between the measurements is short, these variations can be negligible, but for measurements over a longer time frame the UV-induced losses can be a significant part of measurement error.

2.4 UV-HCW

The flexible transportation of light to the point of interest is the main reason to use waveguides of many kinds. Based on an idea of Mercatili and Schmeltzer [Mercatili and Schmeltzer, 1964] to design a waveguide similar to microwave guides with a core of ambient air or gas surrounded by a metallic tube to transmit red laser light for telecommunications purposes, a waveguide for the transmission of Infrared laser light was designed [Miyagi and Nishida, 1980; Miyagi et al., 1983]. Based on a dielectric coating on the inner surface of a silica capillary, the transportation of CO₂ laser light at 10.6 μm and Er:YAG at 2.94 μm became feasible for high power as an alternative to costly chalcogenite and poly crystalline fibres. [Harrington, 1990; Nubling and Harrington, 1996]

Based on this principle a waveguide was proposed and developed for the transportation of ArF (193 nm) and KrF (248 nm) excimer laserlight [Matsuura et al., 2000; Miyagi et al., 1987]. In this technique a film of aluminium is deposited inside a silica capillary with metal organic chemical vapour deposition (MOCVD). The surface roughness of the aluminium film has a great influence on the transmission properties. As shown in [Matsuura and Miyagi, 1999] the deposition temperature of the aluminium has an influence on the surface roughness. Therefore, a pre-treatment with titanium chloride was used to sensitize the inner surface and lower the deposition temperature.

The structure of a hollow core waveguide for the transportation of UV light is shown in figure 2.9: An inner aluminium film is deposited on the inside of a fused silica capillary with an protection buffer of polyimide or UV acrylate. Usually the aluminium film has a thickness between 50 to 500 nm. The aluminium thickness influences the roughness on the inner surface, for a big inner layer. On the other hand, a transmission might occur through the thin aluminium layer. The core is a hollow bore filled with ambient air; alternatively

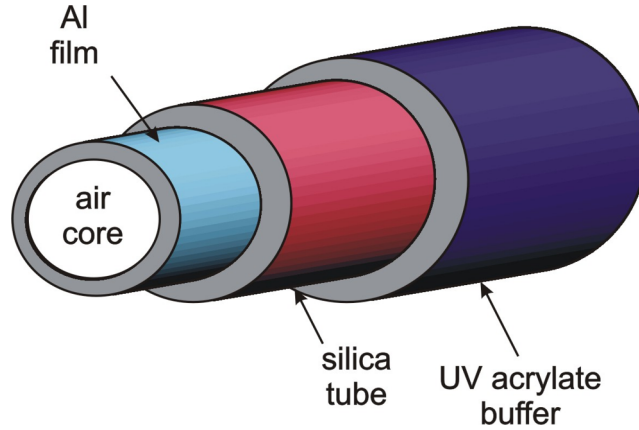


Figure 2.9: Structure of a hollow core waveguide

the bore can be filled with any chosen gas or evacuated.

In contrast to classical fibres the light guidance within the hollow core waveguide is not based on total internal reflection, but by reflection on the inner surface. The degree of reflection R_x can be computed by following equations for perpendicular or parallel polarized light wave incident on a mirror plane:

$$R_p = \frac{\sin(\epsilon) - \sqrt{\left(\frac{n_1}{n_2}\right)^2 - \cos^2 \epsilon}}{\sin(\epsilon) + \sqrt{\left(\frac{n_1}{n_2}\right)^2 - \cos^2 \epsilon}} \quad (2-13)$$

$$R_h = \frac{\left(\frac{n_1}{n_2}\right)^2 \cdot \sin(\epsilon) - \sqrt{\left(\frac{n_1}{n_2}\right)^2 - \cos^2 \epsilon}}{\left(\frac{n_1}{n_2}\right)^2 \cdot \sin(\epsilon) + \sqrt{\left(\frac{n_1}{n_2}\right)^2 - \cos^2 \epsilon}} \quad (2-14)$$

In above formula n_1 represents the refractive index of aluminium and n_2 the refractive index of air. ϵ is the angle between the mirror surface and the incident light ray. Figure 2.10 illustrates the reflection of a light beam on an aluminium wall. For unpolarized light the arithmetic mean value can be used for estimation of the reflectivity. In the UV region the reflectivity of aluminium is superior to other metallic materials. However, the reflectivity decreases with increasing wavelength.

Considering the reflection properties of aluminium a relation between the

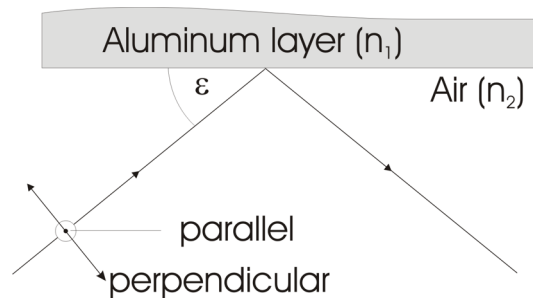


Figure 2.10: Reflection on a wall of aluminium

light's incident angle, the length of the waveguide and even bending of the guide is obvious, because these parameter cause an increasing number of reflections on the inner surface. Due to these influences, the waveguide has a numerical aperture, decreasing with increasing length. In addition to attenuation, depending on the fibre length, an additional bending loss occurs.

2.4.1 Optical properties of hollow core waveguides

During previous work [Kötschau, 2002], the optical properties have been investigated. In figure 2.11 the spectral loss of the UV-HCWs manufactured at Tohoku University is shown. In the case of the UV-HCW, the congruity between the measured and theoretical values are excellent, under the assumption of a certain surface roughness of the Al-layer [Matsuura and Miyagi, 1999; Matsuura et al., 2000]. For straight waveguides, values in the order of approx. 1 dB/m are possible, also in the region below 180 nm; however, the atmosphere in the inner bore has to be exchanged to inert gases in order to reduce the absorption due to ambient oxygen significantly. Furthermore, the additional loss L is influenced significantly by the bending radius R or the curvature $C = 1/R$ [Matsuura et al., 1995]:

$$L \propto 1/R \quad (2-15)$$

$$L \propto C \quad (2-16)$$

There is a linear relationship between losses and curvature, as shown in several papers [Harrington, 2000, 1990; Matsuura et al., 1995; Miyagi and Karasawa, 1990]. Starting with a straight hollow-core waveguide ($C=0$), the additional and total loss is increasing significantly. For large bending radii the additional loss due to bending is negligible [Kötschau et al., 2003].

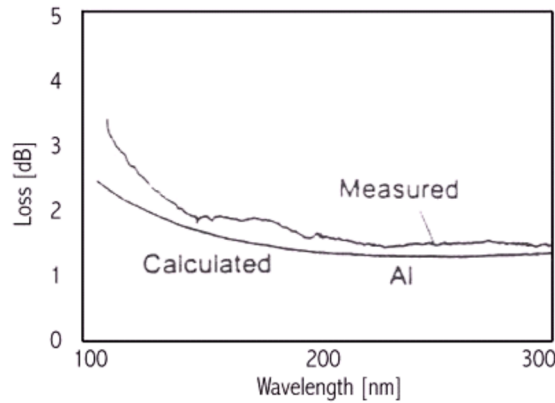


Figure 2.11: Spectral attenuation of a hollow core waveguide

For the efficient use of any waveguide type the coupling efficiency is important, which is related to the maximum acceptance angle Θ_{max} or the numerical aperture NA:

$$NA = \sin(\Theta_{max}) \quad (2-17)$$

For the UV-HCW, this parameter was measured using a modified inverse farfield method [Mohr et al., 2000] with a deuterium-UV-lamp. The measurement principle is illustrated in figure 2.12. A light beam with a numerical aperture significantly smaller than the numerical aperture of the fibre under test is launched into the fibre. The focal point of the light beam is positioned in the center of the fibre endface. The intensity signal is measured at the output end of the fibre. Figure 2.13 shows the measured intensity-profile as a function of the input angle Θ ; the input surface of the HCW was moved

on the axis of rotation. It is obvious, that the 50%-acceptance angle $\Theta_{50\%}$ (equal to Θ_{max} , for the calculation of the NA) is decreasing with increasing length (Figure 2.14), because the light propagating at higher angles will be attenuated more strongly (lower reflectivity and more reflections per unit of length). However, the wavelength-dependence is nearly negligible between 200 and 300 nm.

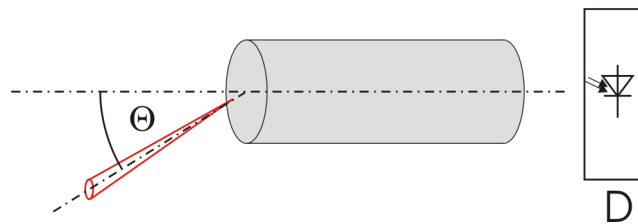


Figure 2.12: Measurement of the numerical aperture by the inverse farfield method

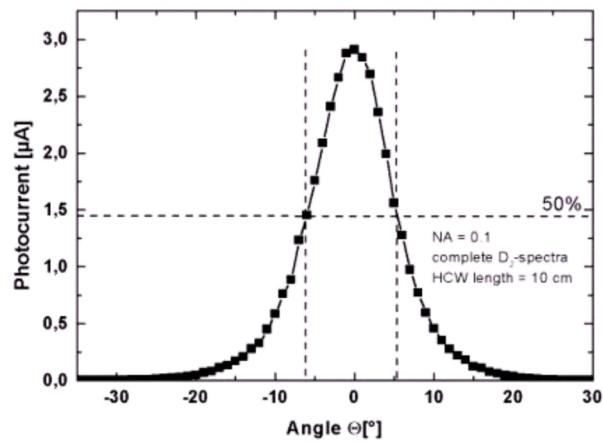


Figure 2.13: Numerical Aperture of a hollow core waveguide [Kötschau, 2002]

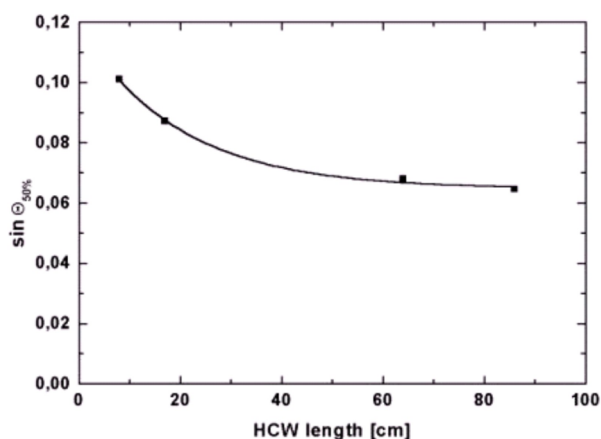


Figure 2.14: Length dependence of numerical aperture [Kötschau, 2002]

2.5 Summary and discussion

Two fibre types are available for the transportation of light in the wavelength region below 250 nm and can be used for fibre-optic based sensor systems. For the measurement of gas spectra, all-silica fibres have to be selected due to their basic attenuation and their UV-induced losses. Principal measurements for the analysis of permanent and transient losses have been carried out. A methodology describing the fibres behaviour and influence on the measured absorbance value has been found in literature. As fibre length has a direct influence on the transmission properties and on the UV-induced losses (with their transient behaviour) a short fibre has to be used for the desired application. As fibre manufacturers often provide typical data on the basic attenuation and on the UV-induced attenuation measurement and preselection is necessary for successfully using fibres in the deep ultraviolet wavelength region.

In terms of its transmission properties hollow core waveguides are superior compared to all-silica fibres, if the core is filled with an inert gas and the waveguide is straight. However, the bending losses and, due to its significantly smaller numerical aperture, the coupling of all-silica fibres to the hollow core

waveguides were identified as potential bottlenecks. As the transmission properties of the hollow core waveguide are influenced directly by the interaction of gas and light within the core, it can be used as an intrinsic sensor.

The characteristics of both waveguides have to be matched for successfully setting up a measurement system for the absorption measurement of gases in the deep ultraviolet wavelength region.

References

- G. Barton, M. van Eijkelenborg, G. Henry, M. Large, and J. Zagari. Fabrication of microstructured polymer optical fibres. *Optical Fiber Technology*, 10 (4): pp 325–335, 2004.
- C. Bates. Temperature dependence on the absorption edge of vitreous silica. *Applied Optics*, 15:2976–2978, 1976.
- M. Belz. *Pollutant monitoring with fiber optic in the deep ultra violet*. PhD thesis, City Uiniversity London, UK, 1998.
- M. Belz, H. Eckhardt, C. Gonschior, G. Nelson, and K.-F. Klein. Quality control of UV-resistant fibers for 200-300 nm spectroscopic applications. *Proc. SPIE.*, 6852-33, 2008.
- A. Bjarklev, J. Jensen, J. Riishede, J. Broeng, J. Laegsgaard, T. Larsen, T. Sorensen, K. Hougaard, and O. Bang. Photonic crystal structures in sensing technology *Proc. SPIE*, 5502:9–16, 2004.
- J. Clarkin, R. Timmerman, S. G.W., and K.-F. Klein. PCS optical fibers for an automobile data bus. *Proc. SPIE 5663*, 122, 2005.
- M. Dressel, W. Neu, and H. Gerhard. All silica fibers for the transmission of high power excimer laser pulses (in german: Quarzglasfasern für die Übertragung von Excimerlaserpulsen hoher Leistung). *Laser und Optoelektronik*, 22:76–91, 1990.
- E. Friebele and D. Griscom. *Treatise on material science and technology*. Academic Press, New York, 1979.
- D. Griscom. Thermal bleaching of X-ray-induced defect centers in high-purity fused silica by diffusion of radiolytic molecular hydrogen. *Journal of Non-Crystalline Solids*, 68:301–325, 1984.

- D. Griscom. Defect structures of glasses. *J.Non-Cryst. Solids.*, 73:51–78, 1985.
- Harrington. *Infrared fiber optics*. OSA Handbook, Vol. III, McGrawHill, New York, 2000.
- J. A. Harrington. *Selected Papers on Infrared Fiber Optics*. SPIE Press, Bellingham, 1990.
- M. Hübner, H. Meyer, K.-F. Klein, G. Hillrichs, M. Rütting, M. Veidemanis, B. Spangenberg, J. Clarkin, and G. Nelson. Fiber-optic systems in the UV-region. *SPIE-Proc. BiOS 2000*, 3911:42–49, 2000.
- N. A. Issa. High numerical aperture in multimode microstructured optical fibers. *Applied Optics*, 43 (33):pp. 6191–6197, 2004.
- C. Kao and G. Hockham. Dielectric fibre surface waveguides at optical frequencies. *Proc.IEE*, 113:1151–1158, 1966.
- V. Khalilov, K.-F. Klein, and N. G. Low-OH all-silica fiber with broadband transparency and radiation resistance in the UV-region. In *Proc. SPIE 5317-09*, 2004.
- V. K. Khalilov, K.-F. Klein, J. Belmahdi, R. Timmerman, and G. Nelson. High-OH fibers with higher stability in the UV-region. In *Proc. SPIE 6083-08*, 2006.
- K.-F. Klein and A. Mühlich. Quarzglas für unterschiedliche Anwendungen im Bereich von $0.2\ \mu\text{m}$ bis $2.4\ \mu\text{m}$. *VDI Bericht, Karlsruhe*, 673:147–177, 1988.
- K.-F. Klein, G. Hillrichs, P. Karlitschek, and K. Mann. Possibilities and limitations of optical fibers for the transmission of excimer laser radiation. *Proc. SPIE*, 2966:564–573, 1997.

- K.-F. Klein, S. Hüttel, R. Kaminsky, J. Kirchhoff, S. Grimm, and G. Nelson. Stability and life-time improvements of UV-fibers for new applications. *Proc. SPIE*, 3262:150–160, 1998.
- K.-F. Klein, R. Arndt, G. Hillrichs, M. Ruetting, M. Veidemanis, R. Dreiskemper, J. Clarkin, and G. Nelson. UV-fibers for applications below 200 nm. In *Proc. SPIE 4258-08*, 2001.
- K.-F. Klein, H. Eckhardt, C. Vincze, S. Grimm, J. Kirchhof, J. Kobelke, J. Clarkin, and G. Nelson. High NA-fibers: Silica-based fibers for new applications. *Proc. SPIE*, 5691:pp. 30–42, 2005.
- R. Kötschau. *Characterization of UV-Hollow Core Waveguides for the application in spectroscopy of gases, in german*. Diploma thesis, University of Applied Sciences Giessen-Friedberg, Germany, 2002.
- R. Kötschau, H. Eckhardt, K.-F. Klein, K. Behler, and G. Hillrichs. Gas-analysis in the UV-region using a long-length hollow core waveguide. *Proc. SPIE Int. Soc. Opt. Eng. 4957, 134 (2003)*, 4975:134–141, 2003.
- L. Lagesson-Andrasko and V. Lagesson. *Handbook of Ultraviolet Spectra, Vapor Phase, 168 - 330 nm*. 2005.
- D. Marcuse. *Principles of optical fiber measurements*. Academic press, 1981.
- Y. Matsuura and M. Miyagi. Aluminum-coated hollow glass fibers for ArF-excimer laser light fabricated by metallorganic chemical-vapor deposition. *Applied Optics*, 38:2458–2462, 1999.
- Y. Matsuura, T. Abel, and J. Harrington. Optical properties of small-bore hollow glass waveguides. *Applied Optics*, 34:6842–6847, 1995.
- Y. Matsuura, T. Yamamoto, and M. Miyagi. Delivery of F2-excimer laser light by aluminum hollow fibers. *Optics Express*, 6:257, 2000.

- E. Mercatili and R. Schmeltzer. Hollow metallic and dielectric waveguides for long distance optical transmissions and lasers. *Bell Syst. Tech. J.*, 43: 1783–1809, 1964.
- M. Miyagi and S. Karasawa. Waveguide losses in sharply bent circular hollow waveguides. *Applied optics*, 29:367–370, 1990.
- M. Miyagi and S. Nishida. A proposal for a low-loss leaky waveguide for sub-millimeter waves transmission. *IEEE transactions of microwave theory and techniques*, MTT-28:398–401, 1980.
- M. Miyagi, A. Hongo, Y. Aizawa, and S. Kawakami. Fabrication of germanium-coated nickel hollow core waveguides for infrared transmission. *Appl. Phys. Lett.*, 5:pp. 430–432, 1983.
- M. Miyagi, Y. Hiratani, T. Taniguchi, and N. s. Aluminum anodizing technique for fabricating optical thinfilm waveguides. *Applied Optics*, 26:970–971, 1987.
- R. Mohr, F. Petri, R. Link, K.-F. Klein, H. Poisel, M. Loch, and U. Greiner. Measurement systems for nearfield- and farfield-profiles of POFs. In *Proc. POF'2000*, pp. 195-199, Boston, 2000.
- R. Nubling and J. Harrington. Hollow waveguide delivery systems for high-power, industrial CO₂ lasers. *Applied Optics*, 34:372–380, 1996.
- R. Taylor, K. Leopold, R. Brimacombe, and S. Mihailov. Dependence of the damage and transmission properties of fused silica fibers on excimer laser wavelength. *Applied Optics*, 27:3124–3134, 1988.
- M. van Eijkelenborg, A. Argyros, A. Bachmann, G. Barton, M. Large, G. Henry, N. Issa, K. Klein, H. Poisel, W. Pokl, L. Poladian, S. Manos, and J. Zagari. Bandwidth and loss measurements of graded-index microstructured polymer optical fibre. *Electronics Letters*, 40 (10):pp. 592–3, 2004.

References

- J. Vydra and G. Schötz. Improved all-silica fibers for deep UV-applications. *SPIE-Proc. BiOS*, 3596, 1999.
- W. Wadsworth, R. Percival, G. Bouwmans, J. Knight, T. Birks, T. Hedley, and P. Russell. Very high numerical aperture fibers. *IEEE Photonics Technology Letters*, 16:843–845, 2004.
- R. Weeks. The many varieties of E'-centers: a review. *J. Non-Cryst. Solids*, 179:1–9, 1994.
- R. Weeks, P. Magruder, and P. Wange. Some effects of 5eV photons on defects in SiO₂. *J. Non-Cryst. Solids*, 149:122–136, 1992.

3 Lamp System

3.1 Abstract

The choice of the light source has an influence on the performance of the entire measurement system. The light intensity provided over the spectral wavelength range, the imaging optics attached for coupling the light efficiency into subsequent components and the noise and drift behaviour have to be considered. Within this chapter the described properties of the lamp system will be discussed.

3.2 Introduction

For spectrophotometric measurement systems in the ultraviolet wavelength region a variety of light sources can be used: Based on the required wavelength range and spectral intensities, xenon discharge lamps and xenon flash lamps, either with or without mercury are an option. However, in analytical instrumentation high stability of the light source is required. Spectral and stability properties, in terms of drift and noise of two types of deuterium lamps, will be discussed in this section.

Deuterium lamps are radiations sources, optimized for the use in dispersive spectrometers and spectrophotometers. The lamp consists of a bulb of fused silica, which is filled with Deuterium under a low pressure. After heating the anode made of a tungsten helix, the discharge is ignited with a stabilized current between the anode and cathode [Perkampus, 1995]. To obtain higher radiation intensity, an aperture with a diameter between 0.3 and 1 mm between anode and cathode restrict the discharge to the area of the aperture. This type of light source offers a continuous spectrum between 160 and 400nm. The emission spectrum might be limited by the transmission properties of the bulb material at lower wavelengths.

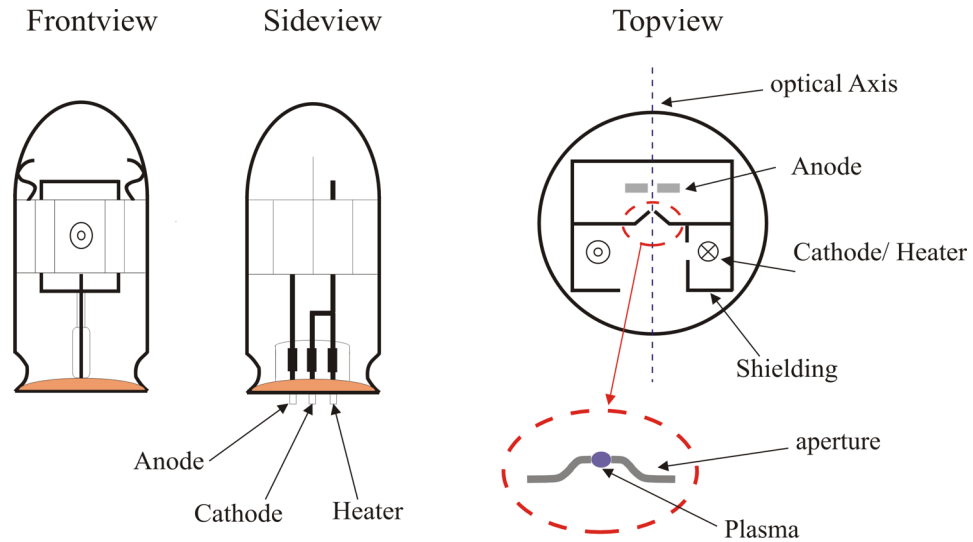


Figure 3.1: Setup of standard deuterium lamps

A further development was a miniaturized deuterium lamp, where the discharge is stimulated by an alternating voltage of high frequency between anode and cathode. The size and power consumption of the lamp is reduced significantly reducing the output light power. However, the stability of the source is suitable for analytic measurements in mobile applications.

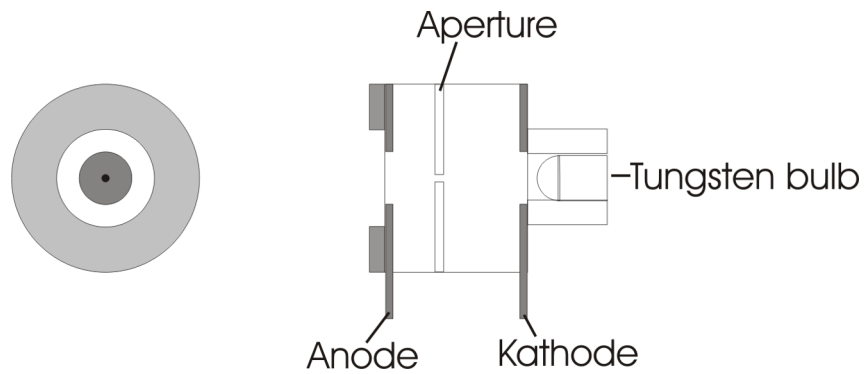


Figure 3.2: Fiberlight setup without fibre coupler

3.3 Influence of coupling optics

The successful use of the different light sources rely on the imaging optics used for the incoupling into the fibre-optics, or other measurement light paths. The spectral behaviour of a light source coupled into a fibre is strongly influenced by the material of the lamp bulb or window used. Additionally, the optical imaging of the deuterium plasma onto the endface of the waveguide has a major influence on coupling efficiency and transmitted spectrum. The following formula describes the relation between the size of the origin G and image B as a function of the distance g between the center plane of the lens and the origin and the distance b to the image on the other side:

$$V = \frac{B}{G} = \frac{b}{g} \quad (3-1)$$

In this formula the desired magnification or reduction can be selected, using:

$$\frac{1}{f} = \frac{1}{g} + \frac{1}{b} \quad (3-2)$$

f describes the focal length of the lens. The dependency is shown in figure 3.3 For a given distance between the origin and the center plane of the lens,

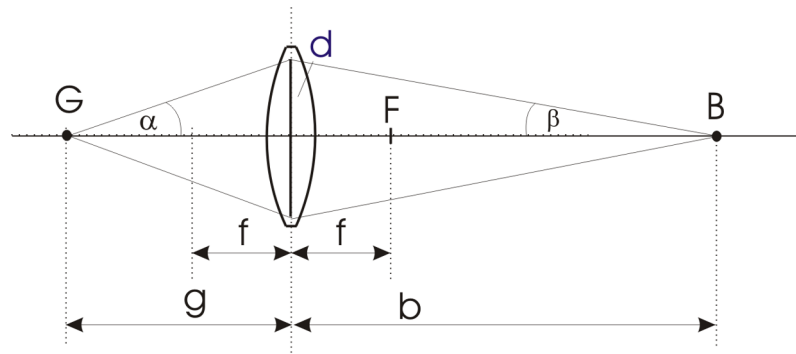


Figure 3.3: The optical projection

g, and the distance between the projection and the lens, b, are a function of the focal length of the lens. Furthermore, some additional information are

available with the usage of trigonometric functions: As a result the used area of the lens, the Numerical Aperture represented as the resulting angles $\alpha = \arcsin(\text{NA})$, and β representing the incident angle towards the fibre can be computed. The diameter $d = 2 \cdot g \cdot \tan(\alpha)$ on the lens is a result of the distance g . This information is evident for the approximation of the incident light on the fibre:

$$\beta = \arctan(d/(2 \cdot b)) \quad (3-3)$$

β is a result of the light radius $d/2$ on the lens $d/2$ and the distance b between the fibre and the center plane of the lens.

As the refractive index changes over the wavelength, the focal length varies

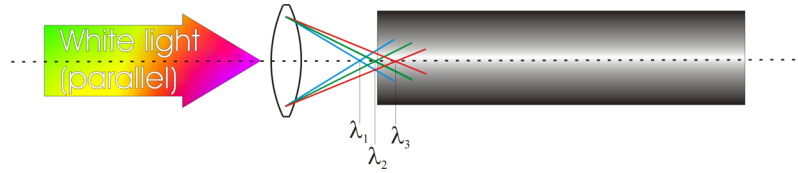


Figure 3.4: Illustration of the Chromatic aberration

in optical systems. This phenomenon can be observed in the UV/VIS and NIR Region using lenses at multiple wavelengths. As in figure 3.4 shown the light with the shorter wavelength (e.g. blue or λ_1) has a minor focal length compared to the longer wavelength (e.g. red λ_3), however, the light has a larger angle of incidence on the fibre endface. In the application the spectral intensity varies over wavelength, depending on the position of the fibre [Belz, 1998]. An achromatic lens, which compensates the wavelength aberration by the use of different base materials, can be used as an alternative. However, for the UV wavelength region no achromatic lenses are available off-the-shelf. As achromatic lenses consist of a doublet or triplet of lenses, the reflection losses can be higher, due to the increased number of interfaces. Alternatively, focussing mirrors might be used. As the transmission of the optical components

and the sensitivity of the detection system decreases strongly with lower wavelength, the fraction of light with lower wavelengths coupled into the incoupling fibre needed to be increased. In addition, the influence of the incoupling numerical aperture on the transmission properties of the hollow core waveguide [Kötschau, 2002] is of high importance. As an optimum, a 1:2 image of the deuterium plasma on the fibre endface, with a resulting diameter of 1 mm and an incoupling numerical aperture of 0.09 was found.

3.4 Nitrogen purge for lamp housing

In order to realize a lamp system which can be used at wavelengths below 200nm, where the absorption of oxygen strongly increases, the entire lamp system needs to be nitrogen purged. With this measure, the generation of Ozone, induced by the high energetic UV light, can be omitted, allowing analytical applications with minimum wavelengths as low as 200nm. In addition, avoiding ozone generation minimizes lamp noise. The volume of the light housing and the attached imaging optics must be minimized to reduce the time for flushing residual oxygen and water vapour out of the cavity. The path of the gas purge was designed to reduce flow rate needed for keeping other gases out of the system. In figure 3.5 the lamp housing and the attached imaging optics are shown.

3.5 Experimental determination of lamp stability

The stability of the lamp for the spectral measurement is of vital interest for spectrophotometric use. Therefore a standard practise for measuring the stability of a system has been introduced [ASTM, 1993]. This measurement method describes the measurement procedure for a whole photometric system. During the progression of this work, measurements have been carried out to select lamps according to their stability. The points of interest for a light

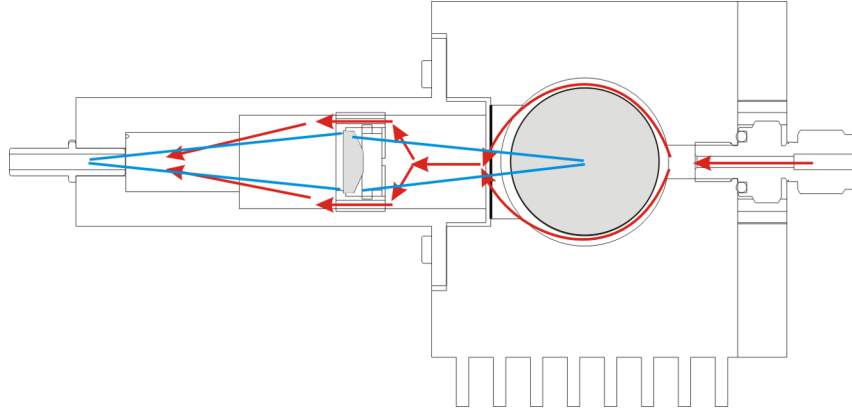


Figure 3.5: Lamphousing and attached imaging optics, illustrated gas flow (red) and light path (blue)

source are the noise, both measured over long and short time, as well as the drifts occurring in the system.

As the stability of the measurement device itself influences the measurement results, the detector choice has a major influence. The detector system should offer a high stability and a low noise level. Therefore, a low noise silicon detector with a band pass filter, or a fibre-optic spectrometer, with superior stability has to be selected. The spectrometer acquires as much spectra as possible within the measurement time. The absorbance is calculated at many points with following formula:

$$A(\lambda, t) = \log \left(\frac{I_{ref}(\lambda) - I_{dark}(\lambda)}{I_{sam}(\lambda, t) - I_{dark}(\lambda)} \right) \quad (3-4)$$

where $I_{ref}(\lambda)$ is the first spectra acquired, $I_{dark}(\lambda)$ is the spectra without illumination of the spectrophotometer and $I_{sam}(\lambda, t)$ are the subsequent spectra. For the determination of short-term drift, the intensity of a light source is measured at one wavelength over a time frame of 15 minutes. The time resolved absorbance is calculated, using the starting value as a reference signal. Depending on the standard, the absorbance is separated in windows with a width of 0.5 minutes (ASTM 0.5) or 1 minutes (ASTM 1). A linear approximation

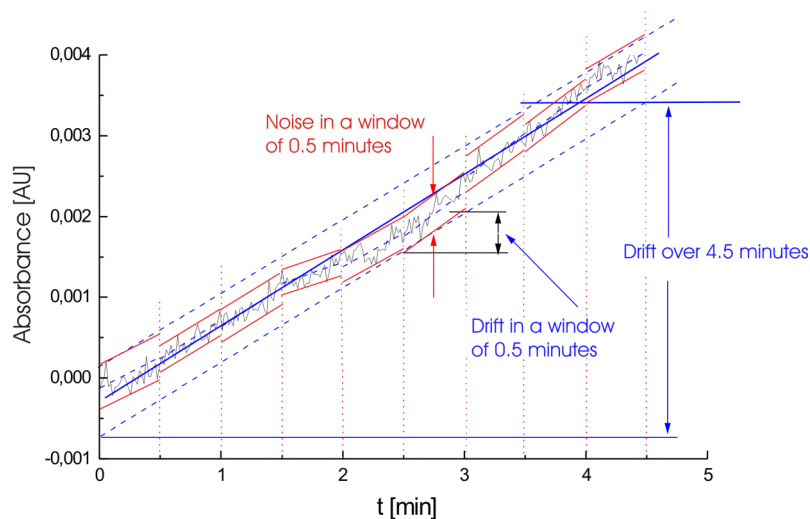


Figure 3.6: Experimental characterization of noise and drift

of the signal is performed over the whole time frame to determine the drift, as shown in figure 3.6. Parallel lines are drawn to the fitted line, enveloping the minimum and maximum of the signal. The vertical distance between the lines is the noise in the window. The short time noise of the lamp is the mean value over the time frame.

The same measurement procedure has been applied to the characterization of the complete measurement system, and will be described in chapter 6.3.2, too.

3.6 Experimental results

During earlier works [Meyer, 1999], the spectral intensity and the stability of two 30W deuterium lamps of different manufacturers were compared. To provide stable measurement conditions, the light sources were tested in the same lamp housing. In addition, a miniature deuterium light source has been tested in terms of spectral intensity and stability.

The spectral intensity has been measured with a Zeiss MCS UV/VIS Spectrometer in a wavelength range between 190 and 1020 nm. For this measurement a

2 m long UV-fibre with a diameter of 200 μm was used. The spectral intensity of the fiberlight source was multiplied by a factor of 100 to be comparable to the measured intensities of the standard light sources. Noise measurements have been carried out over a time frame of 45 minutes, capturing two spectra per second at 90 % of the maximum AD value. Different spectral behaviour of

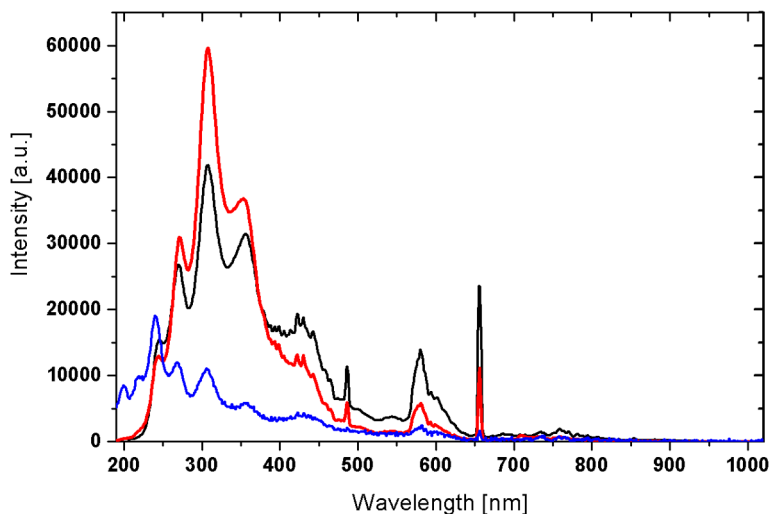


Figure 3.7: Comparison of spectral intensity with spectrometer: supplier A (red), supplier B (black), Fiberlight multiplied by a factor of 100 (blue)

the light sources are mainly caused by the material of the window used and by the optical system for fibre coupling. Noise of the lamps were measured at different wavelengths and is presented in Tables 3-1 for the 30W deuterium lamp of supplier A, 3-2 for the 30W deuterium lamp of supplier B and 3-3 for the Fiberlight lamp. The measurement carried out suggested a stable lamp behaviour of all measured standard deuterium lamps. However, the lamp of supplier B seems to have a higher noise and drift compared to the lamp of supplier A. As measurements were carried out in a lamp housing with the same

power supply, designed for lamps of supplier A, the stability of the other lamp was influenced by the present heating current. The Heraeus Fiberlight lamp has a 4 to 10 times higher noise, compared to the standard lamps. However, due to the compact size of the source, it is very attractive for compact and mobile measurement systems.

3.7 Summary

A variety of lamp systems provide sufficient energy for gas analysis in the ultraviolet wavelength region. However, due to low noise requirements only the deuterium lamps were found to be useful for analytic measurements very efficiently; 30 W deuterium lamps can be used for high stability measurements, mainly in fixed measurement setups. The miniaturized deuterium lamps are an interesting alternative for mobile applications, due to their lower power consumption. In return compromises, such as lower intensity, the resulting longer integration time and the noise figure have to be accepted. For the realization of a gas analysis system, a lamp housing with optimized volume for nitrogen purge and an attached optic was designed. A Heraeus DO 660/05 J lamp with an aperture of 0.5 mm and a pre-aligned socket was selected for this work. The deuterium plasma was imaged onto an optical fibre with either a single or a double lens optic; both are imaging the light with a 1 by 2 ratio onto the endface. The coupling angle on the fibre side approximately equals the numerical aperture of the hollow core waveguide, with a value of 0.09.

References

- ASTM. E685-93: "standard practice for testing fixed-wavelength photometric detectors used in liquid chromatography. Technical report, ASTM International, 1993.
- M. Belz. *Pollutant monitoring with fiber optic in the deep ultra violet*. PhD thesis, City Uiversity London, UK, 1998.
- R. Kötschau. *Characterization of UV-Hollow Core Waveguides for the application in spectroscopy of gases, in german*. Diploma thesis, University of Applied Sciences Giessen-Friedberg, Germany, 2002.
- H. Meyer. *Characterization and test of different spectrometer systems (in german)*. Diploma thesis, University of Applied Sciences Aalen, 1999.
- H. Perkampus. *Eyclopedia of spectroscopy*. VCH, Weinheim, 1995.

References

Table 3-1: D2-Lamp 30W, supplier A

Wavelength [nm]	Noise $[\pm\mu AU]$ ASTM 0,5	Noise $[\pm\mu AU]$ ASTM 1	Drift $[\pm mAU]$ over 45 min.
200	52	60	3,259
250	40	48	2,476
400	49	57	0,241
580	41	47	0,051

Table 3-2: D2-Lamp 30W, supplier B

Wavelength [nm]	Noise $[\pm\mu AU]$ ASTM 0,5	Noise $[\pm\mu AU]$ ASTM 1	Drift $[\pm mAU]$ over 45 min.
200	62	74	3,835
250	38	47	2,58
400	42	51	1,144
580	34	42	1,737

Table 3-3: Fiberlight Lamp, Heraeus

Wavelength [nm]	Noise $[\pm\mu AU]$ ASTM 0,5	Noise $[\pm\mu AU]$ ASTM 1	Drift $[\pm mAU]$ over 45 min.
200	164	205	48,237
240	178	245	9,929
306	194	268	1,215
355	205	266	1,959
580	414	501	2,803

4 Development and characterization of fibre-optic spectrometer

4.1 Abstract

In the following chapter, the different criteria of a spectrophotometer and their dependence on the acquired data are discussed. Starting with the principles of wavelength separation, the influence of the entrance slit width and additional points of interest will be described. In addition, a new-type fibre optic spectrophotometer has been developed and characterized in terms of wavelength resolution and stray light radiant power ratio.

4.2 Different techniques for wavelength separation

[Hardwick, 1998; Loewen, 2005; Margaritondo and Staehli, 1994]

Before linear array detectors were available, the use of monochromators was the only reliable technique to record spectra electronically. For measuring different wavelengths, the grating within the monochromator was turned in order to change the angle of incidence. In some cases, the incident light on the detector had a too low intensity to achieve a sufficient signal to noise ratio (SNR). To improve the SNR the use of a Lock-In Amplifier technique was frequently used. Monochromator measurement time of a spectrum over a certain wavelength range is determined by the time needed to turn the grating, either with a motor or manually in addition to the time needed to obtain a stable signal for each wavelength.

In early days, simultaneous measurement of the full wavelength range within one illumination could be carried out with polychromators with a photographic film at the position of the Rowland circle. With this technique, the qualita-

tive analysis of emission lines became possible. For the use in absorbance spectroscopy polychromators could be used since the development of linear imaging sensors like photo-diode arrays (PDA) and charge coupled devices (CCD). They allow to capture an image of intensities over a certain wavelength range; spectra can be taken with integration times smaller than 10 ms. In addition to the sensitivity and the noise of the detectors, the stability and the noise behaviour of the read out electronics and the resolution of the analogue digital converters used have a great influence on the sensitivity of the measurement system. Spectrometers used for ultraviolet (UV), visible (VIS) and near infrared (NIR) wavelength range can be realized very efficiently with diffraction gratings. They offer improved resolution, luminosity and dispersion compared to prism instruments of comparable size. In addition, the intrinsic losses of the prisms base material reduce the efficiency in the UV region significantly. Grating diffraction relies on interference between wave fronts caused by a series of parallel and microscopically spaced lines. The most common type of grating is the reflection grating. Typically it is ruled on a glass surface and aluminium coated. In contrast to the transmission grating the reflection grating offers a better UV performance due to the aluminium film used as a reflective coating in front of the glass. The intrinsic absorption of the base material is avoided. Reflective gratings are manufactured by two basic principles, mainly: First, the classical mechanical ruling, where the rules are inscribed into a polished master blank or in the mirror surface with a diamond. The ruling engine must perform with very high accuracy, otherwise ghost spectra or wavelength changes are possible. Alternatively, gratings can be produced with a holographic method: An interference pattern is projected onto the mirror blanks surface coated with photoresist. After the illumination the photoresist is developed and the lines are etched into the mirror. With this technique the shape of the groove can be better controlled. Additionally, gratings can be produced as replicas of a master grating for higher quantities. With this

technique, the optical properties of the master grating can be transferred to the replica. Finally, the gratings are coated with a metallic reflection coating. The wavelength of reflected light varies with angle, as defined by the grating equation:

$$m \cdot \lambda = d (\sin \alpha \pm \sin \beta) \quad (4-1)$$

While α represents the angle of incidence in respect to the normal, β represents the angle of diffraction to the grating normal. m is the order of diffraction and has to be an integer value. In addition the grating constant, d , describes the distance between two grooves. In figure 4.1 the relationship between incident and diffraction angle and the grating constant is illustrated.

The shape of the grooves can be controlled in a way that light striking the grating normal to the face of the grooves is diffracted with very high efficiency. The angle of the highest efficiency is referred to as the blaze angle of the grating. The blaze angle θ causes a suppression of the 0^{th} order of the diffraction, while increasing the intensity in the first order. The maximum wavelength of a certain blaze angle can be calculated, according to the following formula:

$$\lambda_{max} = 2 \cdot \frac{d}{m} \cdot \sin(\theta) \quad (4-2)$$

As a criterion of the performance the resolving power R of a grating can be introduced as:

$$R = \frac{\lambda}{\Delta\lambda} \quad (4-3)$$

where $\Delta\lambda$ is the limit of the resolution, the difference between two spectral lines of equal intensities that can be distinguished. Most textbooks describe the resolving power as:

$$R = m \cdot W \quad (4-4)$$

with W describing the total number of illuminated grooves. For negative spectral orders ($n < 0$), the absolute value of R is considered. When m is replaced

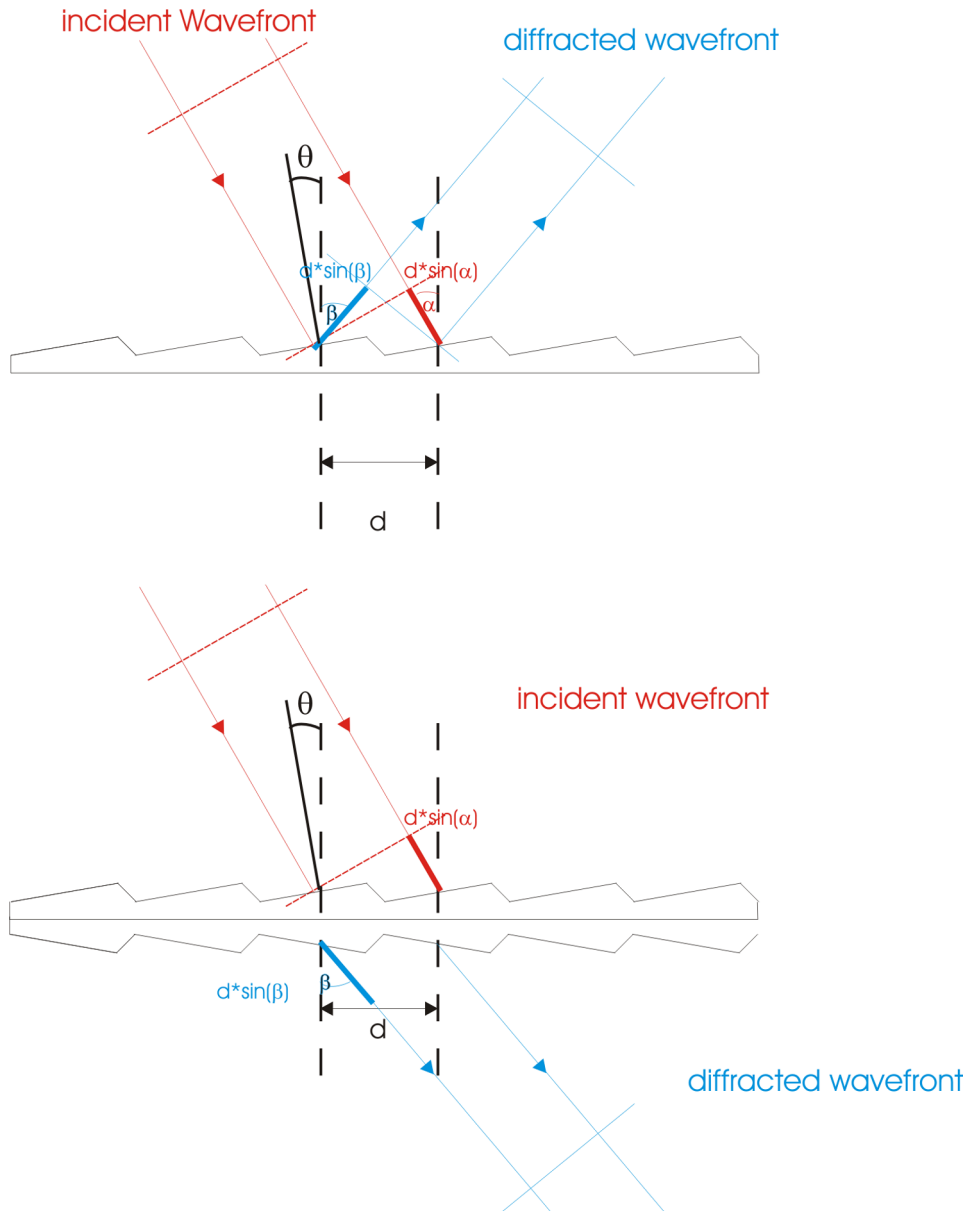


Figure 4.1: Diffraction of incident light on a grating [Loewen, 2005]

with the grating equation 4-1, the resolving power can be expressed as:

$$R = \frac{N \cdot d (\sin \alpha + \sin \beta)}{\lambda} \quad (4-5)$$

If the groove distance is uniform over the surface of the grating and if the substrate is planar, Nd equals the ruled width W . However, the resolving power is not explicitly connected to the spectral order or numbers of grooves; these parameters are contained within the ruled width and the angles of incidence and diffraction, as:

$$|\sin \alpha + \sin \beta| \leq 2 \quad (4-6)$$

and therefore the maximum attainable resolving power is:

$$R_{max} = \frac{2 \cdot W}{\lambda} \quad (4-7)$$

The classical setup of laboratory spectrophotometers are realized with plane gratings. Within these setups focusing mirrors are used to image the entrance slit onto the diffraction grating and the diffracted light onto the exit slit, or the detector. As the mirrors used might cause optical aberrations like spherical aberration, coma, astigmatism and a curvature of field, the efficiency of the spectrometer depends strongly on the careful choice of components minimizing these effects.

The most common type of the plane grating spectrometers is the Czerny-Turner setup. The incident beam is focused on the plane grating by a collimating mirror, where the diffraction occurs. A second condensing mirror is used to image the spectrum onto a detector chip. The Czerny-Turner setup is shown in figure 4.2.

Due to its minimal optical aberrations and flexibility the Czerny-Turner setup is used in many commercial spectrometers for laboratory purposes. However, in terms of stability, light intensity and dimensions it is not the optimal setup for mobile use. Depending on the numerical aperture of the incident light and the diameter of the first mirror after the entrance slit, a larger area might

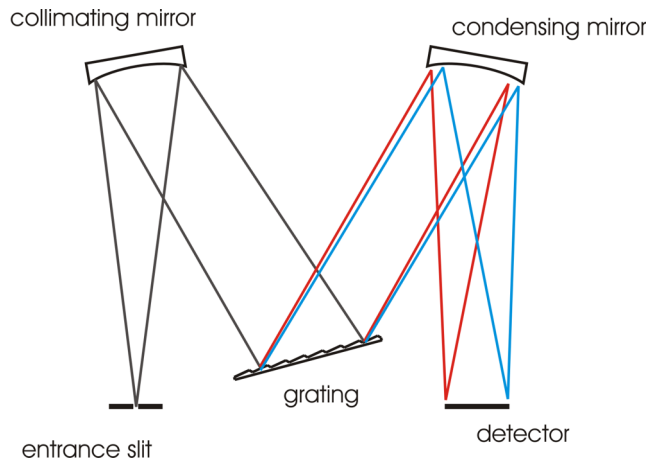


Figure 4.2: Czerny Turner Setup

be illuminated, causing light in the system which is not separated by the diffraction grating, producing additional signal at the detector. Therefore, many commercial spectrometers based on this setup have poor stray light behaviour when used with fibre-optics.

When a concave mirror blank is used instead of a plane mirror as a base for the grating, the use of additional imaging optics becomes obsolete. The concave mirror carries out both the dispersing element as well as the image-forming optics. However, optical aberrations, mainly astigmatism, have to be taken into account because they cannot be compensated by other optical elements. Within a Rowland setup, the wavelengths focal points are located along the outer diameter of the circle, which results in defocusing of the wavelengths on a linear chip. Flat-field gratings are calculated for the use with a linear detector, and the focal points of the spectrum are within a line. This allows a measurement with a constant spectral resolution, avoiding a defocusing on the detector chip.

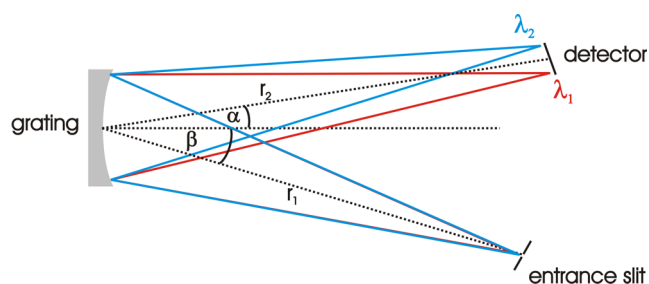


Figure 4.3: Rowland circle setup

4.3 Influence of entrance slit & Cross section converter

Within a polychromator, the selection of the entrance slit has a vital influence of the performance of the system. A fibre illuminates the diffractive grating through the entrance slit, the grating acts as a focussing element and the wavelengths are separated and imaged onto the detector in the width of the entrance slit. While a wide entrance slit allows quick measurements, due to a large amount of incident light on the grating, the width of the entrance slit on the detector increases and the wavelength separation decreases. For small entrance slits the wavelength separations increases, but the amount of incident light is low. Therefore, the choice of the entrance slit width is always a trade off. Additionally, there might be a mismatch between the detector height and the height of the entrance slit used. For the systems designed in this work, a photo diode array (PDA) with a height of 2.5 mm was used. When an optical fibre, with a $600\ \mu\text{m}$ core diameter is used, only a part of the detectors height is used. In addition, a large fraction of the light exiting the optical fibre is cut off by the entrance slit. A cross section converter is an option to optimize the light coupled into the spectrometer. Within this assembly optical fibres with a small diameter between 70 and $100\ \mu\text{m}$ are used. As shown in figure 4.4, the fibres of the incoupling side are combined to a round cross section, on the exit side, they are aligned linear, ideally producing a line with a maximum width

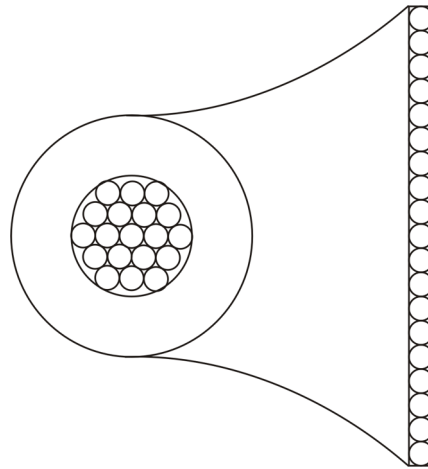


Figure 4.4: Schematic drawing of a cross section converter produced of 19 optical fibres, side of fibre-optic connector (left), side of entrance slit (right)

of the fibres core diameter. At the connection between the fibre and the cross section converter additional reflection losses have to be taken into account. In addition, the light incident onto the gaps between the fibres and their cladding will be lost. However, compared to the losses, which are produced by the area mismatch between the optical fibre and the entrance slit, the cross section converter allows a higher coupling efficiency. In the UV wavelength region, the additional fibres used have to be characterized and selected according to their basic attenuation and their solarization behaviour to ensure a stable measurement.

4.4 Important parameters for spectrophotometers

In order to characterize and quantify the optical and photometric properties of spectrophotometers, a wide range of traceable materials are provided and a variety of guidelines have been published [ASTM, 1993, 2001, 2002, 2004a,b, 2005; Burke and Mavrodineanu, 1977; Mavrodineanu et al., 1994; Travis et al.,

2000]. The different properties of a spectrophotometer, or a spectrophotometric system will be discussed.

The **wavelength range** defines the spectral range of a spectrometer. In general, the different wavelength regions are separated in ultraviolet (UV), visible (VIS) and near infra red (NIR). The wavelength range is influenced by type and position of the detection array, the optical grating and other components used in the optical setup. For the use in the UV, the transmission properties and solarization of materials irradiated by incident light have to be taken into account.

The **spectral wavelength accuracy** describes the correlation of detected wavelengths to the incident wavelengths. The wavelength is mainly dependent on the stability of the relative positions of the optical components in a spectrophotometer. Caused by the manufacturing process and the choice of materials this criterion cannot be fulfilled completely. Therefore, deviations from the wavelength have to be minimized for maximum accuracy.

The **wavelength repeatability** is a measure for monochromators, where the grating has to be turned in order to scan over the wavelengths. For polychromators, the term **wavelength stability** is more appropriate, as there are no moving parts. It describes the shift of measured wavelength over temperature, mainly. Both the mechanical stability of the polychromator, as well as the temperature behaviour of used materials is influencing the behaviour of the measured wavelength. By changing the relative position of the components wavelength deviations might occur.

The **spectral resolution**, also described as spectral bandpass or spectral slit width $\Delta\lambda$ of a spectrometer is influenced by the focus of the spectrometer, the number of lines on the grating, the width of the entrance slit and used detector used. It is a measure of the optical properties of the spectrometer. However, after a wavelength calibration procedure, coefficients are calculated to assign wavelength values to every pixel of the detector chip. However the

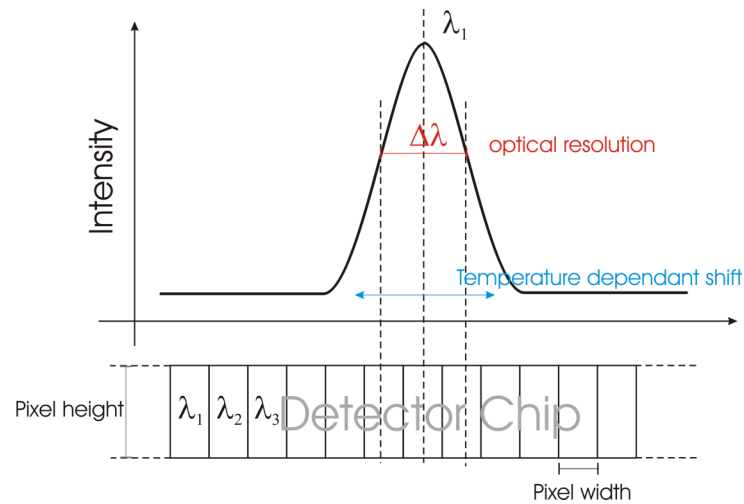


Figure 4.5: Single wavelength illuminating a detector chip. The wavelength accuracy, spectral resolution, pixel resolution and temperature drift can be deduced

pixel resolution does not necessarily represent the spectral resolution, but can be misinterpreted.

In figure 4.5 a single spectral line is shown, which illuminates a detector array. According to the described criteria, the position of the peak can be analyzed if the wavelength accuracy is correct. The spectral resolution is influencing the number of pixels detecting light from the line. The width of spectral lines is mostly determined by a full width method at half maximum (FWHM). The temperature shift causes a change of the detected wavelength, dependent on the thermal expansion coefficients of the different components used.

Stray light, also referred to as stray radiant power ratio (SRPR) is light detected which is different to the assigned wavelength. Stray light can be caused by scattering within the spectrometer or additional light entering the spectrometers housing.

The **linearity** of a spectrophotometer is of interest to be able to measure quantitative amounts, or changes within the incident light. During the integration

time charges are accumulated in the detector. With continuous irradiation, a linear behaviour of the read out value over the integration time should be measurable. Furthermore, with constant integration time, an absorbance series of reference materials in different concentrations should produce linear results. The chosen detector and read out electronic has a major influence on the linearity of a system. Therefore entire detector systems, including electronic and analogue digital converter have to be characterized. Based on former studies [Meyer, 1999] different detectors were compared for linearity and an advantage of PDA detectors over CCD detectors was recognized.

The **signal to noise ratio** (SNR) is defined as the relation between the noise level and the saturation level of a certain detector. In addition to the detector itself the readout circuitry and the analogue to digital converter (ADC) influences the maximal achievable signal to noise value. The noise due to the conversion is depending on the digital resolution b and the uncertainty of one bit. It can be calculated by ten times the logarithm of the fraction of one bit and the maximum number of quantization 2^B :

$$S/N = 10 \cdot \left(\log \frac{1}{2^B} \right) \quad (4-8)$$

In above equation the signal to noise ratio S/N is calculated by the fraction of one bit deviation to the number of quantization achieved by the ADC for ideal values. The **theoretical noise limit** [Klein et al., 2009] for an absorption measurement is described by:

$$\Delta A = \log \frac{2^B}{2^B - 1} \quad (4-9)$$

The calculated maximum signal to noise values and the theoretical noise limit for 3 different digital resolutions are shown in Table 4-1. Due to a variety of additional effects, the real signal to noise ratio of spectrophotometric systems is lower: Electronic irradiation, temperature noise and in the case of CCD detectors noise figures dependent on the illumination have to be taken into account.

Table 4-1: Maximum Signal to noise values for different digital resolutions, considering only noise due to AD conversion

Digital resolution [Bit]	fraction	max. achievable S/N Value [dB]	Theoretical noise limit [μ AU]
12 bit	1/4096	36.1	106
14 bit	1/16384	42,1	26
16 bit	1/65536	48,1	6

The **photometric accuracy** describes the ability of a spectrophotometer to measure an absorption value of different sample concentrations. Usually this test is required as a validation procedure with standard reference materials. The certified absorbance values are compared to the measured.

4.5 Measurements on different spectrometers for gas analysis

During the work on gas analyses, the influence of the spectrometer became obvious. Due to the spectral resolution, stray light and behaviour of the detector, the performance of the whole system is influenced. During the time period of the thesis a synopsis of two CCD-based spectrometers, with a wavelength range in the UV and two spectrometers with a Zeiss MCS Polychromator and different types of detectors where compared. Table 4-2 gives an overview on the compared spectrometers. In principal, the use of CCD detectors for UV light applications is limited, as they are insensitive below 400nm. Therefore, a fluorescence coating on the chip is necessary to allow light detection.

Due to its excellent linear behaviour proportional and superiour signal to noise ratio, the photodiode array is widely used for spectrophotometric detectors. A new development in detectors has been the back-illumination type CCD, where the thickness of the silicon wafer is reduced in a way, that UV light

Table 4-2: Overview on compared spectrometers

	Avantes S2000	UV-Prototype	MCS-CCD	MCS-UVNIR
Detector	CCD	CCD (Sony ILX526A)	BI-CCD Hamamatsu S7031-1006	PDA Hamamatsu S3904-1024Q
Pixels	2048	3000	1024	1024
Wavelength range	154..380 nm	175..210 nm	182..998 nm	187..1040 nm
Pixel resolution	0.15 nm/pixel	0.01 nm/pixel	0.8 nm/pixel	0.8 nm/pixel
spectral width	2 nm	0.015 nm	1.5 nm	1.5 nm
A/D Converter	12 bit	12 bit	16 bit	16 bit

can propagate through it and can be detected in the band gap structure more efficiently. Due to this effect, the back illuminated CCD has a much higher sensitivity to UV irradiation than a classical PDA.

With all of the mentioned spectrometers an absorption measurement is possible. However, depending on the spectral resolution of the spectrometer, the absorption spectrum differs. Depending on the optical bench used for the wavelength separation, stray light has to be taken into account. Finally the sensitivity and signal to noise properties of the detector influences the quality of the measurement.

During the first measurements a principal comparison of the systems was done. The possibility to measure gases could be proven with a low cost CCD type spectrometer. In figure 4.5 the influence of the spectral width and stray light effects become obvious. While the black plot shows a fine structure of oxygen, the blue plot shows the absorption for a calculated spectral width of 1nm. The red plot shows the measured signal from the Avantes spectrometer. The resolution seems to be lower than in the upper wavelength range (0.4-0.7 nm for a 100 μ m slit) and stray light is increasing significantly below 200nm.

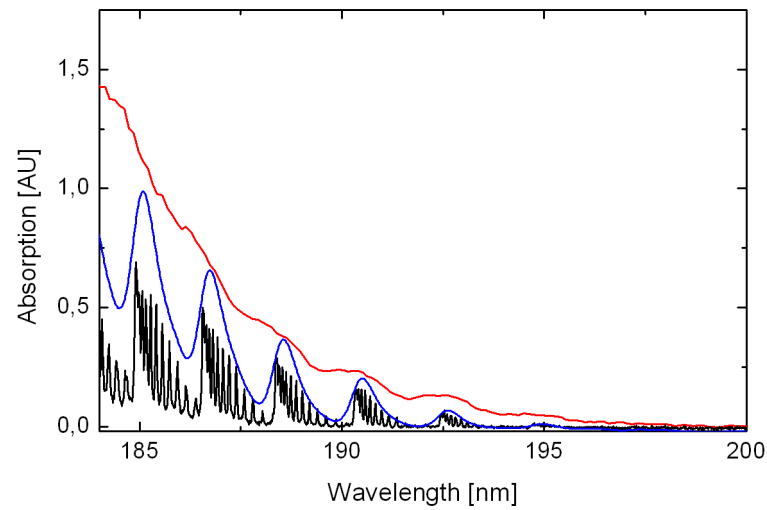


Figure 4.6: Influence of spectral width

4.6 Characterization of HRUV prototypes

Based on the data gathered on available spectrophotometers the development of a fibre-optic spectrophotometer for the deep ultraviolet wavelength with an excellent spectral resolution was decided.

Design criteria have been:

- Excellent spectral resolution within a wavelength region of 120 nm
- Minimum wavelength smaller or equal to 180 nm
- Numerical Aperture matched to optical fibres
- Nitrogen purge or evacuation should be possible
- Excellent stray light behaviour

Starting from these criteria, an industrial partner set up two spectrometers. In order to avoid multiple reflection and transmission losses in this wavelength region, a flat-field polychromator setup was chosen. The numerical aperture of 0.21 is close to that of a multimode fibre aperture (0.24 in the UV wavelength region) and defined by the focal length, $f=166$ mm, and the diameter, $d=70$ mm, of the grating. The wavelength range was decided to be 180 to 300 nm for the prototype. In addition, minimum wavelengths between 168 and 180 nm have been tested. For a sufficient wavelength dispersion, a grating with roughly 12001/mm was chosen. A cross section converter is used to optimize the fraction of light from the fibre which is illuminating the grating. As a detector photo diode arrays have been chosen, with a TSPEC4 read out electronic.

After the design of the prototypes, first tests on stray light and linearity were carried out. For this purpose standard reference materials, as described in [ASTM, 2001, 2004a] were used. As these materials are usually used for laboratory spectrophotometers with cuvette holders, a setup with a fibre-optic cuvette holder as shown in figure 4.7 was assembled. At this time the two prototypes had different entrance slits and different wavelength ranges, as described in table 4-3. According to the procedures described in the ASTM standards, wavelength accuracy, wavelength resolution and spectral slit width can be determined with different reference materials or methods:

Wavelength accuracy is the deviation from an (average) wavelength reading at an absorption band or emission band of known wavelength. For spectrophotometers the average wavelength is determined by extracting the bands from ten spectra. The wavelength bias is the difference between the true wavelength and the average observed reading. Within this standard, a variety of reference wavelengths are given. The mercury arc emission spectrum, starting with an emission at 184.91 nm, which can be measured also with a low intensity in ambient air environment can be used for calibrating the spectrometer [ASTM,

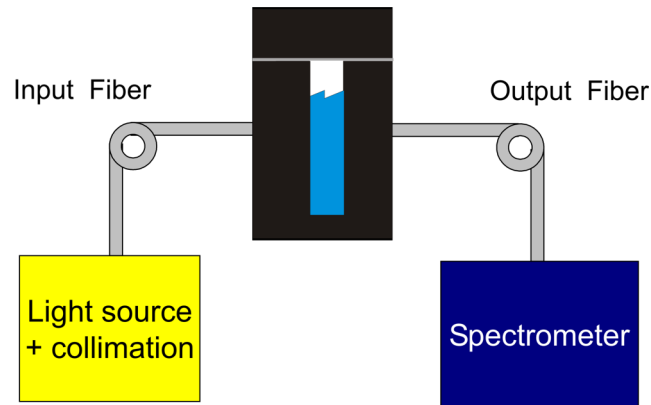


Figure 4.7: Measurement setup for characterization of spectrometer, according to ASTM procedures

2005].

Furthermore, the **spectral resolution** can be determined by a variety of measurements:

- Absorption measurement of **toluene in hexane**, where the absorption minimum at 268.7 nm and the absorption maximum at 267 nm is compared. Depending on the ratio from maximum to minimum, the spectral slit width can be determined.
- Absorption measurement of **holmium Oxide**, which has a series of characteristic absorptions in the wavelength range from 240 to 640 nm. The spectral slit width is determined by the position of the maxima.
- Absorption measurement of **benzene** in the gas phase, which has fine structure in the wavelength range from 230 to 270 nm.

For the determination of the **stray light properties** different liquid mixtures with cut-off wavelengths between 200 and 390 nm are available. Below this wavelength no light is transmitted. The materials used are usually Sodium Nitride (cut-off: 390 nm), potassium iodide (260 nm), sodium chloride (205

Table 4-3: Overview on HRUV prototype spectrometers

	HRUV-prototype 1	HRUV-prototype 2
Detector	PDA Hamamatsu S3904-1024Q	PDA Hamamatsu S3904-1024N
Pixels	1024	1024
Slit	50 μ	75 μ
Wavelength range	168.2..288.3 nm	174.4..294.7 nm
Pixel resolution	0.12 nm/pixel	0.12 nm/pixel
spectral width	0.4 nm	0.6 nm
A/D Converter	16 bit	16 bit

nm) and potassium chloride (200nm). The light measured at this wavelength range is scattered light within the polychromator which influences the quality of measurement, and therefore influences the dynamic of the measurement. In general an absorption measurement against a cuvette filled with solvent is carried out and the absorption value at given wavelengths are specified.

4.7 Measurement results

Wavelength calibration has been carried out with a low pressure mercury arc lamp. The specifications of the spectrometers can be seen in table 4-3.

The spectral width has been determined with different approaches. The absorption measurement of toluene in hexane, is shown in figure 4.8. For both spectrophotometers the minimum and maximum values were determined and the ratio was calculated. The ratio determined was 1.94 for the HRUV1 and 2.01 for the HRUV2, respectively. According to the certificate of the reference material, a spectral slit width of 1.0 ± 0.1 nm was determined for both spectrophotometers.

In addition, the fine structure of benzene vapour was measured. The measured absorption spectra are shown in figure 4.9. For comparison, a measured spectrum with a spectral slit width of approx. 1.6 nm is added. Both characterized spectrophotometers show more details of the benzene absorption. It is obvious

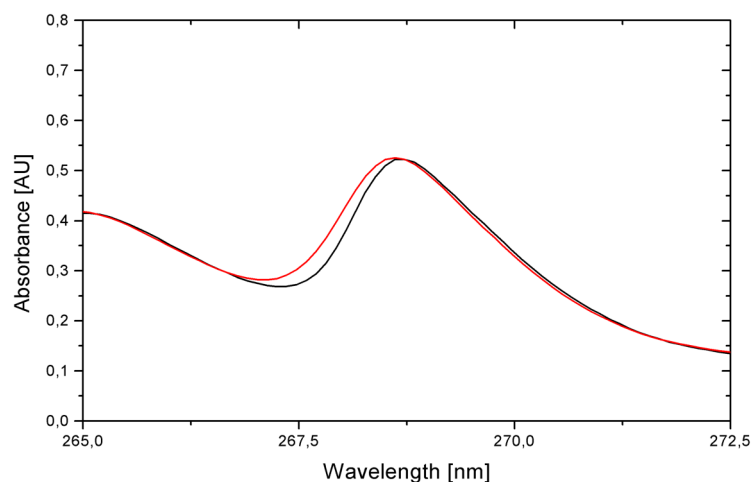


Figure 4.8: Determination of spectral slit width with the ratio of minimum and maximum absorption of toluene in hexane, HRUV1 (black), HRUV2 (red)

that HRUV1 has a better spectral resolution, the fine structure of the benzene absorption are clearly visible.

Additionally, the spectral slit width was estimated with the emission spectrum of a low pressure mercury discharge lamp, within a Heraeus Fiberlight module. The spectral width of the emission lines of mercury in low pressure lamps is approx. 0.02 nm, therefore, detection systems with a spectral slit width equal or greater to 0.2 nm can be tested with this method. The data given in table 4-3 have been determined with the FWHM value of the emission lines measured.

Stray light was determined with a sodium iodide standard set was used. According to the certificate, the standard cuts off the light below 260.53 nm, producing absorptions higher than 2 AU. In figure 4.10 shows the measured Stray light radiant power ratios measured for both spectrophotometers. For

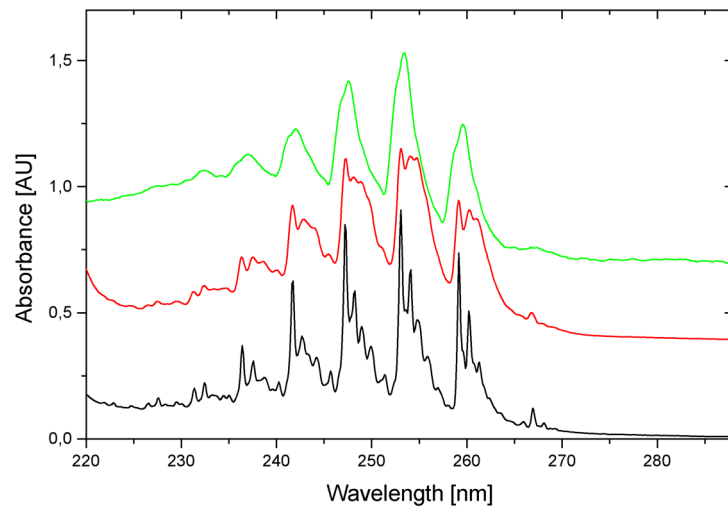


Figure 4.9: Determination of spectral slit width with the absorption of benzene vapour, HRUV1 (black), HRUV2 with an offset of 0.4 AU (red), spectral slit width of approx. 1.6 nm, with an offset of 0.7 AU (green)

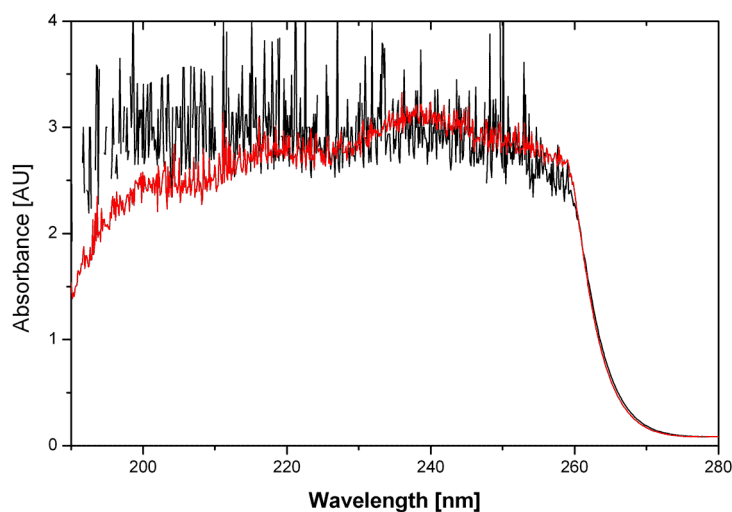


Figure 4.10: Determination of stray radiant power ratio: HRUV1 (black), HRUV2 (red)

both, the SRPR is better than 2.5 AU. The noise on the measured signal is visible. In the wavelength region below 190 nm the absorption of ambient oxygen increases and the reference lamp signal decreases higher stray light values are measured.

The photometric accuracy of the spectrophotometer has been tested with a calibrated set of Potassium dichromate in a perchloric acid. The absorbance at the wavelengths 235 and 257 nm are given in the certificate for concentrations between 20 and 100 mg/l. The absorption spectra for the different concentrations are displayed in figure 4.11. The data is shown in table 4-4 and 4-5 for the spectrophotometer HRUV1 and HRUV2 respectively.

4.8 Summary and Discussion

During the thesis, a variety of fibre-optic spectrometers have been tested and compared. The optical setup of the instruments and their stray light be-

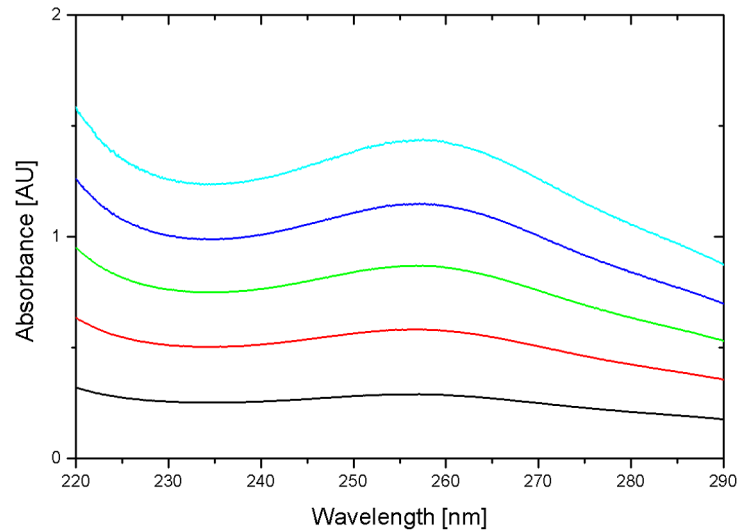


Figure 4.11: Measurement on photometric accuracy: from bottom to top: 20, 40, 60, 80, 100 mg/ml

Table 4-4: Measurement of photometric accuracy, HRUV1 spectrophotometer

Concentration	Cert. Value @ 235 nm	Meas. Value	ΔA	Cert. Value @ 257 nm	Meas. Value	ΔA
20 mg/l	0.240	0.254	0.014	0.278	0.291	0,013
40 mg/l	0.488	0.486	-0.002	0.567	0.564	-0,003
60 mg/l	0.741	0.738	-0.003	0.861	0.858	-0,003
80 mg/l	0.990	0.984	-0.006	1.150	1.137	-0,013
100 mg/l	1.244	1.239	-0,005	1.446	1.442	-0,004

Table 4-5: Measurement of photometric accuracy, HRUV2 spectrophotometer

Concentration	Cert. Value @ 235 nm	Meas. Value	ΔA	Cert. Value @ 257 nm	Meas. Value	ΔA
20 mg/l	0.240	0.251	0.011	0.278	0.288	0.010
40 mg/l	0.488	0.503	0.015	0.567	0.581	0.014
60 mg/l	0.741	0.749	0.008	0.861	0.869	0.008
80 mg/l	0.990	0.987	-0.003	1.150	1.147	-0.003
100 mg/l	1.244	1.238	-0,006	1.446	1.436	-0.010

haviour was found to have great influence on the quality of a measurement. In addition, an attempt to compare the different detector types has been done. However, as these detectors have been combined within different spectrometers, a comparison with comparable condition was not possible. In addition, a new-type fibre-optic spectrophotometer has been developed. The focus of the development was to achieve high spectral resolution and improve stray light behaviour. This was reached with an accepting aperture of the spectrometer close to the fibre NA and a spectral resolution better than 0.6 nm, depending on the entrance slit width. However, the different measurement procedures for the spectral slit width are not producing consistent results. The measurement of benzene vapour and the determination of the spectral slit width by the emission lines of mercury allow reliable characterization. Both spectrophotometers have been tested in terms of Stray light radiant power and one showed results of better than 2 AU, for wavelengths above 190 nm. The tests on photometric accuracy have been performed, with a maximum deviation of 0.014 AU and 0.015 AU, respectively. In respect to the existing characterization procedures, except for the determination of spectral slit width, the performance of both spectrophotometers are far improved to commercially available spectrophotometers.

References

- ASTM. E685-93: "standard practice for testing fixed-wavelength photometric detectors used in liquid chromatography. Technical report, ASTM International, 1993.
- ASTM. E275-01: "standard practice for describing and measuring performance of ultraviolet, visible, and near-infrared spectrophotometers". Technical report, ASTM International, West Conshohocken, PA, www.astm.org, 2001.
- ASTM. E925-02: "standard practice for monitoring the calibration of ultraviolet-visible spectrophotometers whose spectral slit width does not exceed 2 nm". Technical report, ASTM International, West Conshohocken, PA, www.astm.org, 2002.
- ASTM. E387-04: "standard test method for estimating stray radiant power ratio of dispersive spectrophotometers by the opaque filter method". Technical report, ASTM International, West Conshohocken, PA, www.astm.org, 2004a.
- ASTM. E169-04: "standard practices for general techniques of ultraviolet-visible quantitative analysis". Technical report, ASTM International, West Conshohocken, PA, www.astm.org, 2004b.
- ASTM. E958-93: "standard practice for measuring practical spectral bandwidth of ultraviolet-visible spectrophotometers". Technical report, ASTM International, West Conshohocken, PA, www.astm.org, 2005.
- R. Burke and R. Mavrodineanu. Certification and use of acidic potassium dichromate solutions as an ultraviolet absorbance standard - srm935. Technical report, NIST, 1977.
- J. L. Hardwick. *Visible and ultraviolet light spectrometers in Encyclopedia of Applied Physics*. Wiley VCH, Weinheim, 1998.

References

- K.-F. Klein, J. Mannhardt, M. Belz, C. Gonschior, and H. Eckhardt. Optical fibers in instrumental uv-analytics. *Proc. SPIE*, 7173, 2009. doi: 10.1117/12.818663.
- E. Loewen. *Diffraction Grating Handbook*. Newport Corporation, 6th edition edition, 2005.
- G. Margaritondo and J.-L. Staehli. *Monochromators in Encyclopedia of Applied Physics*. Wiley VCH, 1994.
- R. Mavrodineanu, R. Burke, J. Baldwin, M. Smith, J. Messmann, J. Travis, and J. Colbert. Glass filters as a standard for spectrophotometry - selection, preparation, certification and use of srm 930 and srm 1930. Technical report, NIST Spec. Publ. 260-116, 1994.
- H. Meyer. *Characterization and test of different spectrometer systems, in german*. PhD thesis, University of Applied Sciences Aalen, 1999.
- J. Travis, M. Smith, S. Rasberry, and G. Kramer. Technical specifications for certification of spectrophotometric ntrms. Technical report, NIST, 2000.

5 Development of an intrinsic absorption cell for gas analysis

5.1 Abstract

Within this chapter, existing cell concepts for gas analysis will be discussed. However, depending on the application, criteria like optical path length, cell volume, wavelength region or heating of the measurement cell are necessary. The influence of these points on the development and application of an intrinsic absorption cell for gases will be discussed.

5.2 Existing concepts

The analysis of gases has been carried out with different sensor cells: Depending on the extinction of the gas, and the used wavelength range, the cell setup has to be chosen. For gases which require a long or variable absorption length, a so-called white cell, which is a cavity consisting of three spherical concave mirrors, can be chosen. By varying the number of reflections within the absorption cell, the absorption length increases [White, 1942]. In addition, in order to minimize the number of reflections alternative concepts have been realized: By using a retroreflector (corner cube) for folding the path once, the light exiting a fibre can be collimated by a paraboloid, which also focuses the light from the gas cell into an exiting fibre [Schneider et al., 2005]. As the use of mirrors requires a high precision in aligning the system, approaches with lenses, used as optical windows, are an alternative. In a linear setup, as reported by [Chambers et al., 2007], the light from an optical fibre is collimated by the first lens and focused into the detection fibre. However, the chromatic aberration and intrinsic losses of lenses restrict the optical power transmitted through the cell. In [Kötschau, 2002] a system with a single hollow-core-waveguide (HCW) as an intrinsic absorption cell has been introduced. In this setup, the function-

ality of gas analysis by means of UV spectroscopy and first studies on linearity and influences on spectrophotometry were demonstrated in principle. However, the gas exchange in the hollow core waveguide was achieved by flushing the whole system with the gas under test.

5.3 Concepts for new applications

5.3.1 Measurement of trace gases

For the analysis of trace gases, the hollow core waveguide proved to be an interesting alternative sensor cell. Due to its flexibility, the hollow core waveguide could be coiled up to produce a compact absorption cell. In addition, the low volume allows the measurement of small samples in low concentrations. In chapter 7, the aspects of trace gas analysis are discussed further.

5.3.2 Measurement of GC effluent

The coupling of gas chromatography and ultraviolet spectroscopy has been discussed firstly in 1962 [Kaye, 1962]. However, the interconnection between the separation technique and infrared spectroscopy has been discussed on a wider basis [Giss and Wilkins, 1984; Griffiths, 1977; Smith et al., 1983] and became a commercial instrument. The questions regarding measurement technique, such as the design of the optical setup and the optimum dimensions of the absorption cell, which was discussed as a light pipe, and their influence on the measurement results can be applied partly for the development of a UV measurement system. On the other hand, two separate dissertations have been done on the hyphenation of a ultraviolet detection with gas chromatographic separation in 1992. Both approaches identified the advantage of the higher absorptions in the ultraviolet compared to the infrared wavelength region. The approaches for detection have been different: A complex measurement cell [Lagesson, 1992] without the use of fibre-optics, fitting into the

sample compartment of laboratory spectrophotometers, has been designed and measurements have been carried out with scanning monochromators or photo diode arrays. Different work [Müller, 1992] reported the development of a sensor cell based on fibre-optics. However, the solarization behaviour of all-silica fibres was a major problem at this time and the fibres failed to transport UV light after a certain time of irradiation. On the other hand, the idea of coating a capillary with different layers, such as rhodium or aluminium, in order to guide the light through the capillary was proposed.

5.4 Realization of hollow core waveguide sensor cell for the detection of gas chromatographic effluent

After successful testing of the hollow core waveguide as an intrinsic sensor the system had to be improved to avoid problems due to thermal and chemical influences on light source and detector. Further, the gas flow of the sample under test within the system needed to be modified. Optical fibres provide sufficient transmission to be used as "windows" to separate the gas volumes from the measurement system and the absorption cell. In addition, fibres have the advantage that the length of the fibre experiences a temperature gradient and the endfaces within the measurement cell have the same temperature as the cell. A schematic drawing of the new concept is shown in figure 5.1. With classical lightpipe setups the purging of the optical windows and their lower temperature can be critical, as measurands might condensate on colder surfaces. The coupling properties of the hollow core waveguide to the all-silica fibre and the design or selection of couplers have been a vital step for a successful design of the measurement cell.

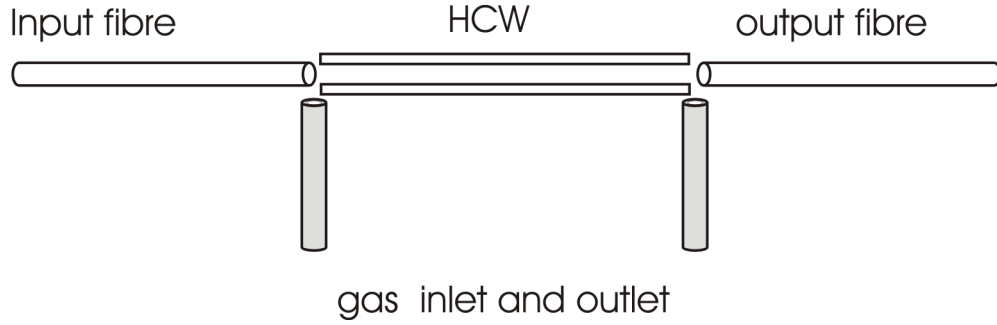


Figure 5.1: Schematic of measurement cell

5.4.1 Coupling efficiency

The coupling efficiency of multimode fibres is affected by the overlap of area a (near-field) and the numerical aperture NA of their acceptance and radiating characteristics (far-field) of both components intended for coupling. At best case, the numerical aperture and the diameter of the optical elements match and the light is coupled into the next optical component, with an reduction of intensity only due to reflection at the endface. In the case of different numerical apertures and areas, the coupling efficiency decreases and can be described as follows:

$$\eta_A = \begin{cases} (A_D \cdot A_S)^2, & A_D < A_S \\ 1, & A_D \geq A_S \end{cases} \quad (5-1)$$

and

$$\eta_{NA} = \begin{cases} (NA_D \cdot NA_S)^2, & NA_D < NA_S \\ 1, & NA_D \geq NA_S \end{cases} \quad (5-2)$$

With η_A and η_{NA} determining the coupling efficiency depending on the area A_i and the numerical aperture NA_i of source and detector fibre, respectively. In order to determine the losses to be expected and tolerances, an experimental approach was chosen: The measurement setup used is shown in figure 5.2. The light of a standard deuterium lamp source was coupled into a all-silica fibre with a core diameter of $600 \mu\text{m}$ and a standard numerical aperture of 0.22 ± 0.02 . A 2 by 1 imaging optics with a numerical aperture close to 0.09

was used. On the exiting side, which was precision cleaved, a hollow core waveguide piece was positioned. With a precision x-y-z stage the influence of misplacement could be determined. Two diameters of hollow core waveguides were tested: 1000 and a 500 μm .

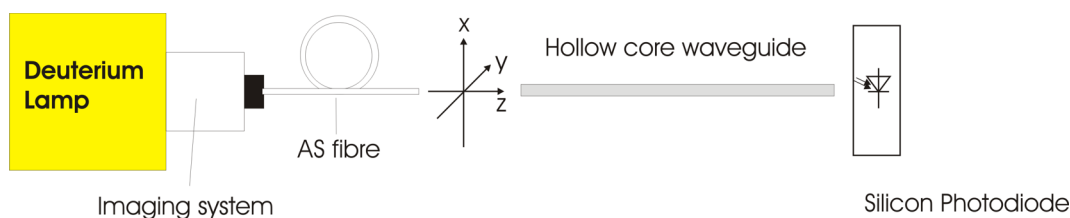


Figure 5.2: Measurement setup for determination of coupling efficiency

The results for the 1000 μm hollow core waveguide for displacement in x direction are shown in figure 5.3. Due to the rotational symmetry of the waveguides, only the measurements for displacement along the x-axis are shown. A displacement in x and y direction is not critical, as long as the displacement of the fibre is smaller than 0.2 mm from the centre of the HCW, which equals half the difference of the diametres.

The results for the 500 μm hollow core waveguide for displacement in x direction are shown in figure 5.4. The coupling of the two waveguides requires a higher precision as displacement of 0.2 mm results in a loss of almost 25 %.

The influence of the displacement in z-direction is shown in figure 5.5. The power at the detector has been normalized in order to simplify the comparison of both measurements. The relative losses due to displacement in the z axis were not that critical, due to the low numerical aperture of the waveguides. In the case of a fibre-optic absorption cell, this property can be used as an advantage as feeding the gas into the hollow core waveguide is necessary.

The coupling efficiency from the hollow core waveguide into the fibre was determined by reversing the system. The amount light coupled from the hollow core waveguide into a fibre is strongly influenced by the overlapping area of

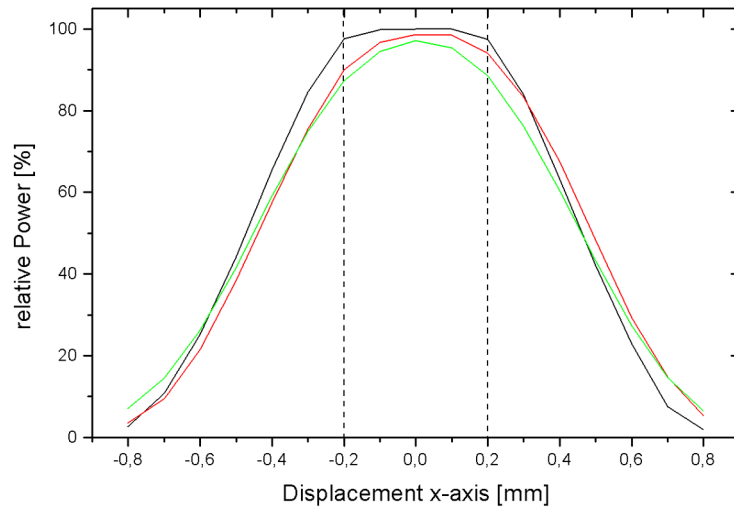


Figure 5.3: Measurement of coupling efficiency with displacement along the x-Axis, Distances fibre endface - HCW1000: 1 mm (black), 3 mm (red), 5 mm (green)

the HCW and the exiting fibre. Measurements have been carried out with the setup shown in figure 5.2, but light source and detector were exchanged. Due to the mismatch in the area of the 1mm HCW compared to the optical fibre a high loss was expected. The measurements showed a loss of 65 %, which can be expected by the ratio of the endfaces, whereas the loss for the small HCW was only 15 %.

If the whole absorption cell setup is compared to two coupled all silica fibres the coupling efficiency is rather low, 25 % transmission were determined in first tests. However, due to the difference in numerical aperture and area, tolerances in the alignment are not critical to the performance of the measurement.

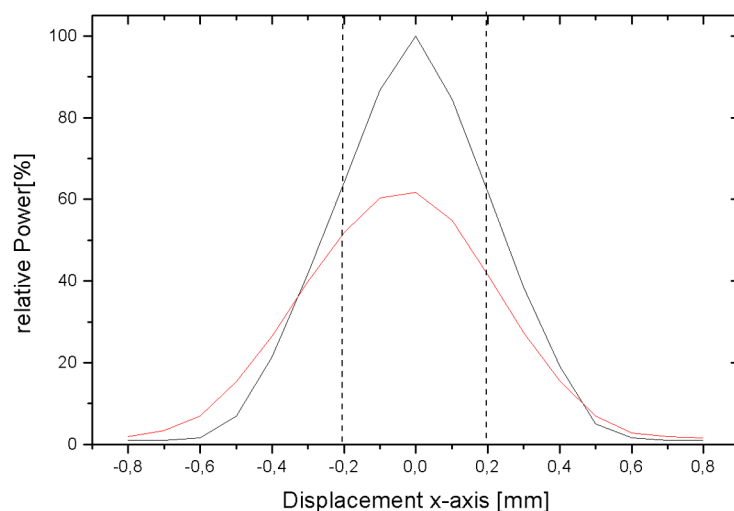


Figure 5.4: Measurement of coupling efficiency with displacement along the x-Axis, Distances fibre endface - HCW500: 1 mm (black), 5 mm (red)

5.4.2 Dimensions of absorption cell

For the use of an optical absorption cell as a gas chromatographic detector the influences of the cell dimensions to the measured signal has to be discussed. For the development of a Infrared [Giss and Wilkins, 1984; Griffiths, 1977] and ultraviolet absorption cell [Müller, 1992] some parameters have been described. The Beer-Lambert-Beer's law states the absorptions linear behaviour depending from the optical path length, as described in formula 1-11. The volume of the cell is dependent from the optical path length, which influences directly the time constants for the GC detection system.

The separated gas compounds reach the end of the separation column as "gas plugs", as shown in figure 5.6. In order to quantify, the grade R of separation has been introduced:

$$R = \frac{2(t_{dr,1} - t_{dr,2})}{w_1 + w_2} \quad (5-3)$$

In figure 5.7, two Gaussian peaks, with their corresponding retention time $t_{dr,i}$

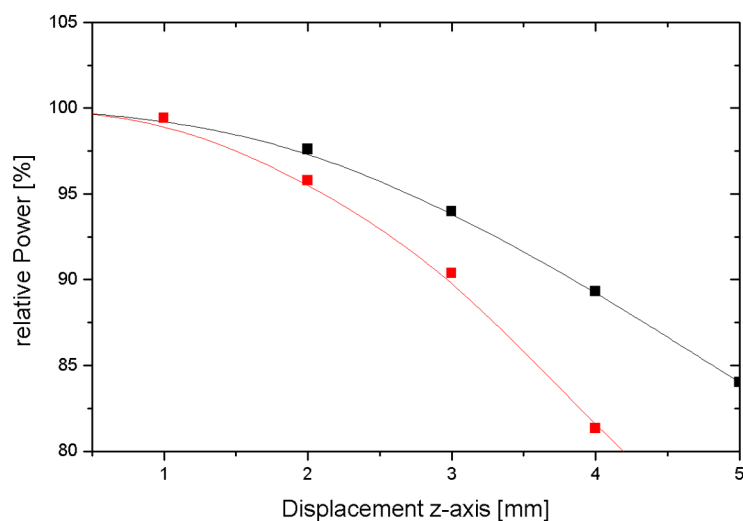


Figure 5.5: Measurement of coupling efficiency with displacement along the z-Axis, HCW1000 (black), HCW500 (red)

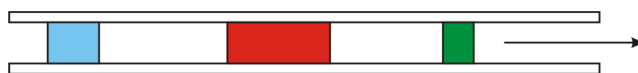


Figure 5.6: Schematic drawing of a "gas plugs" within the separation column

and width w_i are shown. A good grade of separation is reached, when the Gaussian absorption peaks do not overlap ($R > 1$). In the case of a measurement cell with negligible dead volume, a signal $S_{GC}(t)$ can be measured. In the case of larger volumes, the use of make-up gases is accepted for GC detectors: The additional gas compensates the volume difference and the peak is moving with the same speed through the detector. The influence of the cell volume can be described analogue to a convolution:

$$S_{UV}(t) = \int_{-\infty}^{+\infty} w_{cell}(\tau) \cdot S_{GC}(t - \tau) d\tau \quad (5-4)$$

The time-equivalent volume w_{cell} of the absorption cell, estimated as a rectangular window function, is correlated with the time signal of the GC effluent

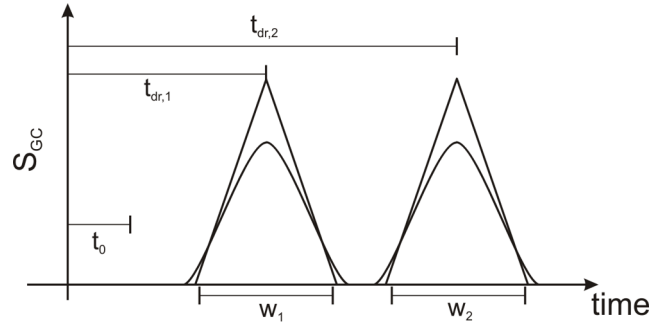


Figure 5.7: Schematic drawing of a chromatogram

$S_{GC}(t)$ and resulting in the detected UV-signal $S_{UV}(t)$. Depending on the cell volume, the resulting signal is shown in figure 5.8: A simulation based on an ideal signal, consisting of a Gaussian peak with normalized height and a width w_p of 2 s. As time-equivalent absorption cell volumes rectangular windows with a width of 0.2, 1, 2 and 4 seconds and a height of 1 have been used. For cell volumes significantly smaller than the peaks width ($w_{cell} \ll w_p$) the resulting peak broadening can be neglected, however, the absorption occurring due to the low absorption length is low, as demonstrated with a time-equivalent absorption cell volume of 0.2 s. With increasing length of the absorption cell, the intensity of the absorption increases, until the approximate peak length is reached ($w_{cell} \approx w_p$), as demonstrated with a window of 2 s. For longer path lengths, the peak is travelling through the absorption cell, without influencing the intensity of the absorption values. However, the peak duration increases, which is influencing the separation of the peaks, as shown with a window of 6 s length. In addition, the optimum situation can be found, when the Signal $S_{UV}(t)$ is differentiated: The gradient of the UV-signal should only intersect the x-axis, when the peak is travelling through the cell. For a time-equivalent cell volume, which is larger, the gradient is zero within the UV-signal. Figure 5.9 shows the UV-signal and its differentiation near the optimum ($w_{cell} \approx w_p$) and for an absorption cell with a significantly larger volume ($w_{cell} \gg w_p$).

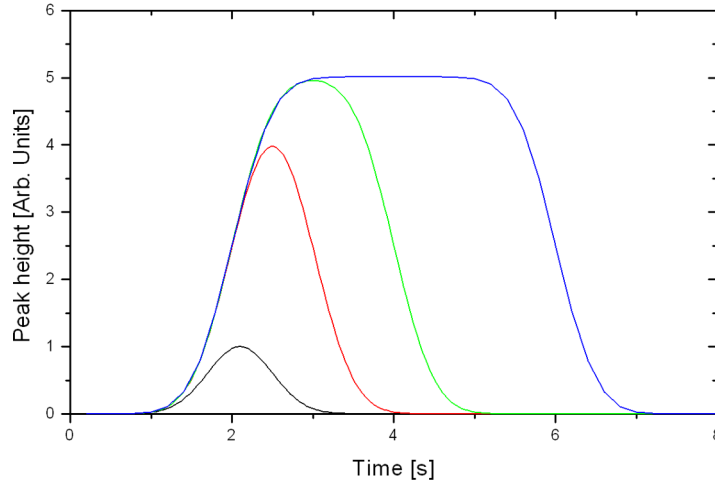


Figure 5.8: Simulated influence of time-equivalent volume on chromatographic resolution: 0.2 s (black), 1 s (red), 2 s (green), 4 s (blue)

According to previous considerations, the optimum length of the absorption cell is depending on the length of the absorption peak L_p . This can be estimated by the volume of the peak, which is the product of the flow rate, F , and the peak duration w_p :

$$L_p = \frac{F \cdot w_p}{A_{cell}} \quad (5-5)$$

In addition, the cross-sectional area (CSA) of the measurement cell A_{cell} influences the peak length:

$$A_{cell} = \frac{(d_{Cell})^2}{4} \cdot \pi \quad (5-6)$$

In table 5-1, the length of the absorption peaks have been calculated for a flow rate of 2 ml/min and a peak duration of 1 s, according to formula 5-5.

Considering an average flow rate of 2 ml/min and an average peak length during the gas chromatographic separation, an absorption length of approx. 10 cm was realized with a 750 μm hollow core waveguide. This hollow core waveguide

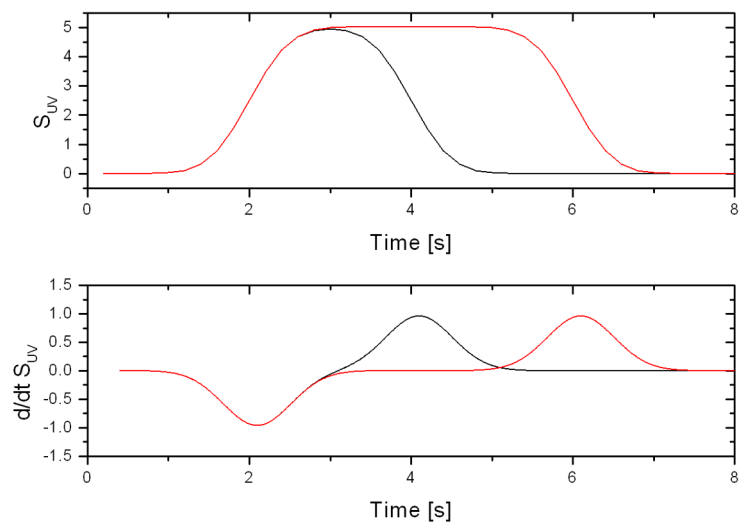


Figure 5.9: Simulated UV-signal (top) and differentiated UV-signal (bottom) for time-equivalent volume of 2 s (black) and 4 s (red)

was chosen for the following tests as the optical coupling efficiency and the absorption length were a good compromise.

5.4.3 Construction and Heating of the measurement cell

The absorption cell, when used after a gas chromatographic separation has to be heated in order to prevent the condensation of vapours and causing an in-

Table 5-1: Absorption peak length for 2 ml/min flow and 1 s peak duration

Capillary ID	0.32 mm	0.5 mm	0.75 mm	1 mm
CSA of Cell $A_{cell}[10^{-3} \cdot mm^2]$	80.4	196.3	441.7	785.4
Velocity [cm/s]	41.45	16.98	7.55	4.24
Peak length [cm]	41.45	16.98	7.55	4.24

creasing absorption within the cell. For this reason, an electrically heated and insulated housing was newly developed, including insulation and a surrounding protective air flow to keep the outer walls at a touch proof temperature. In addition a heated transfer line was constructed in order to transport the GC effluent from the GC-oven into the measurement cell, and eventually back to an additional downstream detector, an overview of a complete system is given in figure 6.5. In order to maximize the light power the optical light path was aligned linear, and the transfer line was attached with a 90 degree angle at the first gas tight fitting. Modified GC tee fittings and precision ferrules have been used for aligning fibres and hollow core waveguide in the measurement cell. Within figure 5.10 the cell setup, the optical light path and the gas flow is illustrated.

During first measurements, thermal stability of the measurement system

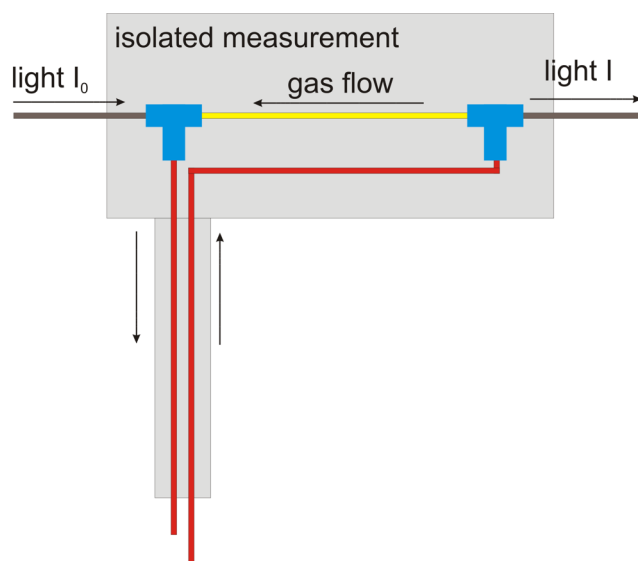


Figure 5.10: Cell setup

was analyzed. The absorption cell was kept at temperatures between 180 and 250 °C, without a measurable degradation of the optical performance, when purged with the carrier gas helium of the GC. As constant heating is necessary

for this type of measurement cell, a flexible heating element from Thermocoax, with a power output of approx. 135 W at a supply voltage of 48 V has been used. The temperature was measured near the absorption cell, with a thermocouple. A proportional plus integral plus derivative (PID) controller connected with a linear power setting circuit was used to control the temperature within the measurement cell.

5.5 Summary

The influence of displacement in the alignment of optical waveguides, have been analyzed in a view of the coupling efficiency. Low tolerances ($\leq 0.1\text{ mm}$) are necessary if the additional loss, due to axial displacement should not exceed 10%. However, low coupling efficiency have to be expected due to the mismatch of diameter and numerical aperture. In addition, the volume situation is a central point for the development of a gas chromatographic sensor. Within this chapter, the influence on tolerances in the alignment on the coupling efficiency have been analyzed. Additionally, the realization of a cell setup with heating and insulation is necessary to avoid condensation of the vapours within the measurement cell, because condensation will influence significantly the sensitivity of the detection system.

References

- P. Chambers, W. Lyons, E. Lewis, T. Sun, and K. Grattan. The potential for development of an NH₃ optical fibre gas sensor. *Journal of Physics, Conference Series*, 85, 2007.
- G. N. Giss and C. L. Wilkins. Effects of lightpipe dimensions on gas chromatography/ fourier transform infrared sensitivity. *Journal of Applied Spectroscopy*, 38, Number 1:17–20, 1984.
- P. R. Griffiths. Optimized sampling in the gas chromatography-infrared spectroscopy interface. *Journal of Applied Spectroscopy*, 31, Number 4:284–288, 1977.
- W. Kaye. Far-ultraviolet spectroscopic detection of gas chromatograph effluent. *Anal. Chem.*, 34:287–293, 1962.
- R. Kötschau. *Characterization of UV-Hollow Core Waveguides for the application in spectroscopy of gases, in german*. Diploma thesis, University of Applied Sciences Giessen-Friedberg, Germany, 2002.
- V. Lagesson. *Micro gas chromatographic separation combined with UV- and IR-spectrophotometric detection/identification with applications within the occupational hygiene field using diffusive and active sampling followed by a direct thermal desorption technique*. PhD thesis, University of Göteborg & University of Linköping, Sweden, 1992.
- P. Müller. *Development of an UV spectrometric detectors for gas chromatographic applications, in German:” Entwicklung eines UV-spektrometrischen Detektors für die Gaschromatographie”*. PhD thesis, University Würzburg, 1992.
- M. Schnaiter, O. Schmid, A. Petzold, L. Fritzsche, K.-F. Klein, M. Andrae, G. Helas, A. Thielmann, M. Gimmler, O. Möhler, C. Linke, and U. Schurath.

References

- Measurements of wavelength-resolved light absorption by aerosols using a UV-VIS extinction cell. *Aerosol Science and Technology*, 39:249–260, 2005.
- S. L. Smith, S. E. Garlock, and G. E. Adams. Industrial applications of a capillary gas chromatography/fourier transform infrared system. *Journal of Applied Spectroscopy*, 37, Number 2:192–196, 1983.
- R. Syms and J. Cozens. *Optical guided waves and devices*. McGraw-Hill Book Company, England, 1992.
- J. White. Long optical paths of large aperture. *J. Opt. Soc. Am.*, 32:285, 1942.

6 Measurements with GC-UV Detection systems

6.1 Introduction

The detection of gas chromatographic effluent by means of qualitative ultraviolet spectroscopy [Kaye, 1962; Lagesson, 1992; Müller, 1992] has already been reported. However, the time necessary for full-spectrum measurements on the one hand and the changes within the components of the detection system, such as solarization effects were taken into account as major drawbacks of this measurement technique. Even in the wavelength range above 200 nm stronger absorptions of gases, compared to the mid infrared wavelength region, have been measured. Within this chapter, gas chromatographic measurements were carried out with different detection systems to optimize an existing system and in addition, to identify possible constrictions for the fibre-optic measurement system.

Essential measurements, such as the determination of the measurement systems linearity was performed. In addition, the first coupling of a gas chromatographic separation with an ultraviolet and a mass selective detector is reported.

6.2 Measurements with existing GC-UV detector

An existing GC-UV detection system, as described in [Lagesson et al., 2000] has been used for the first tests. The schematic setup of this measurement system is shown in figure 6.1. The system consists of a 30 W Hamamatsu deuterium lamp with an attached imaging optics, a gas flow cell with integrated micro separation and an Oriel Spectrograph MS125 with a 1200 l/mm holographic plane grating and a photo diode array with 1024 pixels. The wavelength range was adjusted from 168 to 330 nm and a typical spectral resolution of 1.6 nm was used. The gas flow cell had a length of 10 cm and a diameter of 1.6 mm

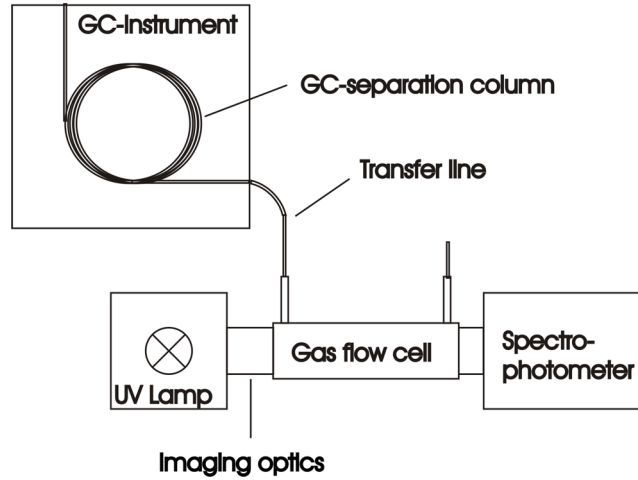


Figure 6.1: Schematic setup

resulting in a volume of approx. 200 μl . In order to compensate the difference in volume compared to a gas chromatographic separation column, make-up gas was added. With the described measurement setup a variety of applications have been reported [Hatzinikolaou et al., 2006; Jones et al., 1995; Lagesson et al., 2000; Nilsson, 2004].

For the determination of the systems stability, a GC run has been performed without an injection. The acquired absorption spectra $A(\lambda, t)$ were stored over time t and converted into a 3 dimensional file. The chromatogram $\bar{A}(t)$, which is a mean value over the absorption in a wavelength range has been calculated with following formula:

$$\bar{A}(t) = \frac{1}{\lambda_{max} - \lambda_{min}} \sum_{\lambda_{min}}^{\lambda_{max}} A(\lambda, t) \quad (6-1)$$

For the measurement described above, the chromatogram can be seen in figure 6.2, with $\lambda_{min}=185$ nm and $\lambda_{max}=300$ nm. The relative high dynamic of the baseline, which is repeating within 25 s influences the systems dynamic strongly: The instable baseline may hinder or inhibit the detection of minor components within the GC effluent. By analyzing this measurement, the in-

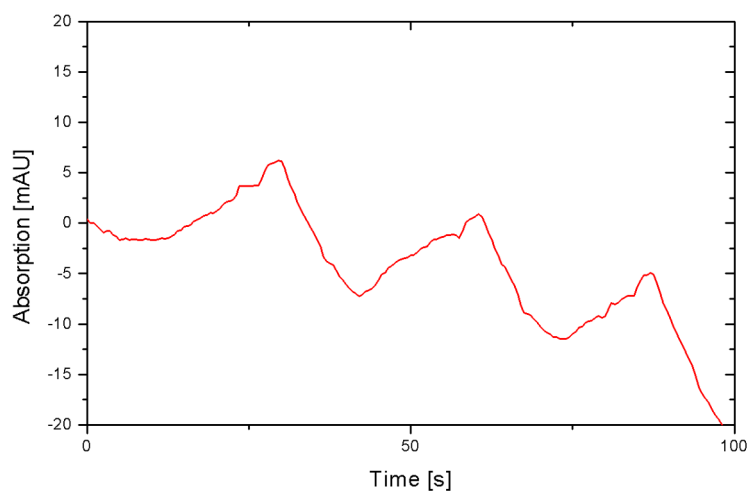


Figure 6.2: Chromatogram for wavelength 185 to 300 nm

stability of the baseline, which is caused by a changing absorption below 190 nm, was related to a change in temperature: The on-off controller, which was used, had a hysteresis which caused an oscillation of 2°C around the set point. For the evaluation of the measurement system an UV test sample was prepared according to table 6-1 and measured. The GC method and data acquisition parameters are shown in table 6-2. In addition, the temperature controller was replaced with a proportional plus integral plus derivative controller and a solid state relay switching the AC heating current. In order to attach the ultraviolet detection system to the gas chromatograph for this experiment, a modification of the transfer line was necessary: A resistance wire and the capillary were put into a silicon hose, which was wrapped with aluminium for insulation.

The chromatogram obtained is shown in figure 6.3, calculated for wavelengths between 185 and 300 nm. The deformed solvent peak, which is not shown in the graph, has a maximum absorption that is higher than the dynamic range of the system. The tail of the absorption peak (A) and the three peaks of the compounds Ethylbenzene (B), Bromobenzene (C) and Butyrophenone (D) are

Table 6-1: Composition of UV test sample

Compound	Concentration [mg/ml]	CAS	Boiling point [°C]
Ethylbenzene	1	100-41-4	136
Bromobenzene	0.9	108-86-1	156
Decalin	1	91-17-8	190
cis-decahydronaphtalene		493-01-6	193
trans-decahydronaphtalene		493-02-7	187
Butyrophenone	0.98	495-40-9	228
Diphenyl Sulfoxide	0.9	945-51-7	70.85
Carbon disulfide	ad 1 ml	75-15-0	46

Table 6-2: GC method and data acquisition parameters

Oven initial temperature	40°C
Initial time	3 min.
Rate	50°C/min
Final temperature	200°C
Final time	2
Injector temperature	250°C
Injection volume	1 μ l
Split ratio	28:1
Temperature of UV Detector & transfer line	180°C
Separation Column	FS-SE-54-DF-0.10, 25 m, 0.32 mm
Carrier gas	Helium
Carrier flow rate	approx. 2 ml/min
Flow rate absorption cell	approx. 5 ml/min
Integration time	500 ms
Accumulations	2
Number of acquired Spectra	500

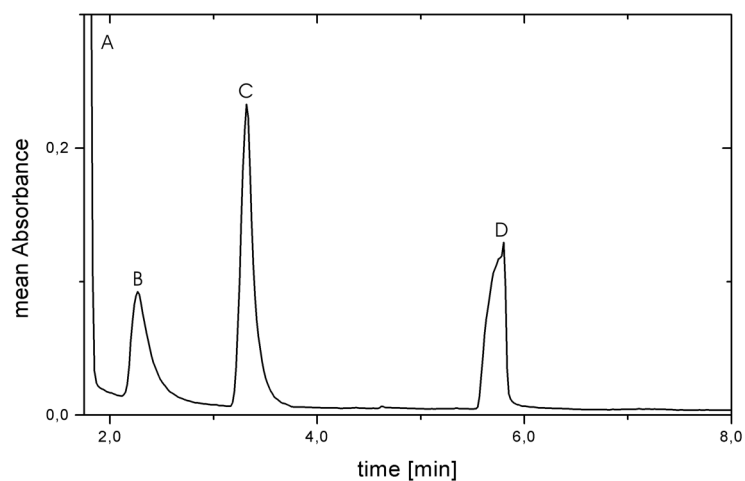


Figure 6.3: Chromatogram of UV test sample, calculated from 185 to 300 nm

clearly visible. The broader peaks can be accounted for the improvisational transfer line, which does not prevent the components within the sample to condensate, due to insufficient heating. However, the stability of the baseline was improved and oscillations over the measurement time were avoided.

For the development of the fibre-optic based detection system the temperature control, the inadequate insulation and heating of the transfer line have been identified as additional constrictions. The measurement of the samples showed absorption spectra, which allow identification of the molecules measured within the gas flow cell.

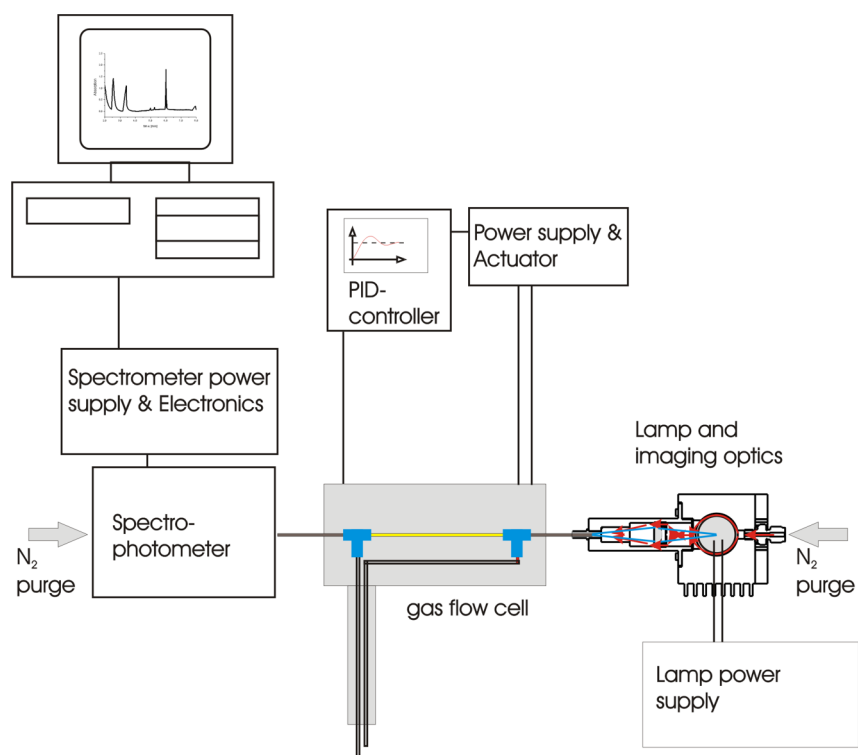


Figure 6.4: Schematic measurement setup of fibre-optic UV detection system

6.3 Characterization of fibre-optic UV detection system for gas chromatography

6.3.1 Fibre-optic UV detector

The fibre-optic UV detection system realized is shown in figure 6.4. The system comprises the following components:

- Nitrogen purged spectrophotometer with electronics and power supply
- Fibre-optic gas flow cell
- Housing for gas flow cell with isolation, heating element and temperature sensor
- Nitrogen purged deuterium lamp system, imaging optics and power supply
- Computer with customized program for data acquisition and analysis

The spectrometer and the lamp source were nitrogen purged. The measurement cell was attached with GC fittings to the gas chromatographic separation column, on the entrance side and to the transfer line of the mass spectrometer downstream. The full measurement setup is shown in figure 6.5, including the illustrated path of GC effluent.

6.3.2 Measurement of systems short-term noise and drift behaviour

As discussed within the introduction, the behaviour of the three intensities measured influence strongly the relative error on an absorption measurement: While the noise of all signals should be rather low, the reference intensity should be high in order to minimize the relative error, as stated in formula 1-20. A blank intensity spectrum is shown in figure 6.6. In the wavelength region below 185 nm the intensity decreases, due to the materials intrinsic

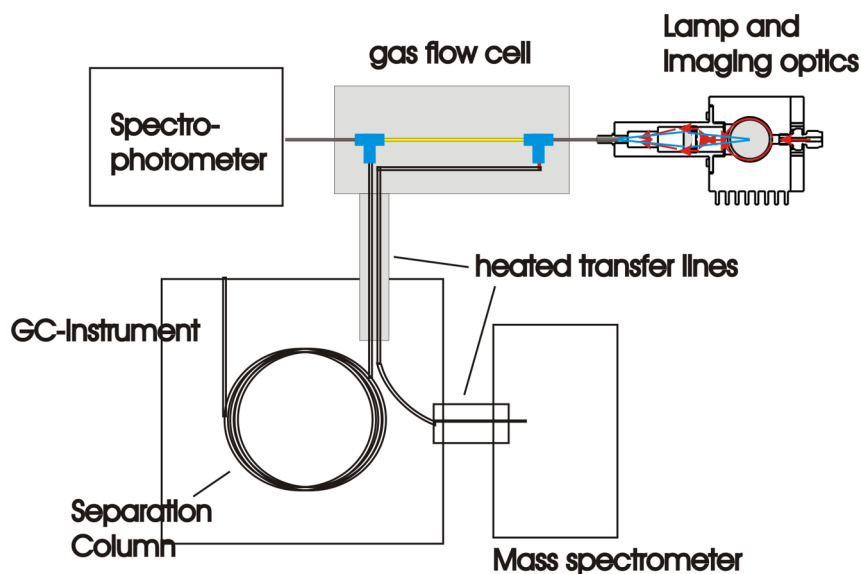


Figure 6.5: Measurement setup for the characterization of the UV detection system, illustrating the path of GC effluent within the system

losses and the decreasing quantum efficiency of the detector. In the wavelength range above characteristic white light interferences of the detectors are visible, with a width of approx. 10 nm. With the measurement procedure described in chapter 3.5, the short-term noise and drift behaviour of the measurement system was characterized. Over a 15 minutes period of time, spectra have been acquired with an integration time of 900 ms. This measurement time was chosen, as the attached mass spectrometer needed the same time for a full scan. During the measurements, the whole system, including GC oven, mass spectrometer and attached vacuum pumps have been in operation. The absorption value was extracted at the wavelengths 180, 186, 200 and 217 nm. Afterwards, the obtained chromatograms have been analyzed according to [ASTM, 1993]. In figure 6.7, the time dependent change of the absorption value at 186 nm is shown. Additional measurement plots are in the appendix A-1.

Within the plots of 186, 200 and 217 nm an oscillation with a period of approx.

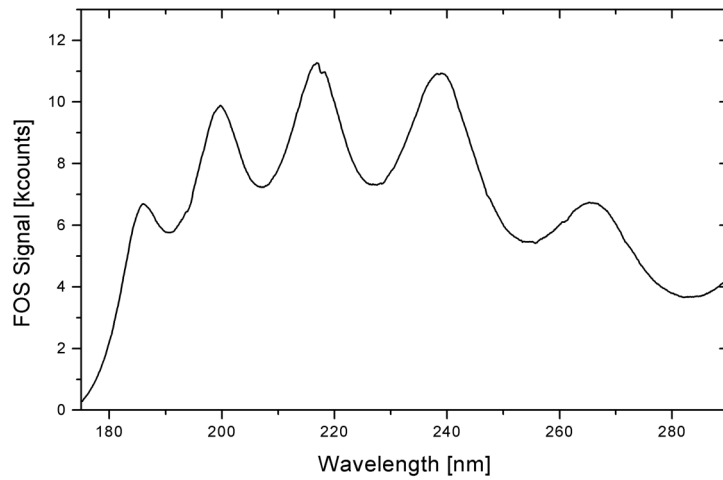


Figure 6.6: Intensity signal of the measurement system, flushed with nitrogen at a temperature of 180 °C

1.2 minutes is visible. This oscillation additionally influence the noise and drift values gathered. The used PID controller with attached temperature sensor indicated oscillating temperatures and an additional temperature offset, when tested at room temperature.

Table 6-3: Noise and drift behaviour of fibre-optic measurement system under operation conditions

Wavelength	Noise [mAU]	Drift [mAU]
180	2.6	5
186	1.3	4
200	1.1	2.25
217	1.1	0.5

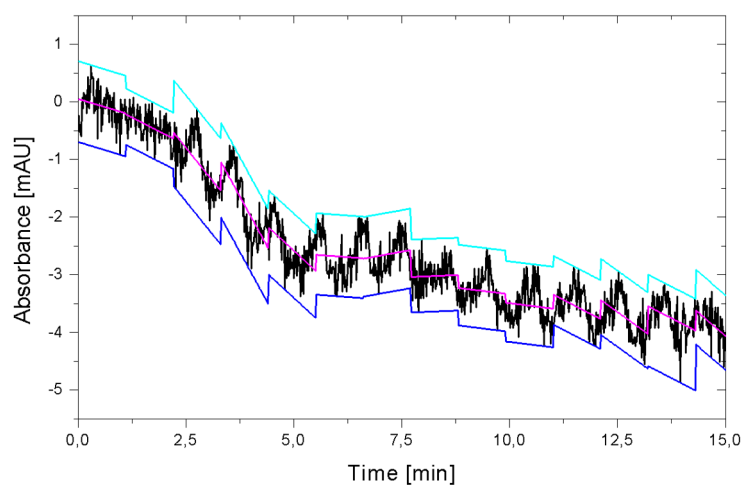


Figure 6.7: Determination of short time stability, at a wavelength of 186 nm, under Measurement conditions

6.4 Measurements with fibre-optic UV detection system for gas chromatography

6.4.1 Measurement of UV Test sample

The UV test sample, as described in table 6-1 was measured with fibre-optic UV detection to gather information on the improvement of the detection system. The measurement program was carried out analogue to the conditions described in table 6-2. The temperature of the measurement cell and transfer line was set to 180°C. The optimized volume of the gas flow cell allowed a measurement without make-up gas. However, due to the higher sensitivity of the measurement and the strong absorption of the solvent, the initial time was increased to 4 minutes to obtain a better separation of ethylbenzene from the carbon disulfide. The chromatogram of the UV detection is shown in figure 6.8. The absorption of the compounds contained within the UV test sample are shown in figure 6.9.

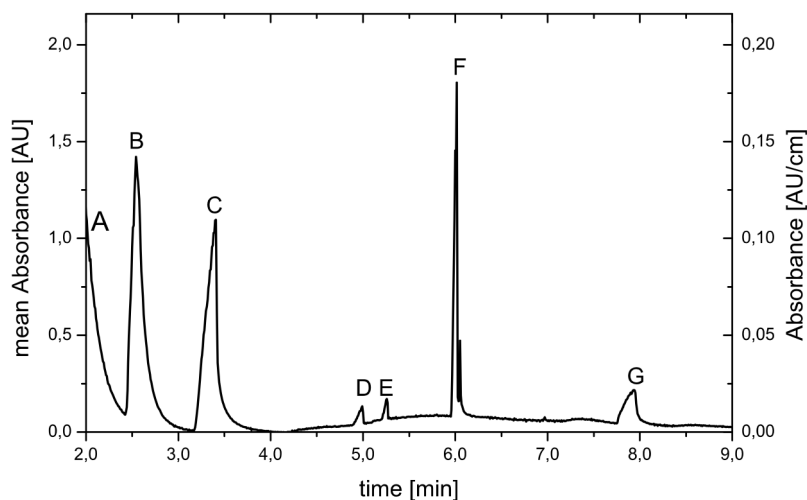


Figure 6.8: Chromatogram of the UV test sample, detected with the UV detector

The gas chromatographic peaks are baseline separated, which would be sufficient for identification. Due to the low dead volume of the absorption cell and the absence of additional make-up gas, the absorbance peaks are very sharp. Again, the tail of the solvent peak is visible (A). It is followed by ethylbenzene (B) and bromobenzene (C). The following two peaks of the isomers of decahydronaphthalene (D and E) around 5 min retention time are rather weak, due to their unspecific absorption in the low wavelength range. Butyrophenone (F) and diphenyl sulfoxide (G) can be detected very well.

6.4.2 Linearity and minimum detection limits

As a test for the linearity of the measurement device, a series of UV test samples were prepared. The lower concentrations have been diluted from the mixture described in table 6-1, by a factor of 5 and 10, respectively. In order to test the linearity for higher concentrations, a new mixture was prepared: In this

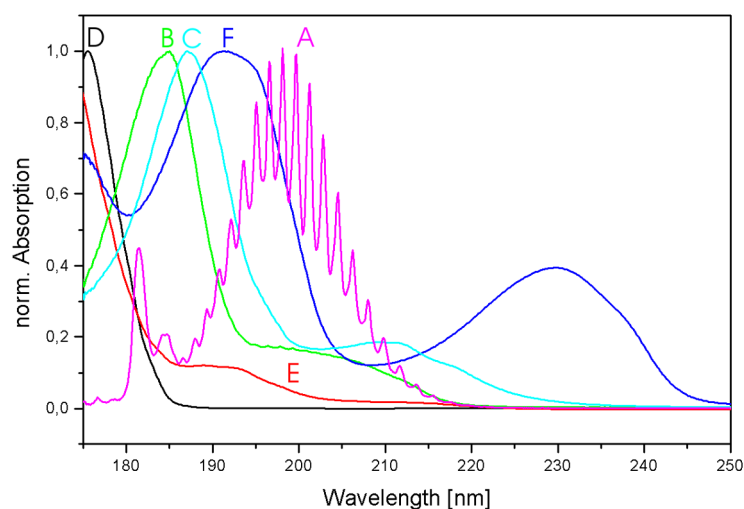


Figure 6.9: Absorption spectra of the compounds within the UV test sample, Carbon disulfide (A), Ethylbenzene (B), Bromobenzene (C), trans-decahydronaphtalene (D), cis-decahydronaphtalene (E) and Butyrophenone (F)

mixture, all components have been prepared in with the double concentration, except diphenyl sulfoxide, which had approx. 5 times the concentration compared to the UV test sample. For the quantification, the chromatograms have been extracted in two ways: Firstly, with the wavelength limits confining the maximum absorption of the compounds, analogue to formula 6-1. Secondly, with an auto correlation of the highest absorption spectrum of the specific component measured, according to the following formula:

$$C(t) = \sum_{\lambda_{min}}^{\lambda_{max}} (A(t, \lambda) * A(comp, \lambda)) \quad (6-2)$$

In above equation, the value of the chromatogram $C(t)$ at a specific time t is calculated as the sum of the product of the single wavelength values of the maximum absorbance spectrum $A(comp, \lambda)$ of the specific compound and the measured absorption spectrum $A(t, \lambda)$. After the chromatogram has been

Table 6-4: Measurement of linearity, absorption peak area based on chromatogram, absolute percentual deviation in brackets

Concentration Compund	2	1	0.2	0.1
Ethylbenzene	27.18 (6 %)	12.86	2.51 (3 %)	1.25 (3 %)
Bromobenzene	30.52 (12 %)	17.26	3.63 (5 %)	1.81 (5 %)
Decahydronaphtalene 1	0.41 (11 %)	0.23	0.03 (35 %)	0.02 (24 %)
Decahydronaphtalene 2	0.32 (6 %)	0.17	0.04 (17 %)	0.02 (21 %)
Butyrophenone	11.25 (14 %)	6.54	1.427 (9 %)	0.73 (11 %)
Diphenyl Sulfoxide	2.47 (34 %)	0.37	0.07 (5 %)	0.06 (69 %)

Table 6-5: Measurement of linearity, absorption peak area based on correlation method, absolute percentual deviation in brackets

Concentration Compund	2	1	0.2	0.1
Ethylbenzene	6261 (4 %)	3271	515 (27 %)	241 (35 %)
Bromobenzene	7981 (11 %)	4431	825 (1.7 %)	456 (2.9 %)
Decahydronaphtalene 1	2.7 (1.8 %)	1.4	0.2 (24 %)	0.1 (28 %)
Decahydronaphtalene 2	1.9 (12 %)	1.1	0.2 (30 %)	0.1 (13.9 %)
Butyrophenone	4746 (14 %)	2709	537 (0.9 %)	268 (0.98 %)
Diphenyl Sulfoxide	85 (8 %)	16	3 (5 %)	1.9 (16 %)

extracted, the area of the absorption peaks have been integrated. The resulting areas are shown in table 6-4 based on the chromatogram. Table 6-5 shows the data based on the correlation. The calculation of the chromatogram according to the first method was resulting in higher deviations.

The measurements of the linearity have been carried out in the time frame of one day, without an internal standard. The measurements of the lower concentrations show low deviation from the expected values for the compounds bromobenzene and butyrophenone. The other compounds show higher deviations from the expected values, especially the two isomers of decahydronaph-

talene, in low concentrations, and ethylbenzene, which is the first compound after the solvent peak. The concentrations of the compounds in the highest concentrations were not verified by an additional detection method. A more detailed study on the linearity of the measurement system needs to be carried out with an additional internal standard. The use of an autosampler unit will additionally reduce the statistical error caused by the manual injection.

However, for the measured components low detection limits can be calculated: With the given split ratio of 28 : 1 and a injection volume of 1 μ l, the absolute weight of all components is in the low nanogram range. Especially Ethylbenzene (3.5 ng), Bromobenzene (7.1 ng) and Butyrophenone (3.5 ng) can be detected very efficiently. The detection of diphenyl sulfoxide with 10 ng. Both isomers of decahydronaphthalene lack a high absorption band in the ultraviolet wavelength region and therefore can not be measured in low quantity.

6.5 Coupling of fibre-optic GC-UV system with a mass spectrometer (GC-UV-MS)

The combination of the mass spectrometer with a gaschromatographic separation is often used if an identification and quantification of complex samples is necessary. However, due to the ionization process, the molecules have been fragmented, when reaching the detector, giving the abundance as a characteristic. For isomers, the information of the structure might not be derived easily by the mass spectrum. The combination of both might be advantageous, as can be seen in figure 6.10: The known test sample has been measured with the UV-Detector (top), and the mass spectrometer (bottom). The data acquisition of the mass spectrometer starts with a delay, which is necessary to protect the instruments filament when the solvent passes through the detector. A too high concentration of ionizable gas might lead to a destruction of the filament. Therefore, the ethylbenzene peak is not detected. Following the

bromobenzene, the both isomers of decahydronaphtalene are clearly visible at a retention time of approx. 5 minutes. In the UV detector these isomers produce significantly lower peak heights in the chromatogram, due to their rather unspecific absorption characteristic above 180 nm. Butyrophenone is detected by both systems, whereas Diphenyl sulfoxide can be measured only in the UV detector.

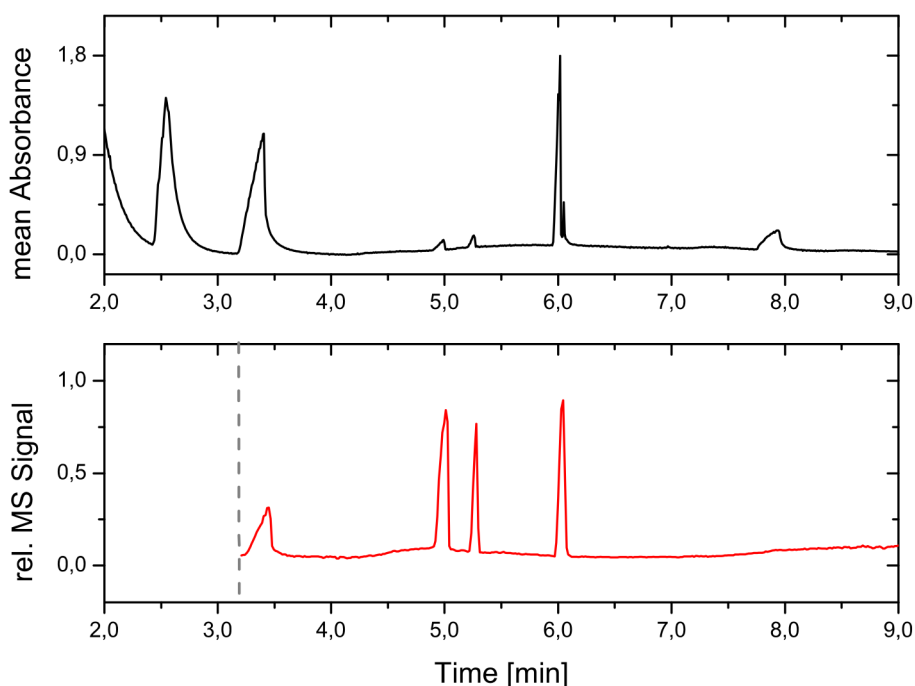


Figure 6.10: Chromatogram of the UV test sample, detected with the UV detector (top) and the mass spectrometer (bottom)

6.6 Comparative measurements with modified sample

The coupling of the fibre-optic UV detector and the downstream mass spectrometer allowed a direct comparison of both detectors. In addition, the mass spectrometer was used as a reference detector. A new test sample was pre-

Table 6-6: Composition of UV/MS test sample

Compound	Concentration [mg/ml]	CAS	Boiling point [°C]
Ethylbenzene	500	100-41-4	136
Bromobenzene	1000	108-86-1	156
Butyrophenone	500	495-40-9	228
Cyclohexane	ad 1 ml	110-82-7	69

pared, according to table 6-6. The test sample has been diluted by the following ratios 1:10, 1:50, 1:100 and 1:500 in order to test the linearity of the detector, and compare the characteristics. The measurement series was carried out with an injection volume of $1\ \mu\text{l}$. The temperature program of the GC instrument was suitable to achieve a good separation of all components. Three measurements have been carried out for all concentrations in order to gather information of the systems uncertainties.

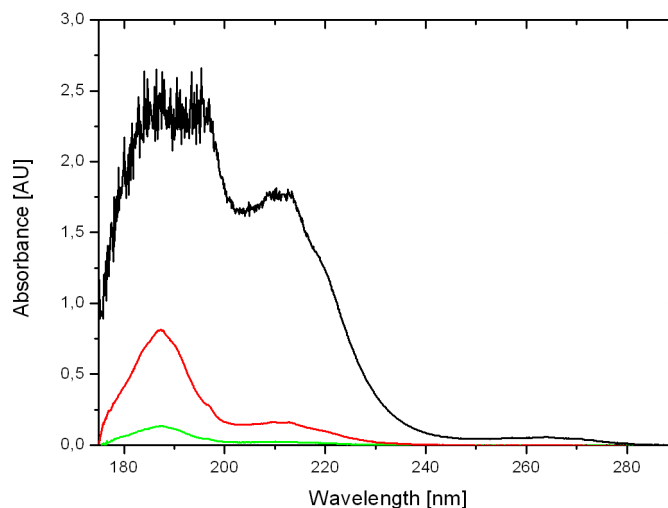


Figure 6.11: Absorbance spectra of bromobenzene for a sample containing 1000 (black), 100 (red) and 10 ng (green)

In table 6-7 the calculated peak areas for the UV and the MS detector are

Table 6-7: Calculated peak areas of the UV and MS detector, values with an asterisk have not been used

Dataset	Peak area UV			Peak area MS		
	Ethyl- benzene	Bromo- benzene	Butyro- phenone	Ethyl- benzene	Bromo- benzene	Butyro- phenone
<i>500μg</i>						
M500_1	370.68*	550.08*	235.26	5.558*	4.667*	14.300
M500_2	239.77*	567.65*	235.29	7.310*	11.650*	11.270
M500_3	234.41*	535.68*	223.85	5.675*	5.150*	7.542
<i>50μg</i>						
M50_1	53.98	120.59	23.56	1.499	3.605	1.813
M50_2	57.07	127.67	24.09	1.503	2.690	1.477
M50_3	52.23	116.26	22.90	1.652	2.902	1.504
<i>10μg</i>						
M10_1	9.50	20.68	4.27	0.369	0.489	0.268
M10_2	12.24	26.25	5.69	0.302	0.653	0.237
M10_3	10.45	22.04	5.16	0.342	0.608	0.321
<i>5μg</i>						
M5_1	5.90	15.69	2.65	0.187	0.458	0.134
M5_2	4.24	11.12	2.61	0.160	0.587	0.101
M5_3	4.93	12.60	2.17	0.153	0.335	0.126
<i>1μg</i>						
M1_1	1.37	3.40	0.65	0.077	0.211	0.035
M1_2		1.99		0.016	0.279	0.037
M1_3	1	2.06	0.52	0.013	0.330	0.018

shown. The data points, which are not used for the further analysis of the linearity are marked with an asterisk. At a total mass of $500\mu\text{g}$ and $1000\mu\text{g}$ for ethylbenzene and bromobenzene, respectively, the increase of the peak area is not proportional to the increase in concentration in both detection systems. The spectra in figure 6.11 explains the not linear increase of the peak area, as the absorption measured beyond the systems linear dynamic range. As an alternative, the quantification could be carried out in different wavelength intervals: Small quantities could be detected by correlation or in the maximum absorbance between 180 and 200 nm. For higher concentrations, the wavelength interval between 220 and 240 nm might be used, where the absorbance

Table 6-8: Correlation coefficients (R) and standard deviations (SD) of linear fit

Compound	UV detector		MS detector	
	R	SD	R	SD
Ethylbenzene	0.9975	7.6234	0.9975	0.46618
Bromobenzene	0.9981	3.2149	0.9811	0.24633
Butyrophenone	0.9996	2.7247	0.9909	0.63786

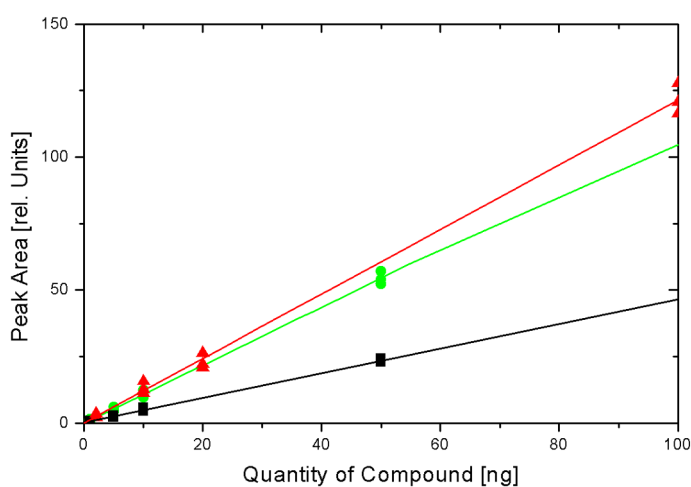


Figure 6.12: Linearity of Ethylbenzene (green), Bromobenzene (red) and Butyrophenone (black), measured with UV detector

signal is not saturated. With this procedure, the addition of make-up gas could be avoided. The additional volume flow of the make-up gas needs to be controlled precisely but would add another source of error to the measurement system. In addition, depending on the vacuum pump of the mass spectrometer maintaining the vacuum might be a problem. However, in respect to the data measured, the procedure was not tested, as the mass spectrometer showed a non-linear behaviour as well. The results in respect to linearity are displayed in 6.12. The peak areas of ethylbenzene (green), bromobenzene (red) and butyrophenone (black) increase linear with increasing quantity of the sample.

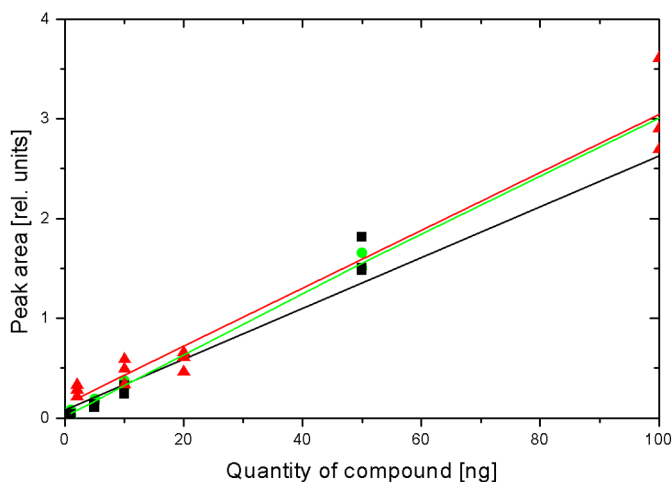


Figure 6.13: Linearity of Ethylbenzene (green), Bromobenzene (red) and Butyrophenone (black), measured with the MS detector

The slope of the linearity plots are depending on the molecules extinction coefficient. A calibration for all molecules is necessary in order to perform quantitative measurements. For the plots of the MS, which are displayed in figure 6.13 the slope show smaller dependency on the molecule. This may be attributed to the Abundance measured in this detector, which gives a total ion count as a result. However, the MS detection system requires a calibration for the specific components as well, when used as a quantitative detector. Correlation coefficients and standard deviations are shown in table 6-8.

6.7 Measurement on polycyclic aromatic hydrocarbons

In environmental testings, the presence and quantity of polycyclic aromatic hydrocarbons (PAH) is regularly tested. These compounds are insanitary and hazardous to the environment. A variety of methods have been developed to quantify the PAH in complex samples. Some of them require a different steps of

sample pretreatment in order to separate the PAH from interfering compounds. For known compositions, a gas chromatographic separation followed by FID detection may be sufficient as a quantitative analysis. If an identification of the components within a sample is desired, a mass spectrometer is used in most cases.

In the case of an insufficient separation the identification and quantification of the compounds might be difficult: In figure 6.14 the mass spectra of anthracene and phenantrene are shown. The ionization process causes the molecules to fragment in identical ions, due to the same total formula of both molecules ($C_{14}H_{10}$). The difference in structure accounts for a isotopic abundance.

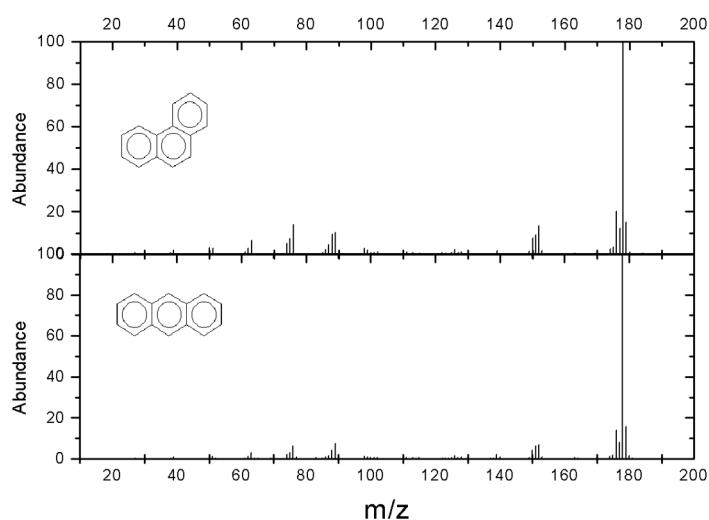


Figure 6.14: Mass spectra of phenantrene (top) and anthracene (bottom)

The detection in the ultraviolet wavelength region gathers information from the intact molecule in the vapor phase. Therefore, significant differences can be noticed in the absorption spectra of both molecules, as shown in figure 6.15. In addition to the peak near 237 nm, which can be observed in both molecules, phenantrene shows a unique absorption peak with a centre wavelength of 200 nm.

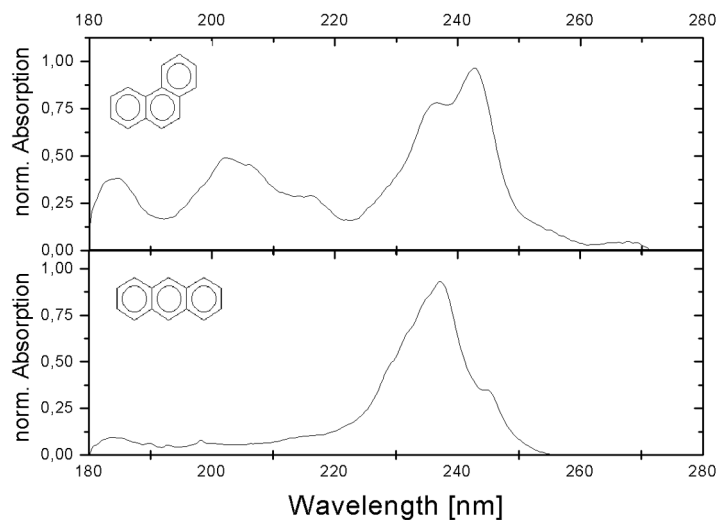


Figure 6.15: UV absorption spectra of phenantrene (top) and anthracene (bottom)

In order to compare both detectors in respect to their capability of identifying different molecules a sample containing 13 PAHs with a concentration of $10 \text{ ng}/\mu\text{l}$ was injected in the GC instrument. The obtained chromatograms are shown in figure 6.16. Most constituents can be detected and identified in a retention time between 5 and 25 minutes. An absorption peak is observed at 35 minutes which might be fluoranthene. The last detected compound is pyrene, with a corresponding retention time of 40 minutes. An overview on the detected PAHs, their chemical formula, molecular structure and boiling point is shown in table 6-9.

The high boiling points of these compounds afford a good choice of the separation column and temperature program. The influence on the temperature can be seen in figure 6.16, where the peak width increase with increasing retention time.

Due to the high boiling point of the PAHs some residual matter was moving through the cell rather slowly. On the reference spectra a decrease in inten-

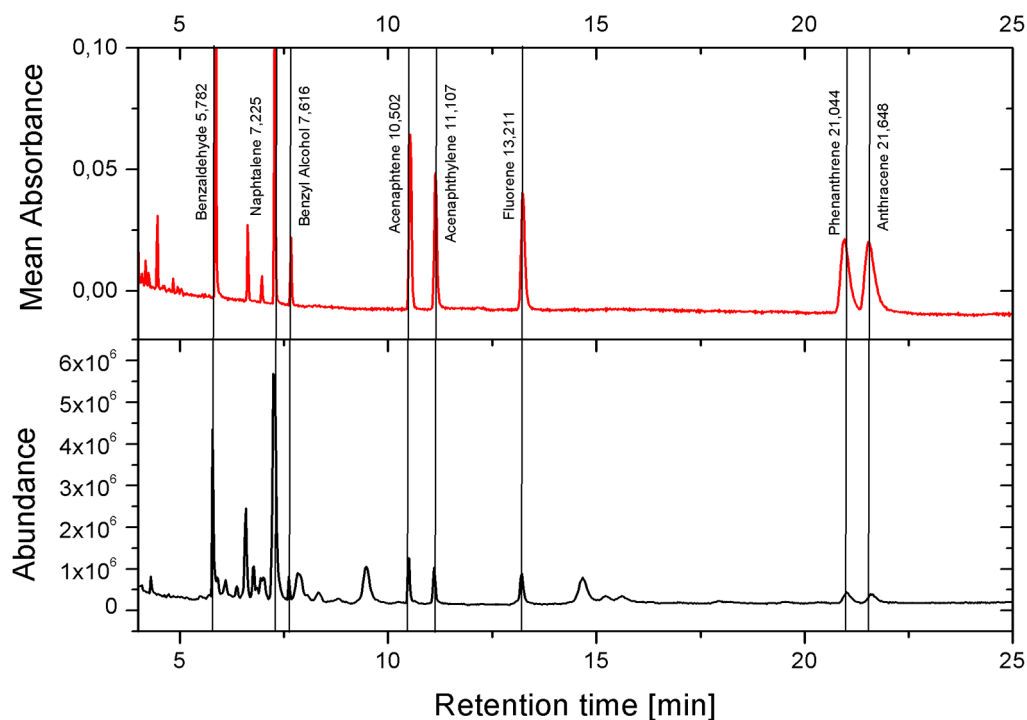


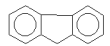
Figure 6.16: Chromatogram of the PAH sample, UV detector (top), MS detector (bottom)

sity was noticed. However, a heating of the measurement cell over night in combination with a continuous nitrogen flow could be used for the cleaning of the cell. Gas chromatographic separation columns are also heated in order to remove the residual analytes. Therefore, the cleaning procedure is well suited in the gas chromatographic context.

6.8 Summary

Within this chapter measurements with two ultraviolet detectors for gas chromatography have been discussed. The volume of the absorption cell, influencing the need for additional make-up gas, and the heating of the gas flow cell and the transfer lines have been identified as critical constrictions for the

Table 6-9: Overview on detected PAHs

T_{ret}	Compound	Total formula	Structure	boiling point [°C]	CAS
5.782	Benzaldehyde	C_7H_6O		179	100-52-7
7.225	Naphthalene	$C_{10}H_8$		217	91-20-3
7.616	Benzyl alcohol	C_7H_8O		205	100-51-6
10.502	Acenaphthene	$C_{12}H_{10}$		279	87-32-9
11.107	Acenaphthylene	$C_{12}H_8$		280	208-96-8
13.211	Fluorene	$C_{13}H_{10}$		298	86-73-7
21.044	Phenanthrene	$C_{14}H_{10}$		338	85-01-9
21.648	Anthracene	$C_{14}H_{10}$		340	120-12-7
35	Fluorathene	$C_{16}H_{10}$		383	206-44-0
40	Pyrene	$C_{16}H_{10}$		393	129-0-0

systems performance.

With the detectors a mixture of 5 compounds was measured, and the advantage of the absorption cells low volume, resulting in higher sensitivity of the measurement system, due to the absence of make-up gas was recognized.

With the fibre-optic detection system a short-time noise and drift characterization has been performed. The measurement system provides sufficient stability over a time frame of 15 minutes. Additionally, measurement runs with a total time of more than 40 min have been carried out, for the detection of PAHs, providing a good long-term stability. The partly open lamp, the nitrogen purged lamp housing and the stabilization of the cell temperature have been identified as additional points to optimize the stability of the measurement system.

The dilution of the UV test sample showed a good overlap with the expected concentration values for the components with strong absorptions in the ultraviolet wavelength region. Minimum detection limits in the nanogram range have been determined for all compounds within the sample. The first comparison with a mass selective detection system shows that both detection principles may complement each other, when used in a combination after a gas chromatographic separation.

Measurements have been carried out with a modified test sample to test the linearity in comparison with a MS detector. Masses between 1 and 500 μg could be measured linearly with both detection systems. The highest concentrations of ethylbenzene (500 μg) and bromobenzene (1000 μg) lead to a non-linear detector response in both detection systems.

The measurements of a sample containing 13 PAHs confirms the ability of the UV-detection system to detect compounds in the nanogram range. Additionally the molecules were identified by their characteristic absorption spectra. The combination of a UV and MS detection provides valuable additional information and is feasible as a successive detection, due to comparable sensitivities of both systems.

Finally, by heating the cell overnight and applying a continuous nitrogen flow a cleaning of the cell was achieved.

References

- ASTM. E685-93: "standard practice for testing fixed-wavelength photometric detectors used in liquid chromatography. Technical report, ASTM International, 1993.
- D. G. Hatzinikolaou, V. Lagesson, A. J. Stavridou, A. E. Pouli, L. Lagesson-Andrasko, and J. C. Stavrides. Analysis of the gas phase of cigarette smoke by gas chromatography coupled with uv-diode array detection. *Anal. Chem.*, 78:4509–4516, 2006.
- A. Jones, V. Lagesson, and C. Tagesson. Determination of isoprene in human breath by thermal desorption gas chromatography with ultraviolet detection. *Journal of Chromatography B*, 672:1–6, 1995.
- W. Kaye. Far-ultraviolet spectroscopic detection of gas chromatograph effluent. *Anal. Chem.*, 34:287–293, 1962.
- V. Lagesson. *Micro gas chromatographic separation combined with UV- and IR-spectrophotometric detection/identification with applications within the occupational hygiene field using diffusive and active sampling followed by a direct thermal desorption technique*. PhD thesis, University of Göteborg & University of Linköping, Sweden, 1992.
- V. Lagesson, L. Lagesson-Andrasko, J. Andrasko, and F. Baco. Identification of compounds and specific functional groups in the wavelength region 168–330 nm using gas chromatography with uv detection. *Journal of Chromatography A*, 867:187–206, 2000.
- P. Müller. *Development of an UV spectrometric detectors for gas chromatographic applications, in German: "Entwicklung eines UV-spektrometrischen Detektors für die Gaschromatographie"*. PhD thesis, University Würzburg, 1992.

References

- A. Nilsson. *Novel technique for analysing volatile compounds in indoor dust : application of gas chromatography - UV spectrometry to the study of building-related illness*. PhD thesis, Linköping University, Linköping, Sweden, 2004.

7 UV Absorption measurements for Trace Gas Analysis

Analysis

7.1 Introduction

The detection of gases in low concentrations, particularly the monitoring of polluting or harmful constituents within emissions, gain importance due to the increasing environmental standards. In addition, the determination of purity in gases for the food industry and for applications in medicine or semiconductor technology can be applied for minimizing risks for human beings or maintaining high efficiency productions. Finally, there are applications in medicine, where trace gases in exhaled breath are used for diagnosis. In all of the described cases, the precise and reliable detection of gases in low concentrations within complex matrices is necessary. In contrast to the measurement system for the use as an gas chromatographic detector, the volume of the gas flow cell is not as critical, as the gases are mostly available in sufficient quantity. On the other hand, especially for the detection of hazardous or toxic components low detection volumes can be an advantage, as the risk for the person operating the measurement equipment is minimized in this way. In addition, the heating of the absorption cell is not vital for the gases under test which simplifies the measurement setup.

According to Beer-Lambert-Beers law, the absorption measured A is proportional to the extinction coefficient $\varepsilon(\lambda)$, the concentration of the compound to be measured c , and the absorption length l :

$$A(\lambda) \propto \varepsilon(\lambda) \cdot c \cdot l \quad (7-1)$$

The desired minimum detection limit and the extinction coefficient directly influences the size of the absorption path length. A variety of applications have been analyzed to determine the prospective efficiency of an ultraviolet detection system. Based on a database of UV spectra, for qualitative information

of the spectra, and in addition, the measurement of test gases in different concentrations for determining the extinction coefficients, case studies have been carried out. The main obstacle for measurement systems are the restrictions due to the absorption of oxygen, which becomes dominant in a wavelength range below 190 nm, where the fibres used provide a better transmission than ambient air.

7.2 Comparison of extinction coefficients in the UV and MIR wavelength region

In order to quantify the advantage of higher extinction coefficients, which also have been reported in Lagesson [1992], an absorption measurement of sulfur dioxide has been carried out in the UV and MIR wavelength range. In both cases, the absorption cell has been a hollow core waveguide. When coated with a dielectric film of silver and silver iodide, the hollow core waveguide is capable of transmitting IR radiation [Harrington, 1996]. As measurement equipment, a process FTIR spectrometer with a deuterated triglycine sulfate (DTGS) detector, was used. The system is a compromise in size and cost efficiency compared to laboratory FTIR systems, which are mostly used with mercury cadmium tellurite (MCT) detectors which require additional thermo electric or liquid nitrogen cooling. In the ultraviolet wavelength region absorption spectra were measured with the UV-prototype, described in table 4-2. A concentration of 8.4 ppm of sulfur dioxide SO_2 in nitrogen in the infrared wavelength region and a concentration of 1.1 ppm in the Ultraviolet wavelength region have been measured. The extinction coefficients $\varepsilon(\lambda)$ were calculated according to the following equation:

$$\varepsilon(\lambda) = \frac{A(\lambda)}{c \cdot l} \quad (7-2)$$

In above equation, the absorption loss A is divided by the concentration c and the optical path length l .

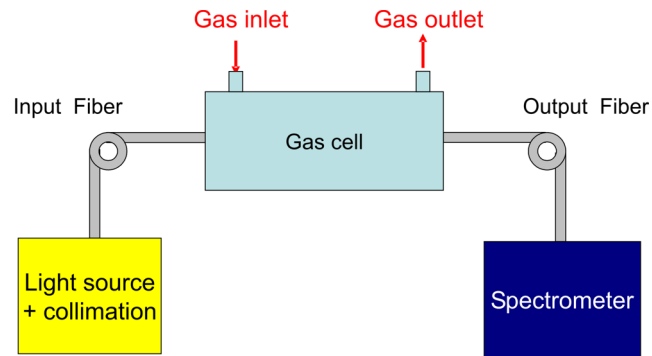


Figure 7.1: Measurement System for trace gas analysis

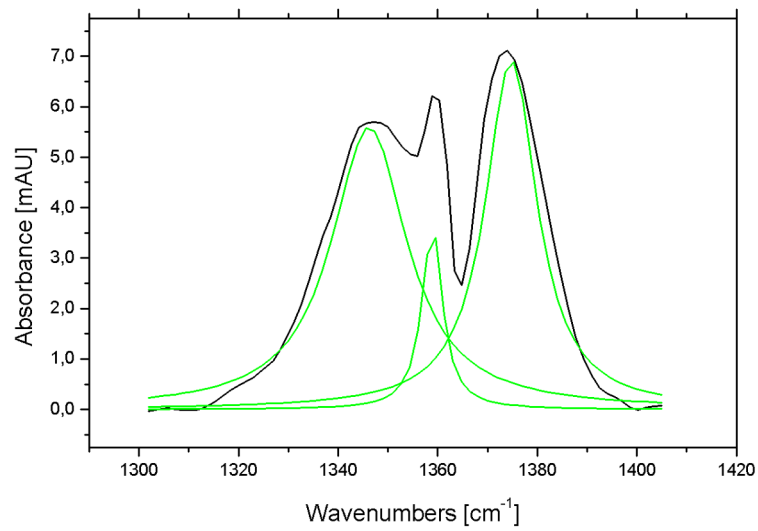


Figure 7.2: Absorption spectrum of 8.4 ppm sulfur dioxide in the infrared wavelength region, measured with a pathlength of 1 m

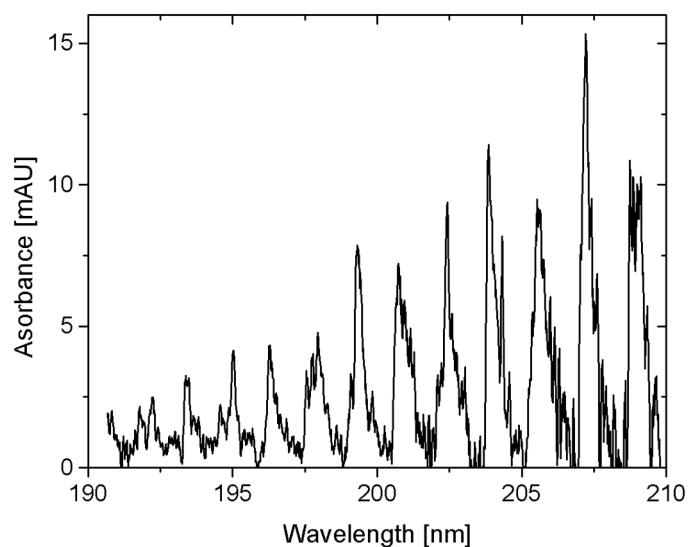


Figure 7.3: Absorption spectrum of 1.1 ppm sulfur dioxide in the ultraviolet wavelength region, measured with a pathlength of 1 m

The absorption spectra are shown in figure 7.2 for the infrared and in figure 7.3 for the ultraviolet wavelength range. The height of all absorption peaks in the infrared and at the wavelengths 202.5, 204.0 and 205.6 nm in the ultraviolet wavelength region have been used for comparison. The extinction coefficients are shown in table 7-1.

Depending on the chosen absorption peaks, the extinction coefficients are at least an order of magnitude larger in the ultraviolet compared to the infrared

Table 7-1: Extinction coefficients of sulfur dioxide

Peak	UV [$mAUm^{-1}ppm^{-1}$]	IR [$mAUm^{-1}ppm^{-1}$]
1	7.95	0.67
2	10.13	0.43
3	9.16	0.83

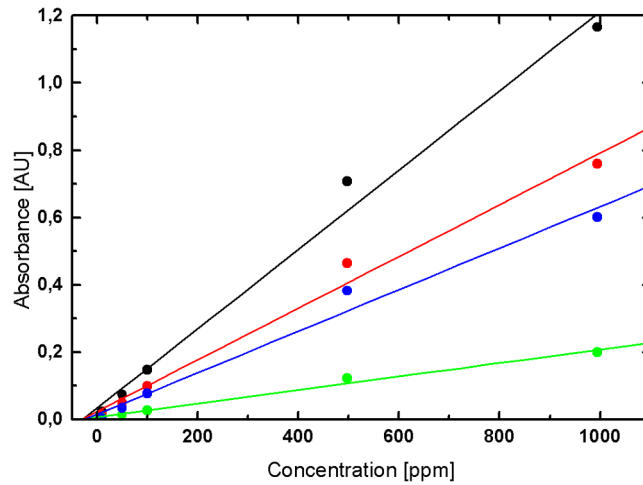


Figure 7.4: Linear regression of concentration over absorptions of Nitrogen dioxide at 220.9 (black), 227 (red), 242.3 (green) and 326.6 nm (blue)

wavelength region.

7.3 Measurement technique / Linearity

For determining the linearity, a measurement series with different concentrations of nitrogen dioxide in nitrogen as a carrier have been carried out. The gases have been blended within a gas blender. Their absorption was measured within a hollow core waveguide providing an optical path length of 1.82 mm, for concentrations between 10 and 995 ppm. In order to determine the linearity of the absorption four wavelengths have been selected and a linear regression has been calculated. The result is shown in figure 7.4.

The measurement is linear, in a range between 10 and 995 ppm. Gradient of the linear fits and their corresponding correlation coefficient R and standard deviation SD are shown in table 7-2. The different extinction coefficients in

Table 7-2: Gradient, correlation coefficient R and standard deviation SD of linear fits

Wavelength [nm]	Gradient [AU/ppm]	Correlation Coefficient R	Standard devi- ation SD
220.9	0.011	0.995	0.580
227	0.0077	0.994	0.396
242.3	0.002	0.995	0.099
326.6	0.006	0.991	0.403

the absorption spectra can be used for determining the actual concentrations in different ranges. As an example, the strong absorption band at 220.9 can be used for concentrations down to 10 ppm. The weaker absorptions at 326.6 nm can be used to determine absorptions for higher concentrations.

7.4 Possible Applications

7.4.1 Medical / health care applications

The importance of analyzing trace gases in human breath gas for biomedical research has been recognized for many years [Phillips, 1992; Risby, 2002; Schubert and Geiger, 1999]. In the past decades, studies have been performed in order to establish the clinical significance of trace gas emission in human breath gas. Results obtained in these studies indicate that the analysis of trace gases in exhaled breath may become a promising and non-invasive tool for medical diagnosis and for monitoring the success of therapy [Diskin et al., 2003; A. T. Society, 1999]. In previous research, mass spectroscopy has commonly been used for the analysis of the exhaled breath, with different types of ionization applied. If methods based on optical absorption spectroscopy could be used as an alternative, a precise and possibly 'turn-key' application could be realized. Taking this approach, a system employing a quantum cascade

Table 7-3: Exhaled trace gases indicating illnesses [Diskin et al., 2003; Fetzer et al., 2003; A. T. Society, 1999]

	Concentration (min..max)	Indicated illness	Measurable in the UV
	ppb		
Ammonia	400..2500	Renal failure	Yes
Acetone	200..1000	Diabetes	Yes
NO	5..1000	Asthma	Yes
Ethanol	20..150	Glucose level	Yes
Isoprene	20..150	Biochemical stress	Yes

laser as a light source in the mid-infrared (MIR) wavelength region, which is tuneable over a narrow wavelength range, was developed and reported. The minimal detectable concentration resulting was approx. 50 ppb NO in nitrogen [Fetzer et al., 2003]. The measurements were carried out within a 9 m long piece of Hollow-Core-Waveguide. The concentration of trace gases in human breath which are of relevance to clinical diagnosis are shown in Table 7-3. For all gases of interest the absorption spectra allow a detection in the ultraviolet wavelength region, with the described measurement system in an ambient air environment. In contrast to the MIR wavelengths, the absorption of the components is not masked by main components of exhaled breath, which is water, carbon dioxide and oxygen.

7.4.2 Monitoring of exhaust gas compounds

Combustion processes convert a mixture of ambient air and fuel into a wide variety of different gases, depending on the combustion parameters and the substances in the fuel. A complete combustion of the components, while using

Table 7-4: Typical exhaust gases from automobiles

	Ambient Air	Petrol ex- haust	Diesel ex- haust	measurable in the UV
	Vol-%	Vol-%	Vol-%	
Nitrogen	78.08	72.80	77.60	No, inert
Oxygen	20.95	1	13.5	Yes
CO ₂	0.03	10.9	4.60	Not in air
Water	1.30	13.10	4.20	Not in air
CO		1.40	0.03	Not in air
Hydrogen		0.04	0.03	
Hydro carbons		0.13	0.03	Some:Yes
Nitrogen Oxides		0.10	0.03	Yes
Ammonia		<0.01	<0.01	Yes
Aldehyde groups		<0.01	<0.01	Some: Yes
Patricle			<0.01	scattering

ambient air, can not be reached. Furthermore, due to the complexity of the reactants, a prediction of resulting exhaust gases is limited. For environmental reasons, a quantitative analysis of the described components is of vital importance, especially to obtain information about the hazardous components in lower concentrations. In addition, quantitative information on the processes within and the efficiency of the catalytic converter could be determined. Typical gas compounds of automobile exhaust are shown in table 7-4, according to [AG, 1988]. In figure 7.5 the absorption spectrum of oxygen within ambient air and of a mixture of 5% oxygen and 828 ppm of nitrogen dioxide within nitrogen, shifted by 0,4 AU. The absorption peaks of the minor gas component are clearly visible.

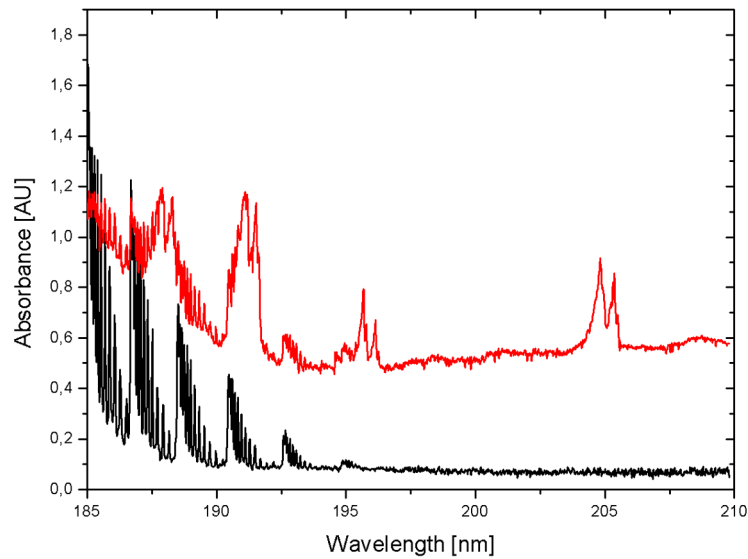


Figure 7.5: Absorption spectra of oxygen (black) and 828ppm of nitrogen dioxide in oxygen (red), with an offset of 0.5 AU

7.5 Summary

The measurement of gas absorptions in the UV offers the opportunity to measure multiple gases in low concentrations when multi-component analysis techniques - known and accepted for NIR and MIR measurements – are adapted for different applications. Furthermore, components in low concentrations can be monitored with a view to improving diagnostic possibilities and as a result ambient conditions. Several drawbacks of currently accepted techniques, such as the costly consumables requirements for a precise determination of trace gases in mobile (e.g. automotive) applications can be avoided. Depending on the path length and quality of the signals produced from the system components in the device, the measurement of trace gases is feasible in nitrogen. Most of the gases can also be measured in an ambient air atmosphere, because the absorption spectra offer peaks in a wavelength region where the absorption of oxygen is no longer dominant.

References

- Volkswagen AG. Non limited automobile exhaust gases, in German: Nicht limitierte Automobil-Abgaskomponenten. Technical report, Volkswagen AG, Wolfsburg, 1988.
- A. Diskin, P. Spanel, and D. Smith. Time variation of ammonia, acetone, isoprene and ethanol in breath: a quantitative SIFT-MS study over 30 days. *Physiol. Meas.*, 24:pp. 107–119, 2003.
- G. Fetzer, A. Pittner, and P. Silkoff. Mid-infrared laser absorption spectroscopy in coiled hollow core waveguides. In *Proc. SPIE Int. Soc. 4957, 124*, 2003.
- J. A. Harrington. Coherent, flexible, coated bore hollow-fiber waveguide and method and making same. Technical report, US Patent 5.567.471, 1996.
- V. Lagesson. *Micro gas chromatographic separation combined with UV- and IR-spectrophotometric detection/identification with applications within the occupational hygiene field using diffusive and active sampling followed by a direct thermal desorption technique*. PhD thesis, University of Göteborg & University of Linköping, Sweden, 1992.
- M. Phillips. Breath tests in medicine. *Scientific American*, Jul; 267 (1):74–79, 1992.
- T. Risby. *Disease Markers in Exhaled Breath*. IOS Press, 2002.
- J. Schubert and K. Geiger. Importance and perspectives of breath analysis. *Anesthesiol. Intensivmed. Notfallmed. Schmerzther.*, 34:pp391–5, 1999.
- A. T. Society”. Recommendations for standardized procedures for the online and offline measurement of exhaled lower respiratory nitric oxide and nasal nitric oxide in adults and children. *American Journal of Respiratory and critical care medicine*, 160:pp. 2104–2117, 1999.

8 Conclusions & Future Work

8.1 Summary of work carried out

Within this report, a fibre-optic system for measuring absorptions in gases in the ultraviolet region was designed and characterized, including the utilized components.

Starting with a review on existing fibre types available for the transmission of ultraviolet light, the requirements for their use in an analytic system have been discussed. In the case of all-silica fibres, their basic attenuation and solarization behaviour influence strongly the applicability of these fibres in the proposed system. However, depending on the base material's purity excellent transmission values can be achieved. The solarization behaviour of the fibre has been seen mostly as an obstacle, due to permanent and transient defects occurring within fibres. However, within the last years, the purity in the base material, and the UV-induced damages within the fibres have been minimized significantly. Therefore, a principal study on the transient UV-defects in current fibres has been carried out. In addition a model for describing their influence on the measurement was discussed briefly. The stability of this measurement system was improved significantly based on fibre-optics.

Subsequently, an overview over the lamp systems available for analytic applications was given, and the spectral characteristics and stabilities of three different lamps were determined. All lamps showed the potential to be used in the desired application. However, the required stability of the measurement system, the sampling time for one spectrum or restrictions in size or supplied energy define the lamp type for the application. Therefore, either a standard or miniaturized deuterium lamp might be chosen. Finally, the construction of the lamp housing and the attached incoupling optics, including path for a nitrogen purge, are vitally influencing the systems performance.

A synopsis of main design parameters for spectrophotometers, which comprise

the setups and properties of the optical bench, the influence of detection arrays and systems and wavelength range were carried out. In addition, criteria for an analytic spectrophotometer were discussed: stray radiant power ratio, wavelength accuracy, thermal stability, linearity and the signal to noise ratio play a major role for the usability in an analytical system. Comparing different spectral detection systems in respect to their characteristics proved, that there was no suitable detection system available, at the beginning of the thesis, which fully complies with the necessary criteria. Consequently a new high resolution fibre-optic spectrophotometer was developed and characterized. Excellent spectral resolution, wavelength accuracy, stray radiant power ratio and a sufficient photometric accuracy has been achieved.

For the construction of the absorption cell, basic studies for the coupling efficiency of a hollow core waveguide with a all-silica fibres were carried out. A methodology for the determination of the optimum absorption cells volume has been described, which strongly influences the time resolution and sensitivity of the detection system. Finally, an optimized coupling for the absorption cell to the gas stream of a gas chromatograph and a insulated and thermally stable housing for the measurement cell has been realized.

With the UV detection system for gas chromatography a variety of measurements have been carried out: A reference mixture has been prepared and separated within a GC instrument. The detection was carried out by the newly developed ultraviolet detection system only, or with an additional downstream mass spectroscopy detector. The in-line combination of both detectors is possible due to the fibre-optic absorption cell, which requires no make-up gas. Both analytical measurement systems operate in the same sensitivity range but provide subsidiary information as they show different response for molecules within the GC-eluate. With the described reference sample, a measurement series for determining the linearity of the system has been carried out showing good overlap with the values of the MS detector used as reference. A

measurement series with a sample containing 13 polycyclic aromatic hydrocarbons has been carried out. The detection and identification of these molecules are of high importance, as these components are insanitary and hazardous to the environment. Ten hydrocarbons have been detected and identified by their characteristic absorption spectra, while the remaining have not reached the detectors, due to their high boiling points. The absolute masses detected are in the lower nanogram range. Finally, a short-term noise and drift analysis has been carried out under measurement conditions. A noise of 1.1 and 2.6 mAU was determined for the wavelengths 217nm and 180nm, with a drift of 0.5 and 5 mAU respectively. The detection system performed steadily through the measurement campaigns, even when long measurement periods (t_i 40 min.) were necessary, for the detection of the PAH sample. The detection cell showed no degradation within the described measurements during a time frame of 1 week, facing temperatures up to 250°C and different solvents. Heating the measurement cell over night while maintaining gas flow and temperature proved to be a suitable method for cleaning the absorption cell.

With the described measurement principle the detection of compounds in low concentrations can be carried out quantitatively. For the analysis of combustion products a case study proved the applicability to detect traces of hazardous or toxic gases within automobile exhaust. In addition, a potential application in the medical diagnosis has been analyzed. In both cases, the gases of interest are not interfering with the absorption of ambient air, which allows a simplification of the measurement setup. The combination of a short, preparative separation column, in order to focus the compounds of interest in the absorption cell could be realized easily.

In conclusion the work carried out demonstrates quite clearly the applicability of the optical fibre based UV sensors for the detection of molecular species in the gas or vapour phase.

8.2 Future Work

The successful development of the fibre-optic based detection system can be transferred to a variety of applications.

The GC detection system was in operation for time frames no longer than a week in a row, and therefore no information is available on the long-term behaviour, exceeding this time frame. In particular, the durability of the heated measurement cell and the HCW with respect to their stability to aggressive solvents and high temperatures should be determined.

Within the future work, a detailed analysis of additional applications, for example the detection and identification of trace elements is necessary. In addition to the reported case studies possible applications might be found in the measurement of technical gases or as an on-line monitoring system for exhaust gases and production processes.

The detection of gas chromatographic effluent is providing additional information on the molecules structure, which is not detected by the most detection systems for gas chromatography. In addition, it might be a valuable tool for the analysis of complex unknown samples, such as flavours, cigarette smoke or oils obtained by pyrolysis.

In order to exploit the full capabilities of the spectrophotometric measurement system, the development of optimized methods data acquisition and, even more important to the end user, the data analysis and data handling procedures have to be streamlined and optimized. The information contained in the absorption spectra, and also on the time axis with chromatographic systems, have to be extracted by a set of mathematical algorithms. Particularly the on-line prediction and classification might be applied for on-line measurements, which potentially lowers the detection limits by an order of magnitude. The intelligent combination of existing off-line methods for data analysis, such as peak detection, library search and, if a calibration set is available for the detected

compound, a quantification might significantly extend the performance of a chromatographic detector.

In respect to available components, there is no alternative to the used deuterium lamps. However, the development of solid state sources in the ultraviolet has been reached wavelength ranges around 300 nm and below. These light sources have shown excellent stability and longevity in the first applications, and the life time of the LED chips can be expected to exceed the life time of a deuterium discharge lamp within the next 5 years. However, the quantum efficiency of the materials used decrease strongly below 300 nm.

9 List of Publications

9.1 Publications related to fibre-optic gas analysis

1. H. S. Eckhardt, K. Behler, M. Frank, K T V Grattan, K-F Klein, R. Kötschau, U. Schröder "Further improvements of high precision gas analysis in DUV region", SPIE Proc. BIOS'04 Vol. 5317 paper 5317-25, (San Jose, USA, Jan2004)
2. H. S. Eckhardt, H. Dominick, M. Frank, KTV Grattan, K-F. Klein: "Gas Analysis in the UV region: a hollow-core waveguide Sensor System", EWOFs 2004, SPIE proc. 5502 paper 5502-60 (Santander, Spain, June 2004)
3. H.S. Eckhardt, K.T.V. Grattan, K.-F. Klein, L. Lagesson-Andrasko, V. Lagesson, T. Sun: "UV-optically based gas sensing with potential application to exhaust gas monitoring" (OFS-17, Bruges, Belgium, 2005)
4. H.S. Eckhardt, K. Graubner, K-F. Klein, T. Sun, K.T.V. Grattan: "Fiber-optic based gas sensing in the UV-region", Proc. SPIE BIOS '06, 6083-10 (San Jose, USA, January 2006)
5. H. S. Eckhardt, K-F. Klein, K.T.V. Grattan: "High precision Gas analysis in the UV wavelength region" in german: "Gasanalyse im UV-Wellenlängenbereich mit hoher Nachweisempfindlichkeit", VDI-Berichte 1959 (Jun 2006)
6. H. S. Eckhardt, H. Dominick, K.T.V. Grattan, K. Graubner, K.-F. Klein, B. Spangenberg, T. Sun: "Fiber-optic detection device for GC-UV", SPIE-BIOS '07, 6433-12, (San Jose, January 2007)
7. H. S. Eckhardt, K.-F. Klein; B. Spangenberg, T.Sun, K.T.V. Grattan:

"Fibre-optic UV Systems for gas and vapour analysis", ICOLAD Conference 2007, Published in IOP Conference Series 85 (2007) 012018

9.2 Publications related to fibre-optic characterization and applications

1. K-F. Klein, K. Behler, H. S. Eckhardt, R. Kötschau, G. Hillrichs: "Status of Hollow-Core-Waveguides", IWKM, Mittweida, Germany 2002
2. H. S. Eckhardt, B.Jüngling, K.F. Klein, H. Poisel "Side- and end-illumination of Polymer Optical Fibers in the UV-region", SPIE Proc. BIOS 03 Vol. 4957 paper 4957-12, (San Jose, USA, Jan. 2003)
3. S. Ferwana, H. S. Eckhardt, T. Simon, K.-F. Klein, R. Haynes, V. Kh. Khalilov, G. Nelson: "All-silica fiber with low or medium OH-content for broadband applications in astronomy", SPIE Proc. Astronomical Telescopes and Instrumentation Vol. 5494 paper 5494-76, (Glasgow, Scotland, UK June 2004)
4. K.-F. Klein, H. S. Eckhardt, C. Vincze, S. Grimm, J. Kirchhof, J. Kobelke, J. Clarkin, and G. Nelson: "High NA-fibers: silica-based fibers for new applications" Proc. SPIE BIOS'05, 5691-7 (San Jose, USA January 2005)
5. M. Bleichert, H. S. Eckhardt, K.-F. Klein, B. Spangenberg, G. Hillrichs, J. Mannhardt: "New components for fiber-optic Thin-Layer Chromatography including fluorescence", SPIE-BIOS '07, Vol. 6433, (San Jose, January 2007)
6. M. Belz, H. S. Eckhardt, C.P. Gonschior, G. Nelson, K.-F. Klein: "Quality Control of UV resistant fibers for 200-300nm spectroscopic applications", SPIE-BIOS '08, 6852-33, (San Jose, CA, USA January 2008)

7. K.-F. Klein, J. Mannhardt, M. Belz, C.P. Gonschior, H.S. Eckhardt:
"Optical fibers in instrumental UV-analytics", SPIE-BIOS '09, 7173-36,
(San Jose, CA, USA January 2009)

A Appendix

A.1 Short-term Stability measurements of fibre optic UV detection system

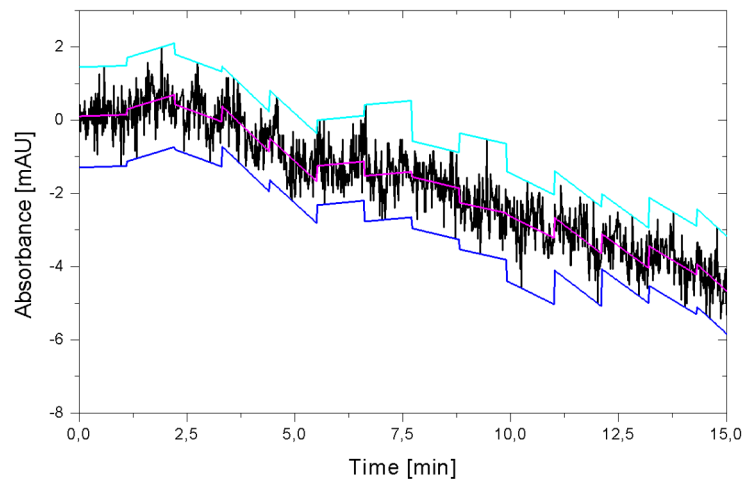


Figure A.1: Determination of short time stability under Measurement conditions at 180 nm

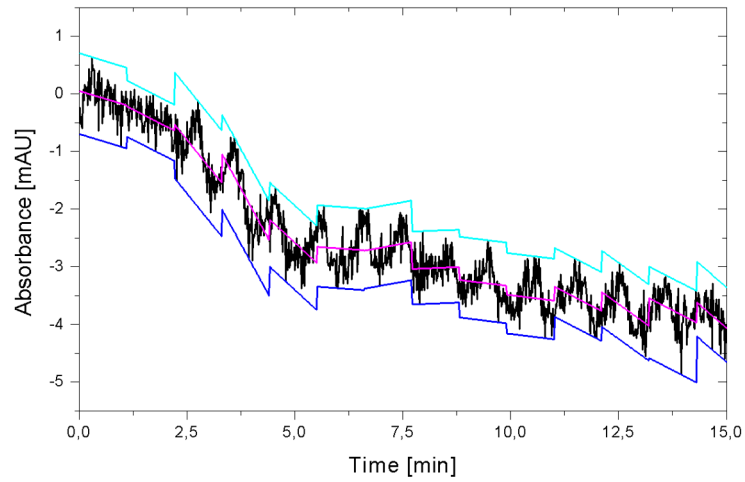


Figure A.2: Determination of short time stability under Measurement conditions at 186 nm

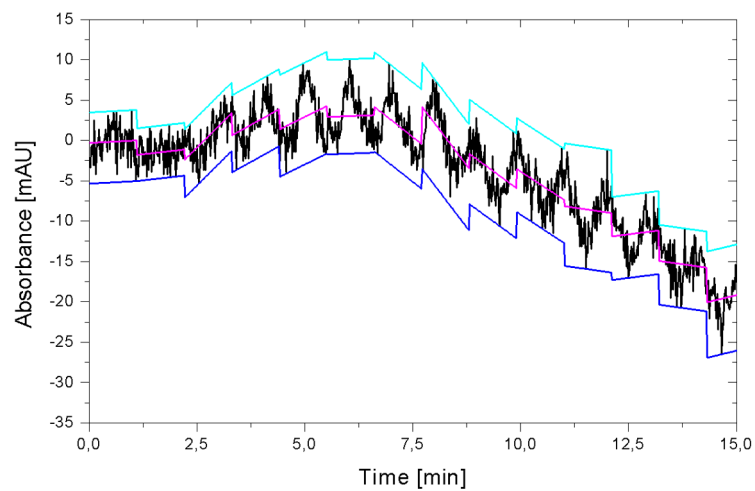


Figure A.3: Determination of short time stability under Measurement conditions at 200 nm

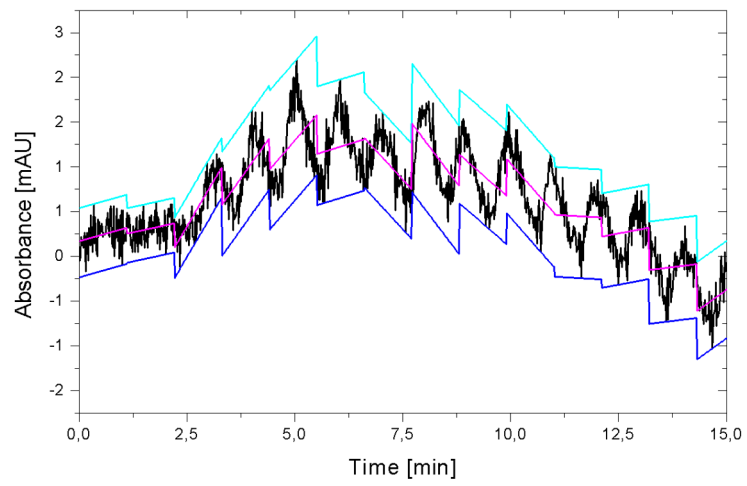


Figure A.4: Determination of short time stability under Measurement conditions at 217 nm

A.2 Engineering drawings of measurement system

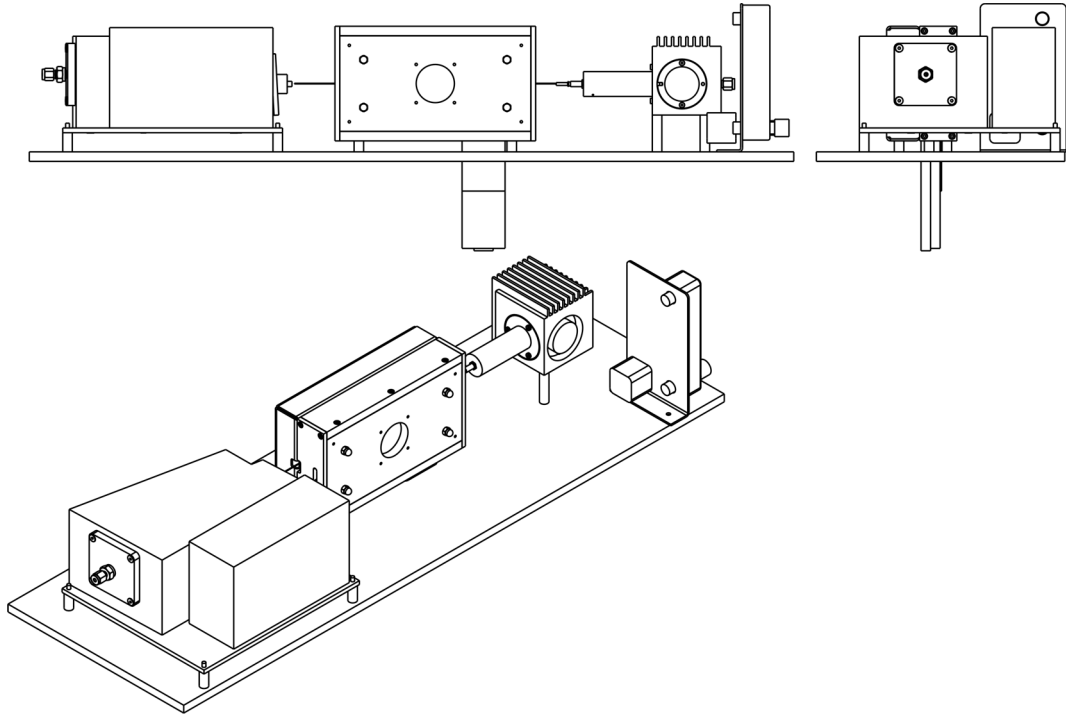


Figure A.5: Overview on measurement system

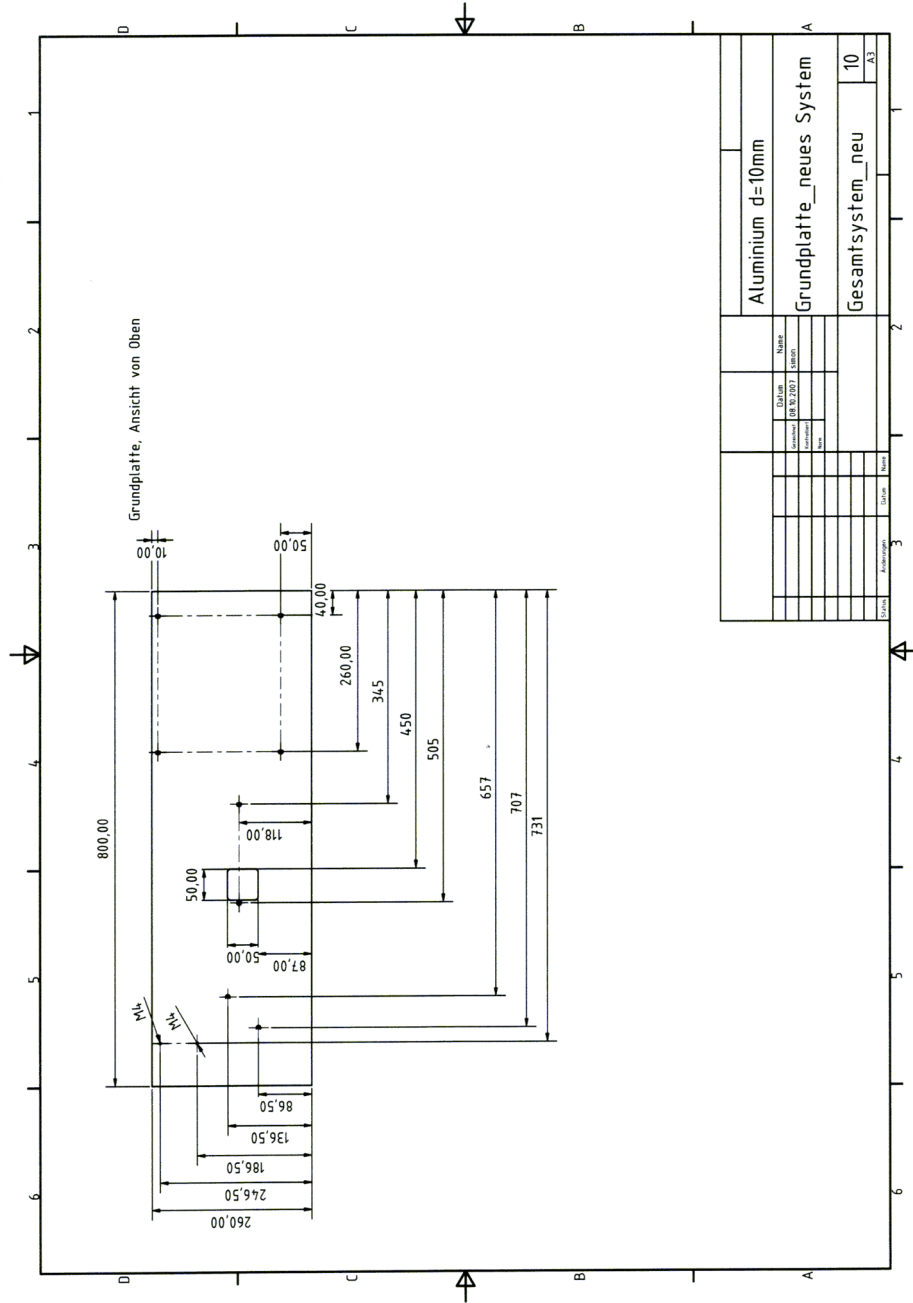


Figure A.6: Drawing of base plate of measurement setup

A Appendix

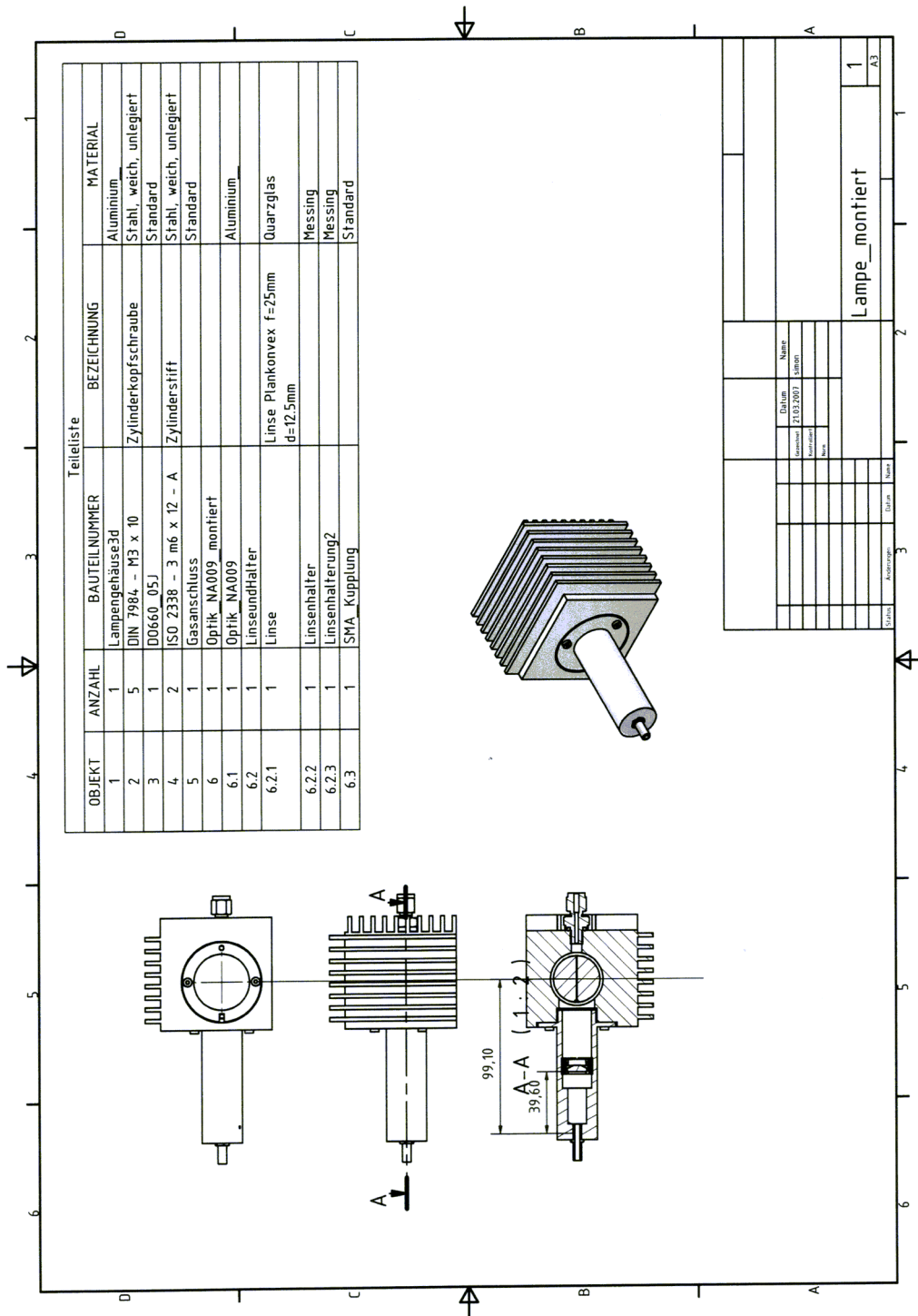


Figure A.7: Overview on lamp setup

A Appendix

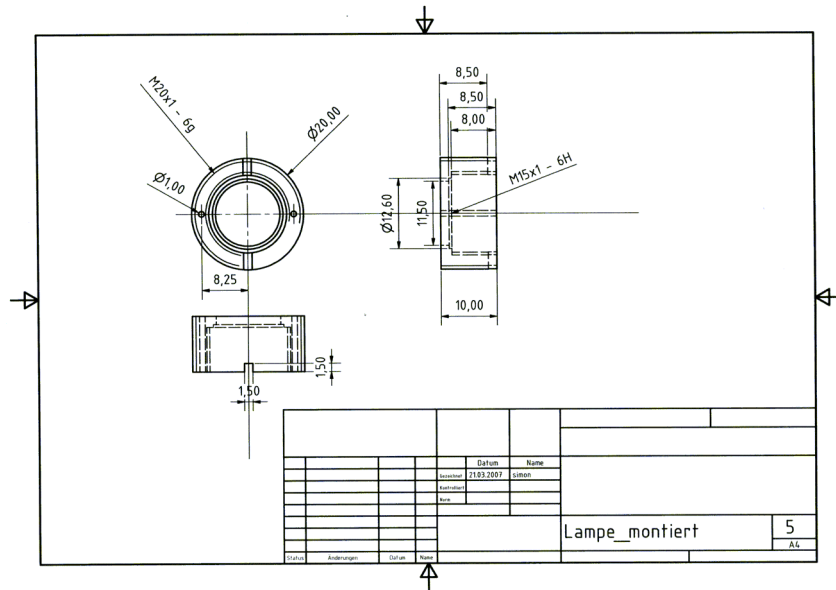


Figure A.10: Drawing of lens holder

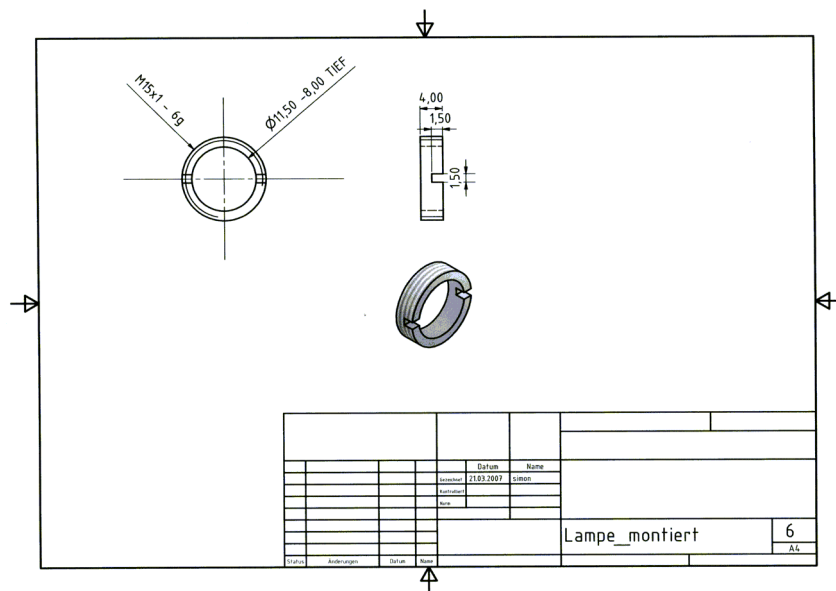


Figure A.11: Drawing of lens ring

A Appendix

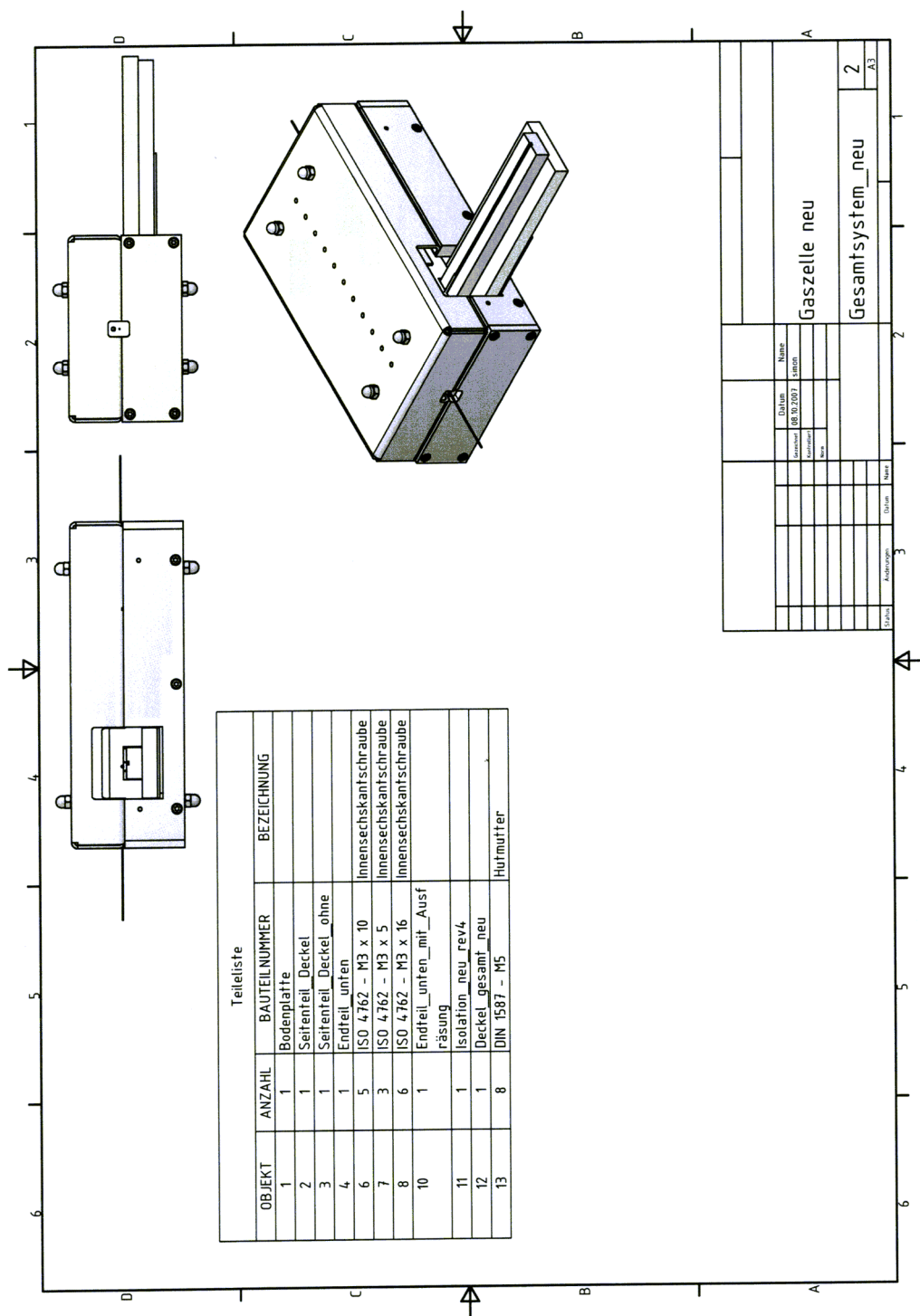


Figure A.12: Overview on measurement cell

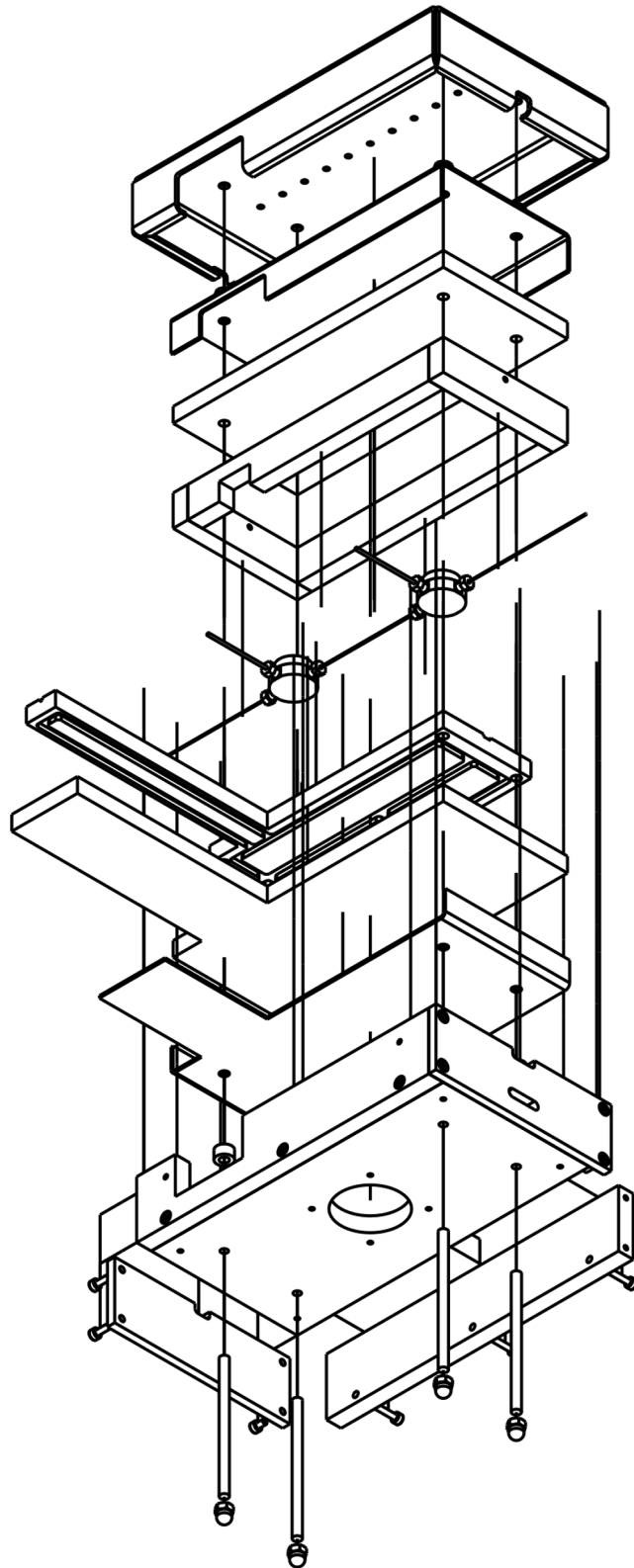


Figure A.13: Explosion drawing of measurement cell

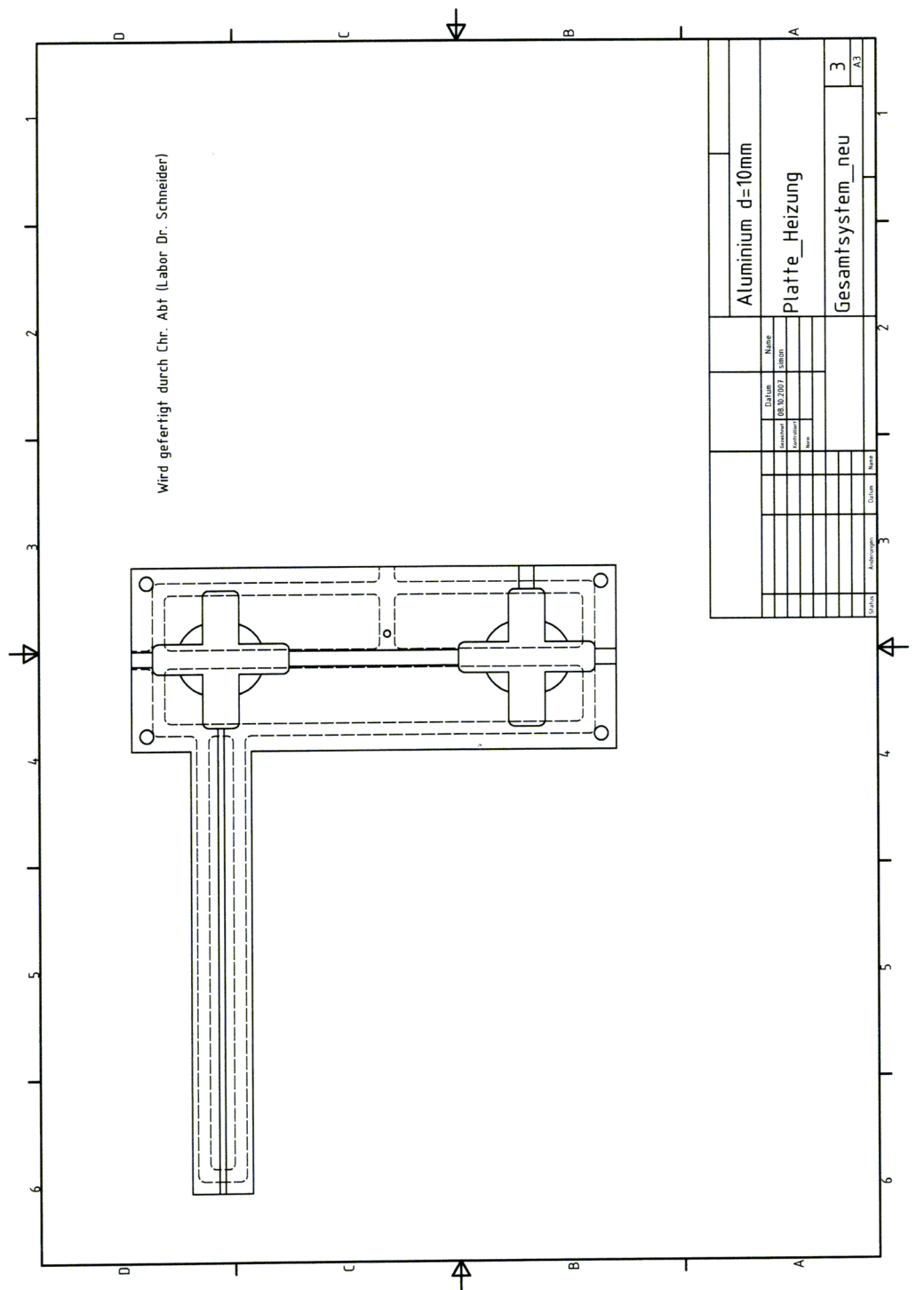


Figure A.14: Drawing of measurement cell - base plate for gas cell

